SOME STUDIES ON MEDICAL IMAGE

PROCESSING AND ANALYSIS

A THESIS

SUBMITTED TO THE DELHI TECHNOLOGICAL UNIVERSITY

FOR THE AWARD OF THE DEGREE OF

DOCTOR OF PHILOSOPHY

HEENA HOODA

DEPARTMENT OF INFORMATION TECHNOLOGY

DELHI TECHNOLOGICAL UNIVERSITY, DELHI

2022

SOME STUDIES ON

MEDICAL IMAGE PROCESSING AND ANALYSIS

By

HEENA HOODA (2K13/PHD/IT/01)

Submitted in fulfillment of the requirement of the degree of
DOCTOR OF PHILOSOPHY

Supervisor

Prof. O.P. Verma

Department of Electronics & Communication Engineering

Delhi Technological University New Delhi

DEPARTMENT OF INFORMATION TECHNOLOGY

DELHI TECHNOLOGICAL UNIVERSITY

DELHI, INDIA

2022

DECLARATION

I hereby declare that the thesis entitled "**Some Studies on Medical Image Processing and Analysis**" to be submitted in partial fulfillment of the requirements for the award of the degree of Doctor of Philosophy in the Department of Information Technology of the Delhi Technological University, Delhi is an authentic record of my own work carried out under the supervision of Prof. O. P. Verma. The thesis has not been submitted either in part or whole to any university or institute for the award of any degree or diploma.

Place: DTU, Delhi   Heena Hooda

Date: 30-05-2022   (2k13/PHDIT/01)

CERTIFICATE

This is to certify that the thesis entitled **"Some Studies on Medical Image Processing and Analysis"** being submitted by **Heena Hooda** to the Department of Information Technology, Delhi Technological University, Delhi, for the award of the degree of Doctor of Philosophy, is a record of bonafide research work carried out by her under my guidance and supervision. In my opinion, the thesis has reached the standards fulfilling the requirements of the regulations relating to the degree. The results contained in this thesis have not been submitted to any other university or institute for the award of any degree or diploma.

(Supervisor)

Prof. O.P. Verma

Professor

Department of Electronics and Communication Engineering

Delhi Technological University, Delhi

ACKNOWLEDGEMENT

Thanks to merciful Lord for everything in my life!!

This thesis work has been a roller-coaster journey and I am indebted to acknowledge a few people who made this journey successful.

First and foremost, it is a great pleasure to express my sincere gratitude and appreciation to my supervisor Prof. O. P. Verma. It is my honor to work under the supervision of such a kind man of values and great expertise. The completion of my thesis work was an uphill task and without the constant support and suggestions of Prof.Verma, this thesis would not have seen the light of the day. He is a professor of wide acclaim and profound knowledge whose valuable guidance and consistent scholarly inputs have helped me to form the basis of this work.

I would also like to thank Dr. S.A. Rao, Sr. Radiologist, Rajiv Gandhi Cancer Institute & Research Centre, Delhi, India for giving me his valuable time and sharing the database with us. This research would not have been possible without his support and guidance.

My extended thanks go to the faculty and staff of the Department of Information Technology, for their assistance and encouragement during my research work.

My deep and sincere gratitude for parents in law Mrs. Ashok Bala and Mr. Davender Singh for their continuous and unparalleled love, help and support throughout my journey towards this thesis.

I am forever indebted to my parents Mrs. Urmila Hooda and Mr. D.S. Hooda for their unfettered love, invaluable blessings and unwavering belief in me. I dedicate this thesis to my parents. Thanks to almighty for being there as my parents. This thesis is your dream come true. I owe them everything.

Some special words of gratitude go to my friends and colleagues who have always been a major source of support when things would get a bit discouraging. Thank you for inspiring me and occasionally pushing me to certain deadlines.

Finally, this is the word of acknowledgment I have saved for my dear husband Ayush Thakran and my son Shivaay Thakran. These two are the pillars of strength in my life. My heartfelt gratitude for my partner who witnessed this journey with me with deep insight and supported me unconditionally with his love. Your continuous motivation helped me to reach my goal. My baby boy Shivaay has been the light of my life whose smile transforms my dull moments instantly. Thank you for being there with me round the clock.

ABSTRACT

Medical image processing is currently the foremost emerging and challenging area of research within the field of image processing. The images used for processing and analysis in the medical domain are captured through imaging technologies like MRI, CT Scan etc. Because of its broad availability and capacity to create high-resolution pictures, magnetic resonance imaging (MRI) is the most commonly utilized imaging technique. MR imaging is a sophisticated visualisation technology that allows for the safe and non-invasive acquisition of pictures of the interior architecture of the human body.

Processing and analysis of human brain images plays a major role in computer aided diagnosis and neuroscience research. It further helps in identification of several neurodegenerative and mental disorder diseases such as tumors, edema, Schizophrenia, Multiple Sclerosis, Alzheimer disease and Parkinson. The segmentation of MRI brain images allows representation of brain image into meaningful segments which helps in analysis and interpretation of image for identifying the area of interest, detecting tumor, and treatment planning. The segmentation of MR brain images is carried out manually within the clinical environment by the radiologist counting on their visual interpretation. This mapping is extremely time consuming tedious task and error prone to human dependency. In order to beat the shortcomings of mapping the tumor manually, the researchers are keen to develop automatic tumor segmentation system. Also, Automatic retrieval of images is of great importance in medical field as it helps in decision making for solving various problems and helps in treatment planning.

This thesis work tries to cater various aspects of MR brain image classification and segmentation. In order to classify the image into tumorous and non-tumorous we have proposed to use binary patterns (LBP) as features. The LBP provides a label to each 3 X 3 window based on the connection between the centre pixel and adjacent pixels. The histogram of these labels is then sent into the classification step as a feature space. The pictures are categorised as tumorous or non-tumorous using the Minimal Complexity Machine (MCM) method. The accuracy computed is used to assess the results of the proposed approaches.

After identification of MR brain image as tumorous, early detection and accurate treatment based on truthful diagnosis are the major concern to cure brain tumor. The precise position, direction, and extent of the aberrant tissues are crucial in the detection of brain tumour. Detection of anatomical brain structure plays a major role in the planning of treatment. This study involves comparative analysis of three image segmentation techniques for detection of brain tumor from sample MRI images of brain. K-Means Clustering, Fuzzy C-Means Clustering, and Region Growing are the picture segmentation algorithms used. A comparative analysis of the above mentioned image segmentation techniques is done and it was found that utilizing solely feature memberships may result in overlapping clusters, emphasising the importance of using both feature and object memberships. To handle this problem in case of MR brain images we introduce the application of Fuzzy Co-Clustering Algorithm for detection of brain tumor. In this algorithm co-clustering is integrated with the Fuzzy approach with a view to obtaining distinct clusters. However, these segmentation algorithms are not able to handle the uncertainty that arises from boundary between different tissues. To handle this type of uncertainty the generalization of fuzzy sets theory is used, known as intuitionistic fuzzy sets (IFS). In order to handle the ambiguity between different tissues we have formulated Intuitionistic Fuzzy Co- Clustering Algorithm. The performance of the

algorithms is evaluated on the basis of match score, accuracy score, Dice score and Jaccard's similarity coefficient.

Also amongst the most essential fields in computer-aided treatment and neuroscience studies is the segmentation of a human brain picture from MRI scans into three brain tissues: cerebrospinal fluid, grey matter, and white matter. Segmentation algorithms such as FCM is very sensitive to noise. To avoid any stuck in local optimal results, ACO technique is used. ACO is used to determine the value of initial cluster centers. The centers thus obtained are fed into the system to perform segmentation. In modified FCM, Mahalanobis distance is used instead of Euclidean distance as Euclidean distance takes into account only the super-spherical shapes about the center of mass for clustering the data points, whereas data points belonging to same cluster may not be located in that area only. Also, the local neighborhood information is also considered as neighboring pixels are more likely to belong to same cluster. Also, we propose one more algorithm for brain image segmentation, a Fuzzy-Gravitational Search Algorithm (GSA) and its application to MRI brain image segmentation. The proposed approach is based on GSA, and uses fuzzy inference rules for controlling the parameter α as search progresses. The results of the system are compared with GSA and recent work on brain image segmentation algorithms for both real and simulated database on the basis of Dice Coefficient values and is found to outperform.

Also, we propose an image retrieval algorithm in this thesis. Automatic retrieval of images is of great importance in medical field as it helps in decision making for solving various problems. The feature extraction in content based image retrieval is a crucial stage whose success is determined on the approach used to extract characteristics from pictures. There are two types of visual content descriptors: global and local. To describe an image, a global descriptor describes the visual features of the entire image, whereas a local descriptor represents the visual features of areas or components.

The feature database is built by arranging these as multi-dimensional feature vectors. In this thesis, we have proposed a novel feature descriptor based on local binary pattern for retrieval of biomedical images.

LIST OF PUBLICATIONS

Journals

1. Om Prakash Verma and **Heena Hooda**, "A Novel Intuitionistic Fuzzy Co-Clustering Algorithm for Brain Images", *Multimedia Tools and Applications,* Volume 79, Issue 41-42, November 2020, pp. 31517–31540

2. **Heena Hooda** and Om Prakash Verma, "Hamming Distance Based Local Binary Pattern for Biomedical Image Retrieval", *International Journal of Advanced Research in Engineering and Technology*, Volume 11, Issue 10, October 2020, pp. 941-950.

3. **Heena Hooda**, Om Prakash Verma, "Fuzzy Clustering using Gravitational Search Algorithm for Brain Image Segmentation", *In Multimedia Tools and Applications*. (2022). Available Online https://doi.org/10.1007/s11042-022-12336-x

Conferences

1. **H. Hooda**, O. P. Verma and T. Singhal, "Brain tumor segmentation: A performance analysis using K-Means, Fuzzy C-Means and Region growing algorithm", IEEE *International Conference on Advanced Communications, Control and Computing Technologies*, Ramanathapuram, 8-10 May 2014, pp. 1621-1626.

2. **H. Hooda**, O. P. Verma, "Classification of Magnetic Resonance Brain Images Using Local Binary Pattern as Input to Minimal Complexity Machine", *In Computing, Communication and Signal Processing, Advances in Intelligent Systems and Computing*, Springer, Singapore, International Conference on Computing, Communication and Signal Processing, Lonere, 26-27 Jan 2018, vol 810, pp. 883-893.

3. **H. Hooda**, O. P. Verma., S. Arora, "Optimal Fuzzy C-Means Algorithm for Brain Image Segmentation", *In Applications of Artificial Intelligence Techniques in Engineering, Advances in Intelligent Systems and Computing*, Springer, Singapore. International Conference on Signals, Machines and Automation, Delhi 23-25 Feb 2018, vol 698, pp. 591-602.

LIST OF ABBREVIATIONS

ACO - Ant Colony Optimization

AFBPNN- Adaptive Firefly Back Propagation Neural Network

ANN - Artificial Neural Network

ANFIS- Adaptive Network Based Fuzzy Inference System

BPNN - Back Propagation Neural Network

CSF - Cerebrospinal Fluid

CT - Computed Tomography

DC - Dice Coefficient

DCT - Discrete Cosine Transform

DWT - Discrete Wavelet Transform

EIFE - Effective Information Feature Extraction

EM - Expectation Maximization

FCCI - Fuzzy Co-Clustering for Images

FCM - Fuzzy C-Means

fMRI - Functional Magnetic Resonance Imaging

FN - False Negative

FP - False Positive

FP-ANN- Forward Back Propagation Artificial Neural Network

GA- Genetic Algorithm

GHSOM- Growing Hierarchical Self Organizing Map

GLCM- Gray Level Co-occurrence Matrix

GM - Gray Matter

GSA - Gravitational Search Algorithm

GRBF- Gaussian Radial Basis Function

GWS- Gabor Wavelet and Statistical

IFCC - Intuitionistic Fuzzy Co-Clustering

IFS- Intuitionistic Fuzzy Sets

JS - Jaccard Similarity

KM - K Means

KNN - K Nearest Neighbor

LBP - Local Binary Pattern

LIPC- Local Independent Projection-Based Classification

MCM - Minimal Complexity Machine

MLP - Multi Layer Perceptron

MR- Magnetic Resonance

MRI - Magnetic Resonance Imaging

NAMIC- National Alliance For Medical Image Computing

NMR - Nuclear Magnetic Resonance

NN- Neutral Network

PCA - Principal Component Analysis

PET - Positron Emission Tomographic

PNN - Probabilistic Neural Network

PSO- Particle Swarm Optimization

RBF - Radial Basis Function

RGCI&RC- Rajiv Gandhi Cancer Institute and Research Centre

SOM - Self Organizing Map

SPECT - Single Photon Emission Computed Tomographic

SVM - Support Vector Machine

TLBO- Teaching Learning Based Optimization

TN -True Negative

TSP- Travelling Salesman Problem

TP - True Positive

VC - Vapnik Chervonenkis

WM - White Matter

WHO- World Health Organization

List of Figures

List of Tables

Table of Contents

Chapter 1

Introduction

1.1 Motivation

Medical imaging is the broad term for a collection of techniques and procedures for generating anatomical or functional pictures of the human body for clinical as well as research reasons. [1]. Medical image analysis is amongst the most important studies in the area of medicine, because the results help field experts with diagnosis, treatment planning, and treatment verification. [2]. Furthermore, recent advancements in medical imaging and medical image processing have reduced the need for intrusive intervention in the treatment of a variety of illnesses and anomalies. In order to be utilised for quantification and analysis of desired characteristics, medical pictures require the sequential use of numerous image post-processing methods, such as restoration, regularisation, segmentation, and registration[2]. These characteristics can be particular portions of the picture, such as specific tissues, tumours, or lesions, or any statistical attribute applied to the full image domain or parts of it.

CT, Ultrasonography, PET, SPECT, MRI, fMRI, and NMR spectroscopy are examples of medical imaging methods that use medical image processing. Computed tomography (CT), magnetic resonance (MR) imaging, single photon emission computed tomographic (SPECT) imaging, positron emission tomographic (PET) scanning, and cerebral angiography are some of the imaging methods used to examine sections of the human body. Because of their broad availability and capacity to create high-resolution pictures of normal anatomic structures and diseased tissues, CT and MR imaging are now the most commonly utilized methods [3].

Because CT is the quickest modality for imaging critically sick or medically unstable patients, it is the recommended assessment. Although their capacity to offer information on tissue biology and physiology can be extremely useful, SPECT and PET imaging play a limited role. PET scanning can also be used to determine the cancer's grade.

For a variety of reasons, MRI is the most often utilised neuro-imaging method for the evaluation and follow-up of patients with brain tumours. CT, SPECT, and PET examinations do not employ ionising radiation. Because it has a higher contrast resolution than the other methods, it is better at identifying tiny lesions and isodense lesions on unenhanced CT. It's also more sensitive than CT when it comes to detecting lesion enhancement. The capacity of MRI equipment to provide pictures in the sagittal, axial, and coronal planes allows for better localisation of a lesion in the 3D space of the brain and more clearly delineation of structures affected by the tumour. Finally, MR imaging eliminates the beam-hardening artefact caused by the skull base on CT, making it more suitable for assessing lesions in the posterior fossa and inferior frontal and temporal lobes. The ability to get both morphological and functional details about the tumour at the same scan may be MR imaging's most significant benefit. MRI has several limits that must be addressed, despite its many benefits [4]. The absence of detail is the most significant. Although enhancement does not necessarily correspond to histology tumour grade, higher grade tumours on MR imaging are more likely to display enhancement. [5]. MRI has several limits that must be addressed, despite its many benefits. The absence of detail is the most significant. Although enhancement does not necessarily correspond to histology tumour grade, higher grade tumours on MR imaging are more likely to display enhancement. A very slow-growing tumour, on the other hand, will commonly exhibit contrast enhancement areas inside the tumour[6]. Likewise, some higher-grade cancers will not improve. [6]. As a result, while MR characteristics of a lesion might be useful, histologic confirmation is sometimes required to make a diagnosis. MR imaging also can't tell the difference between the border of a

tumour and the entire range of illness[6]. Beyond the limits of aberrant contrast enhancement, possible tumour cells have been discovered. [6]As a result, MRI alone cannot be used to detect whether a tumour is present or not after such treatment. MRI is the standard imaging method in human neurooncology, despite these drawbacks.

Image segmentation is important in a variety of image processing techniques. The process of segmenting a picture into its constituent parts based on specific properties or attributes is known as segmentation. Each pixel in an area is identical to the next in terms of intensity, texture, colour, and other factors. The primary objective of segmentation is to extract useful data and make it easier to analyse and visualise. Image segmentation has roots in a variety of fields, including medical imaging, face identification, machine vision, expert systems, autonomous traffic management systems, and dealing with satellite images, among others. Due to its numerous practical uses, medical image segmentation is receiving a lot of attention these days. Different goals may be dealt with in its applicability to brain MRI, such as extraction of tiny specialised structures like brain tumours, or certain key tissues (WM, GM, CSF), [7-9], or dividing the brain into anatomical components, and so on. [10]

Computer-assisted diagnosis and neuroscience research rely heavily on the processing and interpretation of human brain pictures. It also aids in the diagnosis of a variety of neurological and mental disorders, including tumours, edoema, Schizophrenia, Multiple Sclerosis, Alzheimer's disease, and Parkinson's disease. The splitting of MRI brain scans allows the brain picture to be represented in meaningful parts, which aids in image processing and analysis for locating the region of interest, finding tumours, and treatment planning. The radiologist manually segments MR brain pictures in the clinical setting, relying on visual interpretation. This translation is a time-consuming, laborious operation that is prone to human mistake. The researchers are eager to create an automated tumour segmentation method in order to overcome the drawbacks of manually mapping the tumour.

1.2 MRI

MRI is a sophisticated imaging technique that allows for the safe and non-invasive acquisition of pictures of the interior anatomy of the human body. It is formed on the basis of Nuclear Magnetic Resonance (NMR) and may be used to conduct a wide range of visualisations. Due to its capacity to capture signals that can differentiate between various 'soft' tissues, MRI has been particularly useful for generating pictures of the brain (such as grey matter and white matter) [11].

Different techniques can be adopted in acquisition of MRI image. According to Pham *et al.*. the properties and requirements of segmentation should be well known beforehand so as to make a well firmed decision. The density of tissues and its relaxation properties contributes to contrast in an image. The most common and maximum used weightings are T1 and T2.[11] Selection of appropriate one as per the demand of the problem is very crucial and an important step. In brain imaging, T1-weighted and T2-weighted pictures are two of the most widely utilised MRI visualisations. These weightings relate to the main signal (whether it's the T1 time or the T2 time) used to generate the picture contrast [11]. T1-weighted pictures may be thought of as seeing fat locations since regions with high fat content have a short T1 time compared to water. T2-weighted pictures, on the other hand, may be thought of as seeing water locations since areas with high water content have a short T2 duration compared to those with high fat content.

T1-Weighted Images (T1WI)

T1 images exhibits higher contrast among WM and GM. T1 is the time till when X percent (X=63) of the longitudinal magnetization has been restored/recovered. In these types of images gray matter appears dark gray, white matter appears light gray, while some tissues possess low intensity such as CSF and some possess high intensity such as adipose tissue.

T2-Weighted Images (T2WI)

T2 images possess higher contrast between CSF and bone. T2 is the time till when X percent (X=63) of the transverse magnetization has been diminished/decayed. In these types of images both white and gray matter are gray in color i.e. they possess similar intensities.

PD Weighted Image (PDWI)

Unlike T1 and T2 weighted images, proton density (PD) displays the quantity of nuclei in the photographed region rather than the magnetic properties of the hydrogen nuclei. We want to reduce the influence of both T1 and T2 contrast to produce a PD weighted picture. We can see representation of various MRI brain image contrasts in Figure 1.1.

| (a) | (b) | (c) |
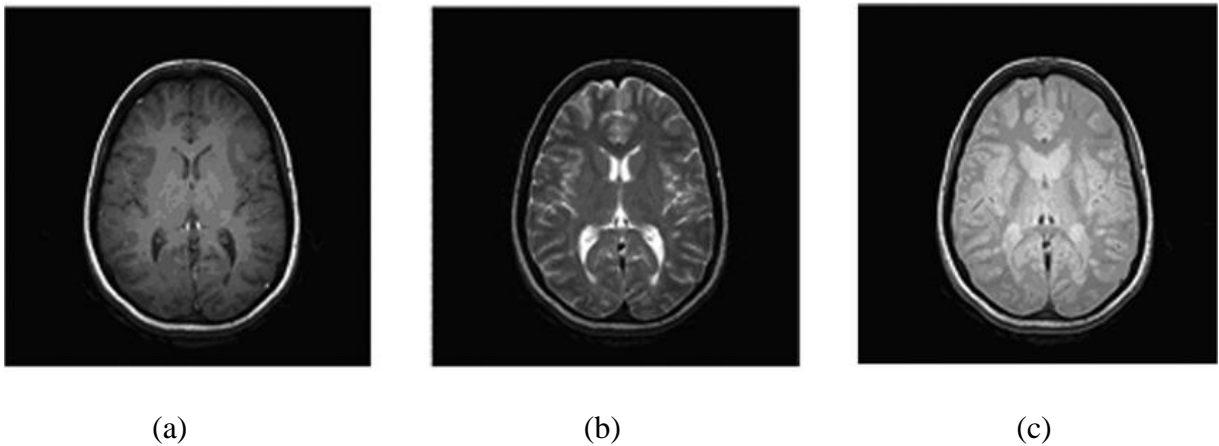
Figure 1.1: Representation of various MRI brain image contrasts:

(a) T1-weighted, (b) T2-weighted and (c) PD

Two important parameters, TR (Repetition Time and TE(Echo Time)in the spin echo (SE) are used to increase the contrast of the images. The period between the 90° Radio Frequency pulse and the MR signal sampling, which corresponds to the maximum of echo, is known as Echo Time (TE). At time TE/2, the 180° RF pulse is used. The time between two excitation pulses is referred to as the repetition time (TR). Depending on the TR and TE sequences, the

primary three sequences are T1-weighted, T2-weighted, and Proton density (PD) weighting.

Proton density-weighted is a term for a sequence with a long TR and a short TE. T1-weighted

is produced by a short TR and short TE sequence. T2-weighted[11] is often produced by a

lengthy TR and extended TE sequence. In Figure 1.2, they are shown clearly.
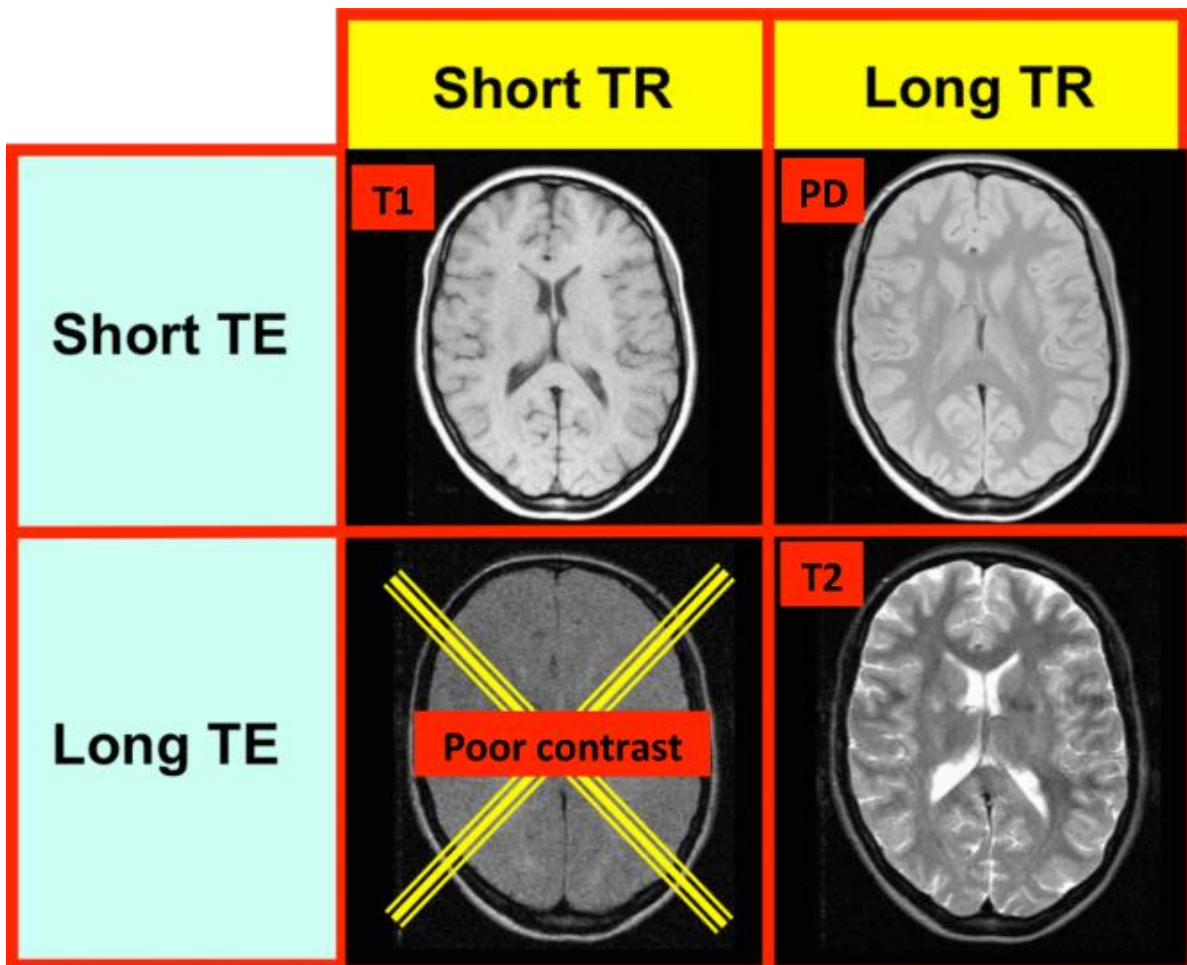
Figure 1.2 Generation of MRI brain image contrasts

1.3 Brain Anatomy

Brain is extremely focused organ of the human body which helps us to cope with the

environment. Human brain serves as the manager for all the functions performed by the body

such as words, actions, thoughts, and feelings that are centered in the brain. In this section we describe the brain tissue structure and its anatomical parts.
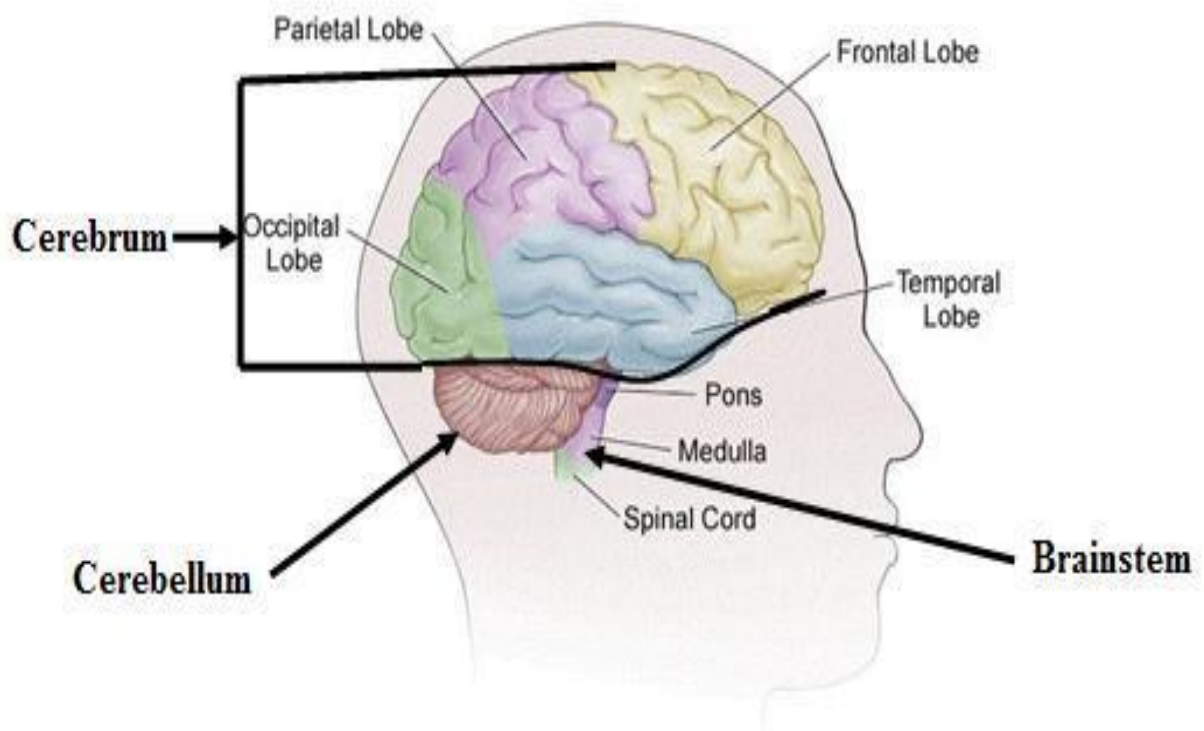
Figure 1.3 Anatomy of human brain

The cerebrum, cerebellum, and brain stem are the anatomical components of the brain, as depicted in Figure 1.3. The Cerebrum is the biggest region of the brain and is responsible for regulating conscious thinking, movement, and feeling in the human body. It is divided into two parts, the right and left cerebral hemispheres, each of which is in charge of a different portion of the body [12]. The frontal, temporal, parietal, and occipital lobes are the four lobes that make up each hemisphere. The cerebellum is the second biggest portion of the brain, and it assists in regulating motor activities such as walking, balance, posture, and coordination of human movement. It is linked to the brain stems and is located at the rear of the brain. Both the cerebrum

and the cerebellum have a thin grey matter outer cortex, interior white matter, and dense grey matter masses. The brainstem is a part of the brain that connects to the spinal cord. Many essential processes, including as motor and sensory pathways, cardiac and repository functions, and reflexes, are controlled by it. The midbrain, pons, and medulla oblongata are its three structures [12].

1.3.1 Brain Tissues

MRI is a powerful imaging technique to study brain disorder diseases such as tumors, edema, Schizophrenia, Multiple Sclerosis, Alzheimer disease and Parkinson. The brain mainly comprises of three types of tissue as shown in Figure 1.4: gray matter (GM) and white matter (WM) and Cerebrospinal fluid(CSF).

- Neuronal and glial cells, also called neuroglia or glia, as well as the basal nuclei, make up grey matter (GM). The former is responsible for brain activity, whereas the latter is made up of grey matter nuclei deep inside the white matter.

- White matter fibres are myelinated axons that link the cerebral cortex to other brain regions. They are made up of the caudate nucleus, putamen, pallidum, and claustrum. The corpus callosum, a thick band of white matter fibres that connects the brain's left and right hemispheres [12].

- The cerebrospinal fluid (CSF), which includes glucose, salts, enzymes, and white blood cells, is found in the brain. To protect the brain and spinal cord from damage, this fluid flows via ventricles surrounding them. Meninges are a kind of tissue that covers the brain and spinal cord and acts as a membrane. [12].

8
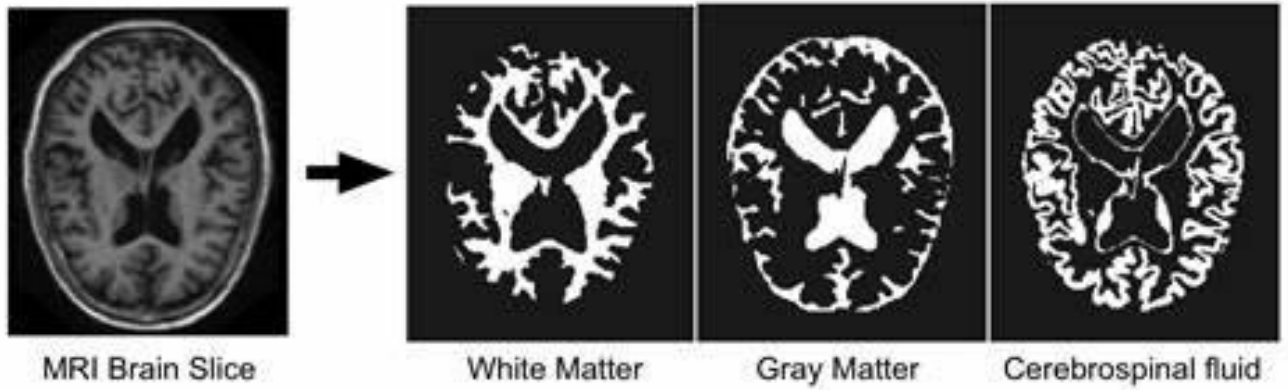
Figure 1.4: Brain Image with three main tissues

(a)   (b)   (c)
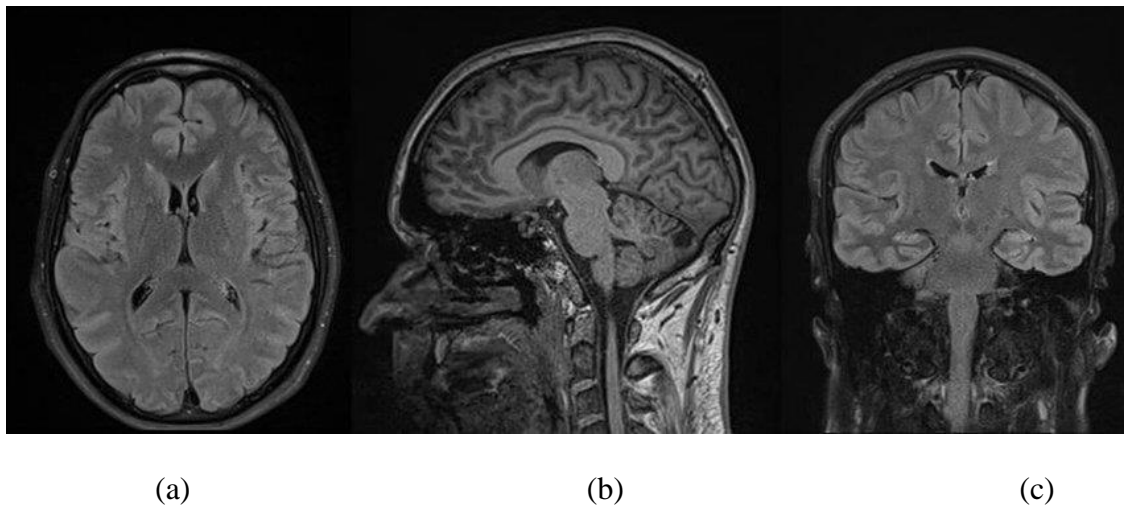
Figure 1.5: Representation of three plane views of MRI brain image:(a) Axial view,

(b) Sagittal view, (c) Coronal view

GM looks darker than WM in T1-weighted MRI, but WM appears darker in T2-weighted MRI. In T1 weighted pictures, CSF looks black, grey in PD images, and brilliant in T2-weighted images. Figure 1.4 depicts the difference between these tissues. The strong contrast between the different brain tissues such as WM, GM, and CSF is provided by the T1-weighted MRI brain picture. PD and T2-weighted images, on the other hand, show little difference between GM and

WM tissues but a lot of contrast between the brain parenchyma and CSF. The brain MRI scans may be seen in three planes: sagittal, axial, and coronal, as shown in Figure 1.5.

1.3.2 Brain Tumor

A brain tumour is an unnaturally growing mass of tissue caused by uncontrolled cell proliferation. The development of a tumour occurs within the skull and disrupts normal brain functioning. Tumors can damage the brain by raising internal pressure, pressing on the skull, and targeting and destroying nerves and other brain cells [13].

The location of the tumour, the kind of tissue, whether it is noncancerous (benign) or cancerous (malignant), and the site of origin (primary or secondary) are all used to classify brain tumours [14]. The World Health Organization (WHO) divides brain tumours into over 120 different kinds. According to the World Health Organization, brain tumours are classified from benign to malignant based on cell origin and behaviour. Tumor types are also given a grade, ranging from Grade I to IV, based on the pace of malignant development; however, grading methods differ depending on the tumour type [13].

1.4 Challenges of MR Brain Image Segmentation

Because of the various practical uses of segmentation results, medical picture segmentation has gotten a lot of attention. The automatic detection and segmentation of brain tumours from brain MR images provides a way to avoid the time and effort required for manual segmentation of huge datasets. It also offers repeatability, which is influenced by observer variability both within and across groups. However, automated systems have substantial challenges in achieving these goals. Because of the nature of brain MRI images, pixel intensities violate the independent and identically distributed assumption within and across pictures, and MRI images contain a considerable number of artefacts and intensity inhomogeneity [15, 16].

As a result, in order to produce consistent segmentation findings and create clinically acceptable automated methods, automated methods need take into account these issues. Our goal is to separate white matter, cerebrospinal fluid, and grey matter tissue types in MRI scans of the brain. Dealing with picture declension aspects such random noise during acquisition, bias field, and partial volume impact can be time-consuming and difficult. A brain tumor is the mass of tissue that grows abnormally due to uncontrollable cell multiplication. The growth of a tumor takes place within the skull and interferes with normal brain functions. Tumor can harm brain by increasing pressure inside it, pushing against the skull, and by attacking and damaging nerves and healthy brain tissues [13].

1.5 Objective of the thesis

The main objective of this thesis is to develop content-based image retrieval and segmentation system for Brain MR images so that the tumor if any, is accurately segmented and the similar cases are retrieved from the database.

This involves three steps: Classification of brain image into normal and abnormal brain, to segment the tumor from the image and also give its location and to retrieve similar cases from the database for help in treatment planning.

The main objectives of the thesis are as follows:

- To study existing methods for brain image classification, tumor detection and brain image segmentation, brain image retrieval and compare their relative segmentation performance on two publicly available real and simulated MRI brain data.
- To propose new algorithms for brain image classification, tumor detection and brain image segmentation, brain image retrieval and compare their relative segmentation performance.

11

1.6 Organization of the thesis

This thesis consists of eight chapters that are organized as follows:

- **Chapter 1: Introduction**

It provides a fundamental idea about the motivation of the work described in this thesis. A brief overview of MRI, Brain Anatomy and brain tumor is given to understand the basics. Problem formulation and thesis objectives are also discussed.

- **Chapter 2: Literature Review**

This chapter presents a brief study of the existing techniques present in literature for MRI Brain Image Classification, Segmentation and Tumor Detection and Brain Image Retrieval.

- **Chapter 3: Classification of Magnetic Resonance Brain Images using Local Binary Pattern as Input to Minimal Complexity Machine**

The objective of this chapter is to introduce a novel scheme for brain Image classification. LBP algorithm is discussed in this chapter for extraction of features. Classification algorithms like KNN, SVM and MCM algorithms are discussed in this chapter. This algorithm is compared with many states of art techniques and shows superior results. Experimental results are given at the end of the chapter.

- **Chapter 4: Brain Tumor Segmentation: A Performance Analysis using K-Means, Fuzzy C-Means and Region Growing Algorithm**

This chapter initially describes the Segmentation algorithms namely, KM, FCM and Region Growing algorithm. Further, brain tumor detection algorithm is proposed and comparative performance analysis of the algorithms is carried out.

- **Chapter 5: Intuitionistic Fuzzy Co-Clustering Algorithm for Brain images**

A novel Intuitionistic Fuzzy Co-Clustering (IFCC) algorithm for MRI brain image segmentation is described in this chapter. The intuitionistic fuzzy set theory is incorporated as it is more suitable for handling uncertainty as compared to fuzzy sets theory. The algorithm is based on the Co-clustering approach as it offers the advantage of assigning membership functions for both object as well as features. The parameters in the IFCC algorithm are optimized using Particle Swarm Optimization (PSO).

- **Chapter 6: Optimal Fuzzy C-Means Algorithm for Brain Image Segmentation**

In this chapter, an automatic framework for segmentation of brain tissue classes namely, white matter, gray matter and cerebrospinal fluid has been proposed. ACO algorithm is explained in this chapter which is further used for optimization of well-known FCM algorithm. Finally, segmentation performance of the algorithm is evaluated and compared quantitatively with existing methods.

- **Chapter 7: Fuzzy Clustering Using Gravitational Search Algorithm for Brain Images**

In this chapter, a clustering approach, Fuzzy-Gravitational Search Algorithm (GSA) and its application to MRI brain image segmentation. The proposed approach is based on GSA, and uses fuzzy inference rules for controlling the parameter α as search progresses. The results of the system are compared with GSA and recent work on brain image segmentation algorithms for both real and simulated database on the basis of Dice Coefficient values and is found to outperform.

- **Chapter 8: Hamming Distance based Local Binary Pattern for Biomedical Image Retrieval**

The application of image retrieval in the medical field can be very useful for the diagnosis of disease and further treatment planning. In this chapter, we will have an overview

of existing image retrieval algorithms. Also, a new image retrieval algorithm is proposed and discussed which shows significant improvement over existing local binary pattern based image retrieval algorithms.

- **Chapter 9: Conclusion and Future Scope**

The work is summarized in this chapter. The thesis concludes with the contributions of thework done in this thesis along with the discussion of their future scopes.

Chapter 2

Literature Review

This chapter presents a brief study of the existing techniques present in literature used for brain MRI images. The initial section discusses about brain image classification. In section 2.2, we have discussed the works related to brain image segmentation. In section 2.3, studies related to brain tumor detection have been mentioned. Section 2.4 discusses about the work done in the field of image retrieval for brain images. In the last section we can see the limitations of the work that we have gone through that motivated us to work in the right direction and achieve the desired results.

2.1 Brain Image Classification

Magnetic resonance imaging may be used to automatically classify tumorous and non-tumorous human brain pictures, which is critical for research and clinical investigations. Recent research has demonstrated that supervised approaches like support vector machine [17] and unsupervised classification techniques like self-organization map (SOM) [18] and fuzzy c-means (FCM) [19] can be used to classify magnetic resonance brain images. Sayed et al. [20] provide a comprehensive study on computer-aided diagnosis of human brain tumours using MRI, as well as a new method that consists of three stages: segmentation, feature extraction and reduction, and classification of MR images into normal or abnormal. This method can be improved by extracting more efficient features and increasing the training data set. Also we can see in the paper there is still much room for additional researcher to utilize other machine learning techniques and integrate them into a hybrid one system. Zhang et al. [21] presented a hybrid approach for MRI brain image classification in 2011, which uses a neural network (NN)

based algorithm to categorise a given MR brain picture as normal or abnormal. Hybrid intelligent techniques for MRI brain images classification. Sayed *et al.* [22] presents a hybrid technique for the classification of MRI images. Two classifiers have been proposed by the author in the classification stage. The first classifier uses a feed forward back propagation artificial neural network (FP-ANN), while the second uses a k-nearest neighbour algorithm (KNN). Classification of magnetic resonance brain images using wavelets as input to SVM and NN is proposed by Chaplot el al [18] in which a novel method using wavelets as input to NN is used and SOM and SVM is implemented for classification of magnetic resonance (MR) images of the human brain. The feature extraction and reduction needs to be carried out for classification of MR images. The features of the brain image can be extracted using a discrete wavelet transform (DWT) as done by N. Hema Rajini *et al.* in [23]. Nandpuru *et al.* [24] have extracted features using gray level co-occurrence matrix (GLCM) and further classified them using SVM. Feature reduction can be carried out using principal component analysis (PCA) as illustrated by Ibrahim *et al.* in [25]. In [26] Sridhar *et al.* proposed an algorithm for extraction of features using Discrete Cosine Transform (DCT) and classifying the images with the help of Probabilistic Neural Network (PNN). In neural network, we cannot determine how or why a decision is made and brain tumor classification is very critical problem for which we need to have proper justification. Hence, neural network usage is not a good advice for classification of brain tumors. A hybrid method is given by Yazdani *et al.*[27] by integrating the modified Expectation Maximization(EM) and GLCM features and feeding them for classification into SVM algorithm. Also a hybrid classifier [28] was given by Macchale *et al.* by integrating the features of KNN and SVM classifier. Gupta *et al.* proposed an algorithm for multi sequential image classification of brain images by using Effective Information Feature Extraction (EIFE) and SVM [29]. Tazin et al. proposed a novel classification algorithm based on deep neural networks [30] for classification of brain tumor images. The major disadvantage of using deep

neural network is that enormous data is required for training so that the algorithm can perform efficiently as compared to other classification algorithms. Also we can see from the literature review that most of the techniques uses KNN and SVM as a classifier. KNN is computationally inefficient and it is difficult to pick the correct value of K for good classification. The problem with SVM is that they have large and infinite Vapnik Chervonenkis(VC) dimension and it does not provide good generalisation. Hence there is a need to choose some other classification algorithm that requires less number of support vectors and provides good generalization and robust learning. Also, many techniques for extraction of features from brain images have already been proposed but keeping in mind their limitation there is a scope to investigate some novel feature extraction technique as proposed in chapter 3.

2.2 Brain Tumor Detection

In recent years, many approaches for automating the identification and segmentation of brain tumours have been developed. Morphological operations, edge detection, fuzzy sets theory, classification, region growth, neural networks and clustering, and other image segmentation methods are used in these approaches. Vidhya S. Dessai et al. [31] developed a multithreaded framework for segmenting multiple MRI images utilising k-means clustering and morphological procedures in parallel. Kiran Thapaliya et al. [32] presented a method that uses morphological gradients and morphological operations to identify brain tumours. Ishita Maiti et al. [33] proposed a color-based brain tumour segmentation approach based on a watershed method and an edge detection algorithm. Dr. M. Karnan et al. [34] used ant colony optimization in conjunction with the fuzzy c-means technique to segment brain MRI images. H. B. Kekre et al. [35] used a vector quantization segmentation approach in combination with morphological procedures to identify malignant masses in MRI images. Sudipta Roy et al. [36] used symmetric analysis and watershed segmentation to provide a completely automated system for brain tumour identification. For brain tumour segmentation, Rajendran et al. [37] developed a region-

based fuzzy c- means clustering method. The approach starts the area based algorithm using the tumour class output from fuzzy clustering, and the region based algorithm proceeds towards the ultimate tumour border. M.A. Jaffar et al. [38] suggested an automated brain MR image segmentation approach that uses the curvelet transform to remove noise and FCM to segment brain MR images automatically. For tumour extraction from brain MRI images, R. B. Dubey et al. [39] compared the level set technique, modified watershed approach, and modified region growth method. The above techniques proposed for brain tumor detection are all based on manually defining the tumor area and then classifying. The detection becomes easier but it prevents the system from being fully automated.

In the recent years, various methods have been developed by the researchers for automatic tumor detection but they suffer from some limitations. These techniques are based on morphological operations, edge detection, fuzzy sets theory, classification, region growing, and clustering and other image segmentation methods. Ming–Ni Wu et al. [40] presented a color-based segmentation method that uses k-means clustering and histogram clustering to separate tumours from other objects in input MRI images. N. Nandha Gopal et al. [41] have proposed an intelligent system that uses Fuzzy C methods and optimization approaches to identify brain tumours. In 2014, Melegy *et al*. proposed a new approach by reformulating the popular FCM algorithm to take into account any available information about the class center [42]. Also, local independent projection-based classification (LIPC) method was introduced by Huang *et al*. [43] to solve the tumor detection problem. The proposed LIPC used local independent projection into the classical classification model, and a novel classification framework was derived. In 2015, Nabizadeh *et al*. [44] proposed brain tumor detection and segmentation technique for MR images using Gabor wavelet and statistical (GWS) features. Also, Maksoud *et al*. [45] developed an efficient image segmentation algorithm using KM clustering technique integrated with FCM (KIFCM) algorithm. Sompong *et al*. [46] proposed brain tumor segmentation method

18

based on gray-level co-occurrence matrix based cellular automata (GLCM-CA) and improved tumor-cut algorithm. A meta-heuristic optimization approach is proposed by Rajinikanth *et al*. [47] to assist the brain MRI examination. This approach enhances and extracts the tumor core and edema sector from the brain MRI integrating the Teaching Learning Based Optimization (TLBO), entropy value, and level set/active contour based segmentation. In 2018, Deepa *et al*. [48] proposed adaptive firefly backpropagation neural network(AFBPNN) for detection of brain tumor based on fusion of features using Gaussian radial basis function(GRBF). Javeria *et al*. [49] also gave a feature fusion based method for finding brain tumor in the year 2018. Various methods have already been proposed for brain tumor segmentation [50-52], but still there is scope to develop significant tumor detection techniques.

Thresholding based tumor detection and segmentation methods [53] which integrated with watershed and histogram analysis have been proposed. Kadam D. B. *et al*. [54] have used eight textural features to train the MLP network in segmenting brain tumor. Perceptron networks can only classify linearly separable datasets hence it does not perform efficiently in detecting tumors as it is a non-linear problem. Automated brain tumor segmentation with two phases is proposed by Khontalou *et al*. in [55]. In first phase tumor is detected and segmented by combination of histogram analysis with symmetry analysis using morphological operations. Then tumor is detected by applying fuzzy classification method or symmetry analysis and some morphological operations. A supervised hybrid fuzzy ANN based method for tumor detection is proposed in [56] by Pradhan *et al*. The major problem with this approach is its black box nature. It does not give an idea to the user that how a certain result is achieved. A comparative study of adaptive network based fuzzy inference system (ANFIS), k-nearest neighbors (KNN) and fuzzy c-means (FCM) for brain tumor segmentation is conducted in [57] by Khalid *et al*. But in presence of noise FCM doesn't copes up with the expected results. Since it takes into account random values in its initialization step and also no spatial information is considered in

complete algorithm. Salama et al. [58] proposd a new system for detection of brain tumor. The proposed system is a two stage process where convolutional neural network is used so that dataset is balanced in the first stage and detection of tumor is done in the second stage. We can see from the literature that large amount of dataset is required to achieve the desired results using neural network method. Also, working on large datasets increases the time used to calculate the tumor.

Various methods have already been proposed for brain tumor segmentation [59-61], but still there is a scope to develop significant segmentation technique. There are two major challenges in segmentation of brain images as seen in the literature. First is to handle the uncertainty that arises on boundary between different tissues and second is to obtain distinct or non-overlapping clusters. Hence, we need to devise an algorithm that caters to both the problems identified from the literature.

2.3 Brain Image Segmentation

Different image segmentation techniques, both supervised and unsupervised have been proposed and been applied to numerous applications in real world [62]. Unsupervised segmentation techniques requires less human intervention in obtaining clinically useful results. We are basically concerned with unsupervised techniques based on soft clustering in which an object can belong to more than one cluster/class with varying degree of membership. The most commonly studied soft clustering algorithm is FCM which was introduced by Bezdek in 1981 [63]. This approach is simple to implement and performs clustering in an efficient way. As already discussed in section 2.2, FCM doesn't work efficiently in the presence of noise as it does not take spatial information into consideration. Several works have been done to include spatial data/information [64-65]. Mahmood *et al.* proposed a framework [66] by integrating Bayesian-based adaptive mean shift, a priori spatial tissue probability maps and FCM. Ahmed

et al. [67] introduced FCM-S in which the objective function was changed to include information of gray levels but this approach was computationally expensive. Kalaiselvi *et al*. also modified the FCM algorithm by incorporating spatial parameter for minimizing the objective function of conventional FCM and new weighting parameter for centroid initialization[68]. Chen and Zhang [65] proposed another variant of FCM in which the neighbouring term for each data point is computed well in advance to avoid computational delays. Also, the Euclidean measure is used in FCM to calculate the distance between data points and cluster centres. Euclidean distance always takes into account the data points in spherical shape from the point being examined. It does not consider the correlation among the data points. The possibility of data point belonging to same cluster is not only dependent upon the distance but also on the direction. Mahalanobis distance introduced by P.C. Mahalanobis in 1936 considered both these issues. Kim and Krishnapuram [69] tried to show that mahalanobis distance cannot be directly applied to any of the clustering process. Gustafson and Kessel (GK) [70] used Mahalanobis distance with fuzzy terminology i.e. introduction of fuzzy co-variance matrix was done in this work. Also meta-heuristic approaches are introduced to deal with NP-hard problems and the problems for which the data is uncertain and not readily available. These optimization techniques include Particle swarm optimization, Genetic Algorithms(GA), ACO. [71] Thomas A. Runkler showed the extension of simplified ant colony system to be compatible with FCM. Yucheng Kao and Kevin Cheng [72] introduced ACOA in which array based graph is constructed and ants are moved randomly to from the solution set.

A proportionally significant amount of research effort has been devoted to certain body parts or modalities, such as the segmentation of brain pictures in MR imaging. MRI brain picture segmentation has been suggested using a variety of approaches, and it is a hot topic of research. Ortiz suggested a hybrid technique based on a probabilistic clustering algorithm and a developing hierarchical self-organizing map classifier[73]. Chen[74] updated the fuzzy c-

means(FCM) algorithm's objective function to use basis functions to correct for intensity inhomogeneities and enhanced non-local information to compensate for noise. Benaichouche et al. utilised a metaheuristic optimization approach for initialisation[75] and integrated Mahalanobis distance in the objective function to decrease the influence of geometrical forms of various clusters to address the problem of FCM algorithm trapping in local minima. These techniques, however, are susceptible to noise, which is a typical issue with intensity-based systems. Furthermore, most intensity-based techniques tend to over-segment the picture, resulting in sub-optimal outcomes. For brain picture segmentation, Verma developed an enhanced intuitionistic FCM algorithm [76], which utilises local spatial information in an intuitionistic fuzzy approach. The method deals with uncertainty using an intuitionistic approach, and the noise impact is mitigated by adding local data. Moeskops et al. presented a Convolutional Neural Network-based approach for automatically segmenting brain pictures into tissues[77]. Using non-local information and incorporating the covariance and prior probability in the distance function, Chen et al. presented an enhanced FCM clustering technique (FCM)[78]. Namburu et al. offer the Generalized Rough Intutionistic FCM method to eliminate the need for membership function and parameter adjustment. Lesion Detection in Medical Imaging Based on Unified Gravitational Fuzzy Clustering[79], fuzzy clustering incorporates the Newtonian idea of gravity. Using fuzzy unsupervised learning, an improved MRI Brain Image Segmentation method is proposed [80] by Keyvan *et al.*. Although this initial seed selection technique reduces operator engagement and reduces the method's susceptibility to initialization, it is possible that this procedure may not encompass all regions inside the volume of interest along the depth direction, resulting in tumour under segmentation. It also does not allow the system to be fully automatic.

2.4 Feature Extraction for Brain Image Retrieval

Patient diagnostic databases are available in a variety of formats, including computer tomography, magnetic resonance imaging, ultrasound, and X-ray. However, it is impossible to make use of this information unless it is structured in a way that allows for easy access, search, and retrieval. Content-based biomedical image retrieval was created to solve this issue. Automatic retrieval of images is of great importance in medical field as it helps in decision making for solving various problems. The feature extraction in content based image retrieval is a crucial stage whose success is determined on the approach used to extract characteristics from pictures. There are two types of visual content descriptors: global and local. To describe an image, a global descriptor describes the visual features of the entire image, whereas a local descriptor represents the visual features of areas or objects. These are arranged as multi-dimensional feature vectors and construct the feature database. In this thesis, we have proposed a novel feature descriptor based on local binary pattern for retrieval of biomedical images.

The visual contents of a picture, such as colour, texture, form, faces, and spatial arrangement, are used to represent and index the image database in content-based image retrieval. [82] The research paper contributed by Geetha et al. [83] investigates about various CBIR techniques for for efficient retrieval of brain images. The approach for local binary patterns has been thoroughly explored and updated in several respects. Some of the key changes are made to improve discriminative capability and neighborhood selection while keeping the computational cost low. The LBP operator was first introduced by Ojala et al. [84] as a texture descriptor for image retrieval. The basic LBP technique generates a binary code for each pixel of the picture by thresholding the pixel's 3 x 3 neighborhood with the value of the center pixel. To identify the pixel, the binary codes are translated into decimal numbers, which are referred to as LBPs or LBP codes. [85] Jin et al. [86] presented an Improved LBP (ILBP) for image retrieval, which compares the adjacent pixels, including the centre pixel, with the window's mean value. But

their method has increased the feature vector length by 511 ($2^9 - 1$, as all zeros and ones are the same). Recently, dynamic feature extraction methods have been evolved over the years [87]. There are two spatiotemporal local pattern approaches: Volume Local Binary Pattern (VLBP) and LBP from Three Orthogonal Planes (LBP $-$ TOP) by Zhao *et al.*[88]. They have reported that the LBP-TOP generates significantly less feature vectors as compared to VLBP with comparable accuracy of recognition. The dynamic texture (DT) analysis is performed over the sequence of image frames. Dubey *et al.*[89] proposed this new and efficient feature descriptor for CT image retrieval. They have considered only the diagonal and the center pixels in a 3 x 3 neighborhood to obtain a binary representation of the center pixel. The method has reduced the feature vector dimensionality to 24 as against 59 in case of Uniform Local Binary Pattern. It has been reported by Gupta *et al.*[90] that most of the local information is contained in diagonal elements. This gives the justification behind use of diagonal elements only. Local binary pattern methodology has been extensively researched and modified over different aspects for image retrieval. Some of the major modifications are carried out to increase the discriminative capacity and neighborhood selection to obtain better performance while not increasing much of the computational cost. In [91] Zhou *et al.* proposes a similarity retrieval approach for brain MRI images based on sparse representation and metric learning. For different images and images with different principles, the feature algorithms involved are different. This creates a problem in the real world as medical data is very huge and variant.

2.5 Analysis of the Limitations of State-of-the-art Techniques

In the previous sections, we went through various State-of -the-art techniques in the field of Medical Image Processing. While studying about them we identified some limitations as follows:

- We can see from the literature review that most of the techniques uses KNN and SVM as a classifier. KNN is computationally inefficient and it is difficult to pick the correct value of K for good classification. The problem with SVM is that they have large and infinite Vapnik Chervonenkis(VC) dimension and it does not provide good generalisation.

- In neural network, we cannot determine how or why a decision is made and brain tumor classification is very critical problem for which we need to have proper justification. Hence, neural network usage is not a good advice for classification of brain images.

- The major disadvantage of using deep neural network is that enormous data is required for training so that the algorithm can perform efficiently as compared to other classification algorithms. Also, working on large datasets increases the time used to calculate the tumor. Hence, we do not apply deep neural networks.

- While performing brain image segmentation in the presence of noise FCM doesn't copes up with the expected results. Since it takes into account random values in its initialization step and also no spatial information is considered in complete algorithm.

- Local binary pattern methodology has been extensively researched and modified over different aspects. Some of the major modifications are carried out which works on transitions inside a window. It does not takes into account the transition between the consecutive windows.

The problems identified from the literature motivated us to carry out the work discussed in the following chapters.

Chapter 3

Classification of Magnetic Resonance Brain Images using Local Binary Pattern as Input to Minimal Complexity Machine

3.1 Introduction

The goal of image classification is to group pixels having similar features into one class depending on the features obtained. The process of feature extraction is carried out using LBP that has been explained in this chapter. The proposed system for classifying MRI brain images into two different classes is shown in Figure. 3.1. The techniques used for classification can be either supervised or unsupervised. As we can see from the Figure, the classification system is constituted of two stages, namely training stage and testing stage. In this chapter, we have applied MCM algorithm for which classification offers various advantages over the well-known SVM and KNN algorithm.

3.2 Feature Extraction

We use LBP for extracting features from MRI brain sample images. Originally, LBP was proposed by Ojala *et al*. [84] for deriving the textural features from the image. In his basic LBP method, every pixel of the image is converted into a binary number on the basis of Thresholding the 3×3 window which comprises of the neighbors of the pixel. The Thresholding is done by comparing the value of the center pixel with the neighboring pixels. This Thresholding results in a binary number and these binary values are concatenated by moving in a clockwise direction

26

starting from top-left neighbor as shown in Figure 3.2. The binary codes are converted into decimal number to label the pixel and are termed as LBPs or LBP codes.
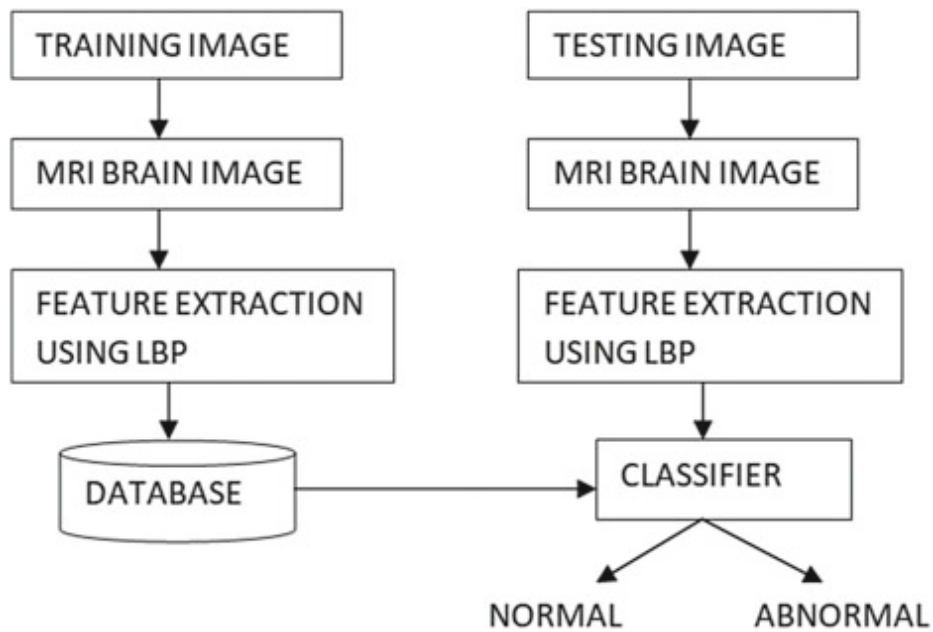
Figure 3.1: Brain Image Classification System

The steps for constructing LBP codes are stated in algorithm 1.
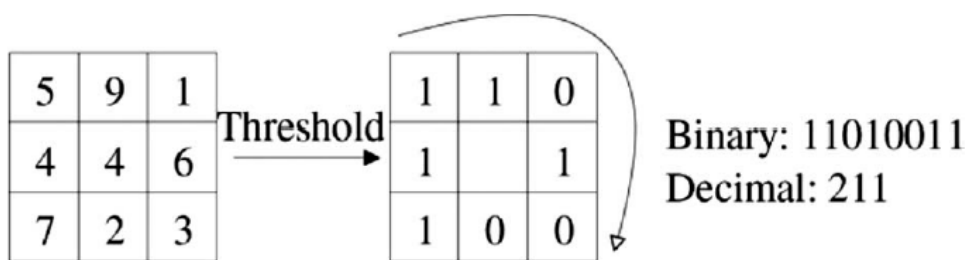
Figure 3.2: The basic LBP operator[92]

Algorithm1: Steps for Constructing LBP Code

    Step 1. Take a 3X3 window in the image.

Step 2. In the window, take central pixel and threshold its eight neighbours by comparing.

Step 3. If the intensity of the central pixel is more than or equal to that of its neighbour, write 1; otherwise, write 0.

Step 4. The result will be a 8 bit binary number for each pixel, just like 11001111.

The local primitives like edges, spots, flat areas etc can be coded by the LPB method as shown in Figure 3.3.

Spot   Spot/flat   Line end   Edge   Corner
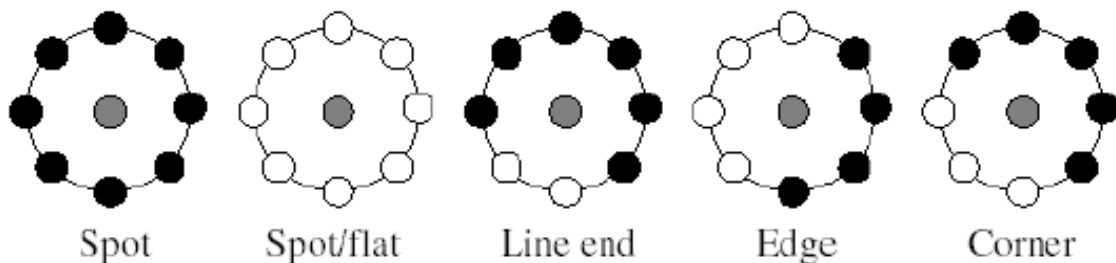
Figure 3.3. Texture primitives which can be detected by LBP[93]

To handle textural features in the image, varying size neighborhood have been proposed by Ojala *et al.*[91]. The local neighborhood has been defined circularly in place of square and bilinear interpolation was employed to obtain value of sampling points not lying on a pixel. This generalization allowed flexibility in number of sampling points and radius of circle as shown in Figure 3.4 below. The *(P, R)* notation denotes *P* equally spaced sampling points lying over the circle of radius *R*.

LBP Pattern thus formed can be either uniform or non- uniform. The binary number is said to be uniform, if the pattern consists of two or less than two transitions between consecutive bits from 0 to 1 or 1 to 0 considered circularly. As an example, we can see that the binary string

00000000, 001110000, and 11100001 are uniform patterns having zero, two, and two transitions, respectively, while 11001001 and 01010011 are non-uniform with four and five transitions, respectively. These uniform patterns carry around 90% of information in (8,1) neighborhood [94]. Ahonen *et al*. [95] reported that 90.6% of patterns in (8, 1) neighborhood are uniform while experimenting on FERET database. The concept of uniform patterns paved the way to a much-reduced feature vector by storing the uniform and non-uniform pattern in two different bins. Following this criterion, the histogram reduced to 59 bins in case of uniform LBP against 256 bins in standard LBP.
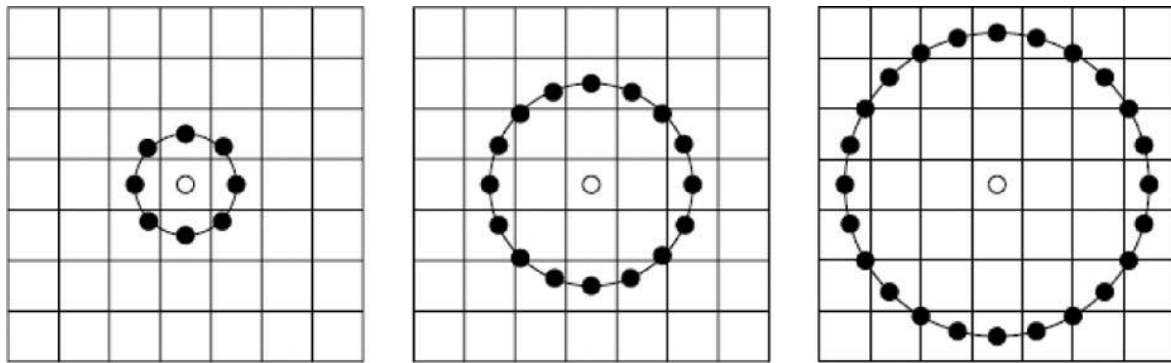
Figure 3.4. Examples of Extended LBP operator [92] : (8,1) , (16,2) and (24,3) circular neighborhood

The histogram of the LBP labeled image can be illustrated as in Equation 3.1 [96].

$$H_i = \sum_{x,y} I(f(x,y) = i), \quad i = 0,1,.....n-1 \qquad 3.1$$

This histogram forms the feature vector having local micro-pattern information like edges, spots, and flat areas over the entire image [97]. Thus, a statistical representation of the image is obtained. The final, spatially enhanced, and global feature vector is derived by joining all the region specific histograms and is shown in Equation 3.2 and Figure 3.5 illustrated the block-based LBP feature histogram. Each region is indicated by R_j where j is the number of regions.

$$H_{i,j} = \sum_{x,y} I(f(x,y) = i) \, I\left((x,y) \in R_j\right) i \ = \ 0,1,\ldots\ldots.n-1 \qquad 3.2$$

$$and \ j \ = \ 0,1,\ldots\ldots.m-1$$
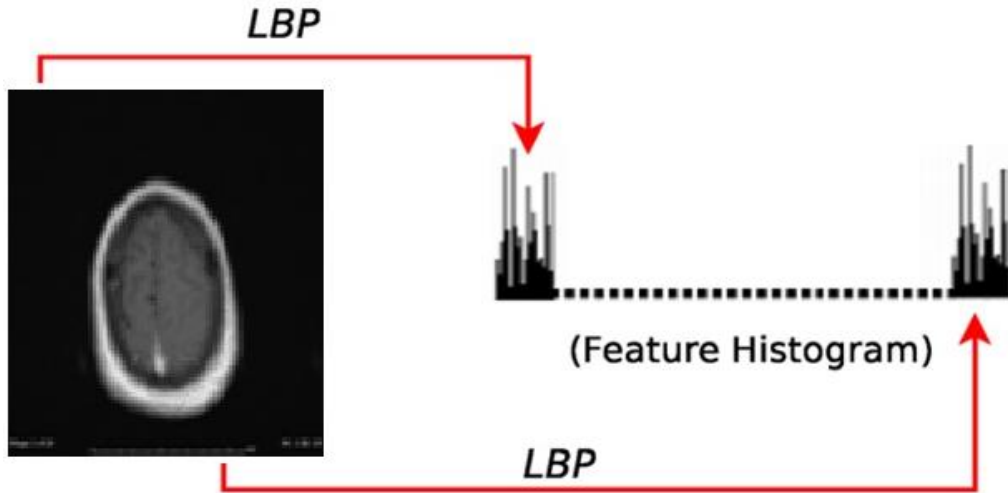
Figure: 3.5 Illustration of Block-based LBP feature extraction [97] .

3.3 Classification Algorithms

3.3.1 Image Classification

Image classification refers to grouping of pixels having similar features into one class depending on the features obtained. The techniques used for image classification step can be either supervised or unsupervised. In this section, we discuss some supervised image classification algorithms namely, KNN and SVM along with their advantages and disadvantages. The model for supervised classification algorithm is depicted in Figure 3.6. We can see from the Figure that in the first stage features are obtained from the training data set along with the known labels for the training data. A machine learning algorithm is applied and then the outcome of testing images is obtained. A novel MCM algorithm for classification of

MRI brain images which also belongs to the category of supervised classification have been discussed briefly in this chapter.
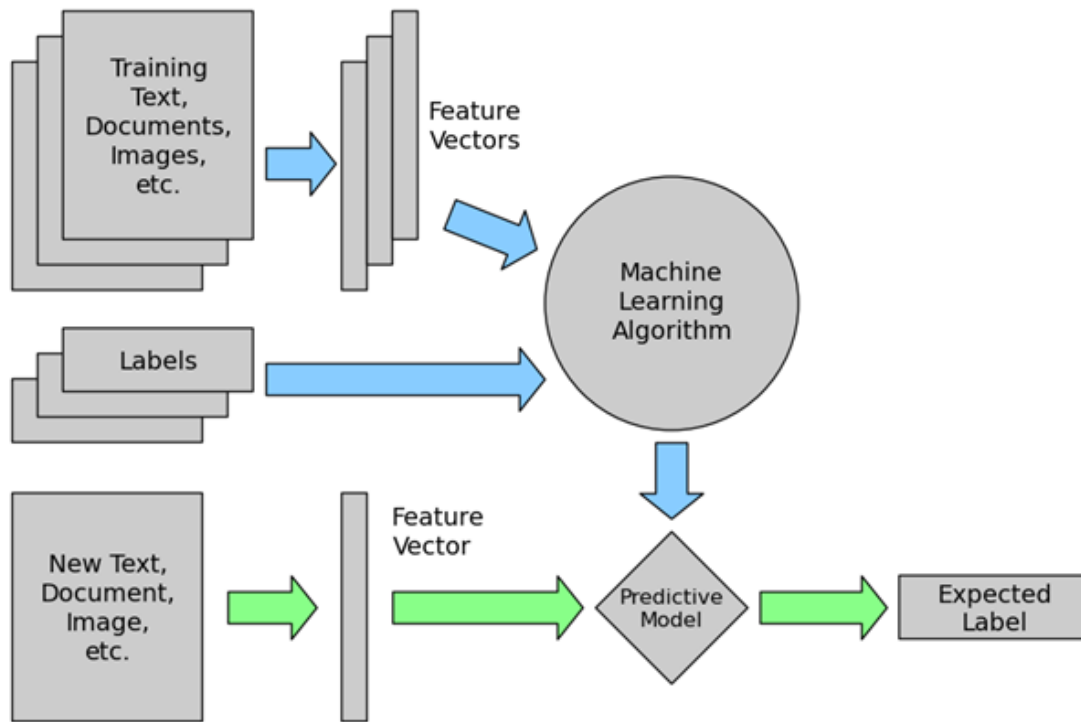
Figure 3.6: Supervised Learning Model

3.3.2 k-Nearest Neighbor

It is the simplest classification algorithm which is used to classify the data in the sample to one of the classes in the training by implementing the nearest neighbor technique. A distance measure is used as a metric to classify the input feature vector V into classes on the basis of training vectors which are closest to the data. The vector I is a member of the class that includes the majority of those k nearest neighbours. The KNN method is based on two functions, namely the distance function and the voting function, which are derived using the k nearest neighbours [97]. The metric for distance function can be Euclidean, cosine similarity, correlation or hamming distance, mahalanobis distance. The KNN classification algorithm[97] is a traditional technique which belongs to a class of supervised algorithms and is not based on any parameters except the value of K. The algorithm works efficiently for optimal values of K.

Similar to other learning algorithms, KNN also comprises of two stages namely, training stage and testing stage. Firstly, in the training stage, data points are allocated in a n-dimensional space. Each training data point is assigned with a label to indicate the class it fits in. Then, in the testing stage, the unlabeled data points are tested for the identification of class. The class is identified by producing a list of K nearest data points to the input data point by making use of the already classified data. The algorithm then returns the class to which the majority of the labeled data belongs. The value of *K* given as input to the algorithm plays an important role in accurately classifying the data.

Step 1: Load the test and training data sets.

Step 2: Select the K value, i.e. the closest data points. Any numeric value can be used as K.

Step 3: Perform the following for each data point in the test data:

• **3.1** Using any of the following methods, calculate the distance between test data and each row of training data: Euclidean, Manhattan, or Hamming distance. Euclidean Distance is the most often used method for calculating distance.

• **3.2** Sort them in ascending order depending on the distance value.

• **3.3** The top K values from the sorted array will then be chosen.

• **3.4** Now, the test point will be assigned a class based on the most common class of these values.

Step 4: Finish

3.3.3 Support Vector Machine

SVM is a binary classification algorithm that takes labeled data as input along with the group or class it belong to and outputs the classes for the unlabeled data on the basis of training. The SVM algorithm given by Vapnik[98] was developed from the idea of minimizing the structural risk. SVM are generally used to classify the data into two classes and are found to be more attractive and systematic as compared to KNN in learning to build a linear or non-linear

boundary between classes. The SVM algorithm also involves two phases, training and testing like any other machine learning algorithm. In the training phase, the known data is fed as input to the SVM along with the correct labels that are known prior. The training phase makes the SVM intelligent to accurately classify the unknown data. SVM classifier makes a hyper plane between the two classes which can be either linear or non-linear[18]. Let there be a data set x $\epsilon\ R^n$ which needs to classified and it belongs to class label denoted by $y = \pm 1$.

In Linear SVM classifier, the input data or images can be separated linearly. It is the simplest case of data classification and linear function used to perform it is given by the equation of the form,

$$f(x) = W^T x + b$$

3.3

such that for each training data or image x_i, the function yields

$f(x_i) \geq 0$ for $y_i = +1$

and

$f(x_i) < 0$ for $y_i = -1$.

Hence, training data from the two different classes are separated by the hyperplane given by the equation,

$$f(x) = W^T x + b = 0$$

3.4

For a given set of data set, many hyperplanes exist to distinguish between the two classes. The SVM classification algorithm chooses the hyperplane in which the distance of the separating margin between the two groups or classes is maximum.

The non-linear classifier is an extension of linear classifier where the input data or image x, is mapped into a higher dimensional space using a non linear operator $\varphi(.)$. The nonlinear classifier obtained is given by the equation,

$$f(x) = W^T \varphi(x) + b,$$

<div align="right">3.5</div>

which is linear in terms of the transformed data $\varphi(x)$ but nonlinear in terms of the original data $x_i \in R^n$.

An optimal hyperplane can be seen in Figure 3.7 where, ρ_0 is the minimal margin. The data points in blue on both side of the optimal hyperplane are the support vectors.
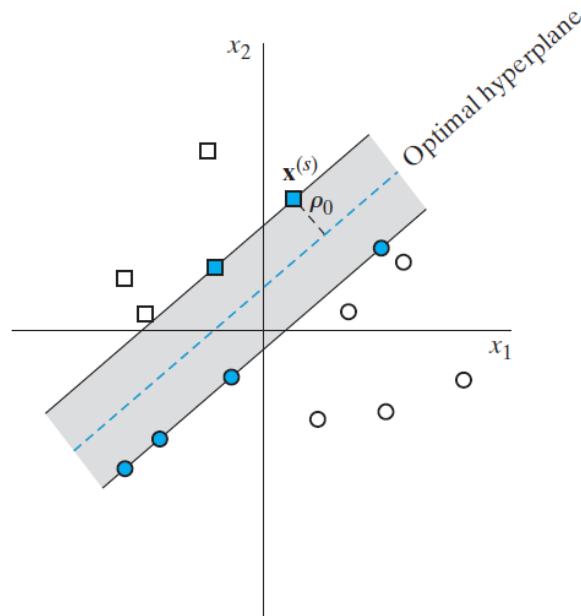
Figure 3.7: An illustration of classification by SVM.

The SVM algorithm's kernel function is responsible for unavoidably converting the input vector into a high-dimensional feature space. Because all real-world issues cannot be divided into two groups in a linear manner, a linear SVM classifier cannot be utilised in all instances. As a result, the introduction of a kernel function that allows data points to enter a class belonging

to a separate class label is required. However, before selecting a kernel function, make sure it's not linked with the inner product of a non-linear mapping. Various kernel functions that are used in the SVM algorithm are polynomial, Radial Basis Function(RBF) and Multi Layer Perceptron(MLP) kernel. During implementation we need to initialize the parameters of each kernel. The order of the polynomial of kernel function should be given initially during the training phase. The value of sigma needs to be specified for the RBF. The MLP kernel requires two parameters, P1 and P2, where P1 > 0 and P2 < 0.

3.3.4 Minimal Complexity Machine

The learning capacity of the machine is calculated with the help of Vapnik Chervonenkis (VC) dimension and computational theory shows that good generalization and robust learning can be achieved using a small VC dimension. Since SVM can have large and infinite VC dimension they do not provide the guarantee of good generalization. The solution to this is proposed by Jayadeva in [99] by finding a hyperplane classifier with small or minimum VC dimension. This algorithm is termed to be the Minimal Complexity Machine(MCM) algorithm[99]. It is shown to be performing better generalization as compared to SVM and uses less than one-tenth the number of support vectors. In this thesis, we have used the MCM algorithm to classify brain MRI images. MCM, like any other machine learning method, has two fundamental phases, termed as the training and testing processes. The known data, as well as the prior knowledge outputs, are fed into the MCM classifier during the training phase. The classifier gains its intelligence from the training step.

The soft margin equivalent of the linear MCM is given by

$$\min_{w,b,h} \; h + C \cdot \sum_{i=1}^{M} q_i$$

3.6

where,
$$h = \frac{\max_{i=1,2,...,M} \left\| u^T x^i + v \right\|}{\min_{i=1,2,...,M} \left\| u^T x^i + v \right\|}$$

3.7

35

$$h \geq y_i. [w^T x^i + b] + q_i, \quad i = 1, 2, ..., M \tag{3.8}$$

$$y_i. [w^T x^i + b] + q_i \geq 1, \quad i = 1, 2, ..., M \tag{3.9}$$

$$q_i \geq 0, \quad i = 1, 2, ..., M. \tag{3.10}$$

Once w and b have been determined by solving equations 3.6 to 3.10, The sign of the discriminant function can be used to determine the class of a test sample x.

$$f(x) = W^T x + b = 0 \tag{3.11}$$

The value of C here provides for a trade-off between the classifier's machine capacity and the classification error. After determining w and b, the class of a test sample x may be calculated using the sign of f(x) in equation 3.11 as previously.

It is possible to prove that the relevant optimization issue for the kernel MCM is

$$\min_{w,b,h,q} h + C . \sum_{i=1}^{M} q_i \tag{3.12}$$

$$h \geq y_i. [w^T \phi(x^i) + b] + q_i, \quad i = 1, 2, ..., M \tag{3.13}$$

$$y_i. [w^T \phi(x^i) + b] + q_i \geq 1, \quad i = 1, 2, ..., M \tag{3.14}$$

$$q_i \geq 0, \quad i = 1, 2, ..., M. \tag{3.15}$$

The steps to implement Minimal Complexity Machine Algorithm are:

Step1: The training dataset is marked with label +1 and -1.

Step 2: In order to spherize the data we need to subtract mean and divide by variance.

Step 3: Now input the values of parameters such as C.

Step 4: Set up constraints of linear programming from equation 3.8-3.9 or equation 3.13-3.14, depending on whether the linear programming is used or kernel MCM is being used.

Step 5: Set up lower and upper bounds on variables $h, b, q_i,$, where $i = 1,2,...M$ and w_i, where $i = 1,2,...n$ or λ_i, $i = 1,2,...M$, depending on whether the linear programming is used or kernel MCM is being used.

Step 6: Set up the coefficients of objective function (for h and $q_i,$ $i = 1,2,...M$)

Step 7: Call the *linprog* function in MATLAB to solve the MCM linear programming problem.

A flowchart depicting the algorithm is shown in figure 3.8.
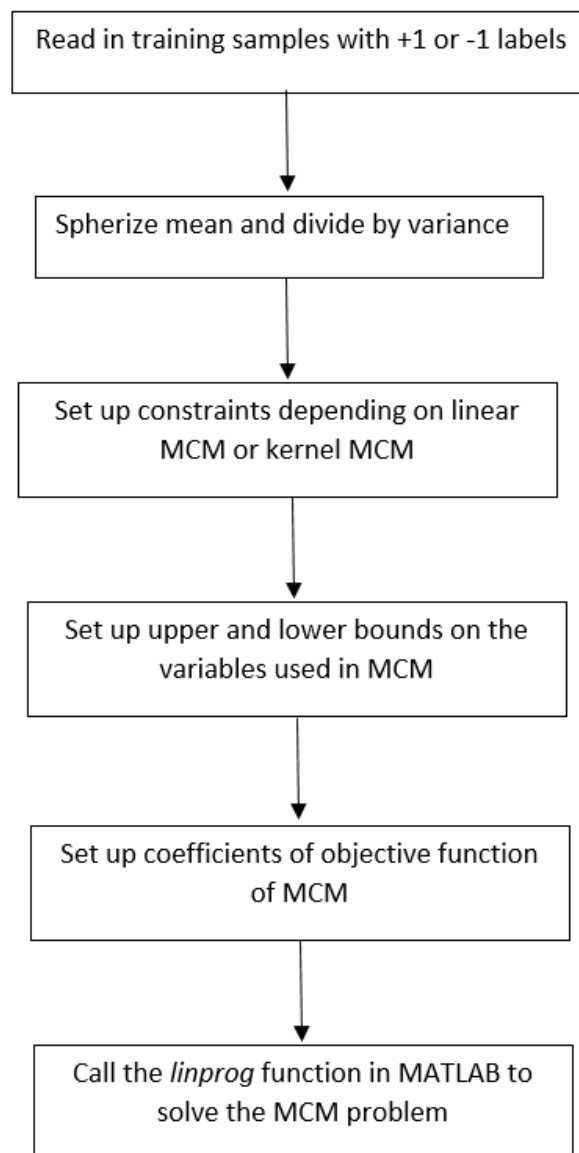
Figure 3.8: Flowchart of Minimal Complexity Machine Algorithm

3.4 Experimental Results

The algorithm is implemented on personal computer (Intel Core i7 @ 2.0 GHz CPU, 8GB RAM) using MATLAB 7.9.0 (2009b). T2-weighted brain MR images in the axial plane with 256×256 in plane resolution make up the datasets. The pictures were obtained from the Harvard Medical School website[100], a few examples of sample images are shown in Figure 3.9. The dataset consists of 80 T2-weighted axial MRI brain images of which 24 are of normal and 56 are of abnormal brain.

(a)   (b)

(c)   (d)
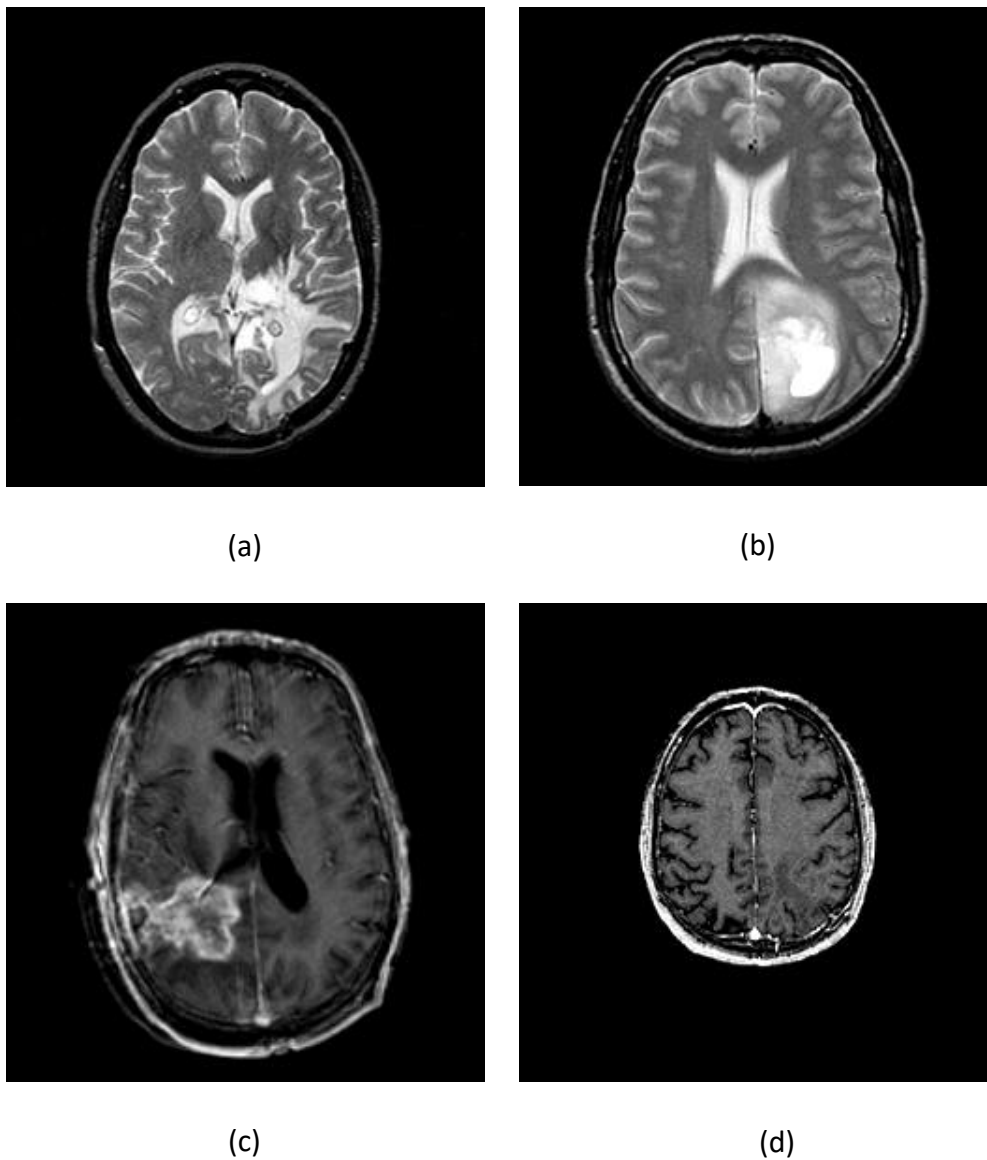
Figure 3.9: Sample of brain MRI Images: (a-c) abnormal brain; (d) normal brain [100]

The experiments are also conducted on real time database taken from Rajiv Gandhi Cancer Institute and Research Centre(RGCI&RC), Delhi as shown in Figure 3.10. To check the accuracy of the algorithms, the system is first fed with the same training and testing set, and the match rate of 100 percent is achieved.

(a)   (b)

(c)   (d)
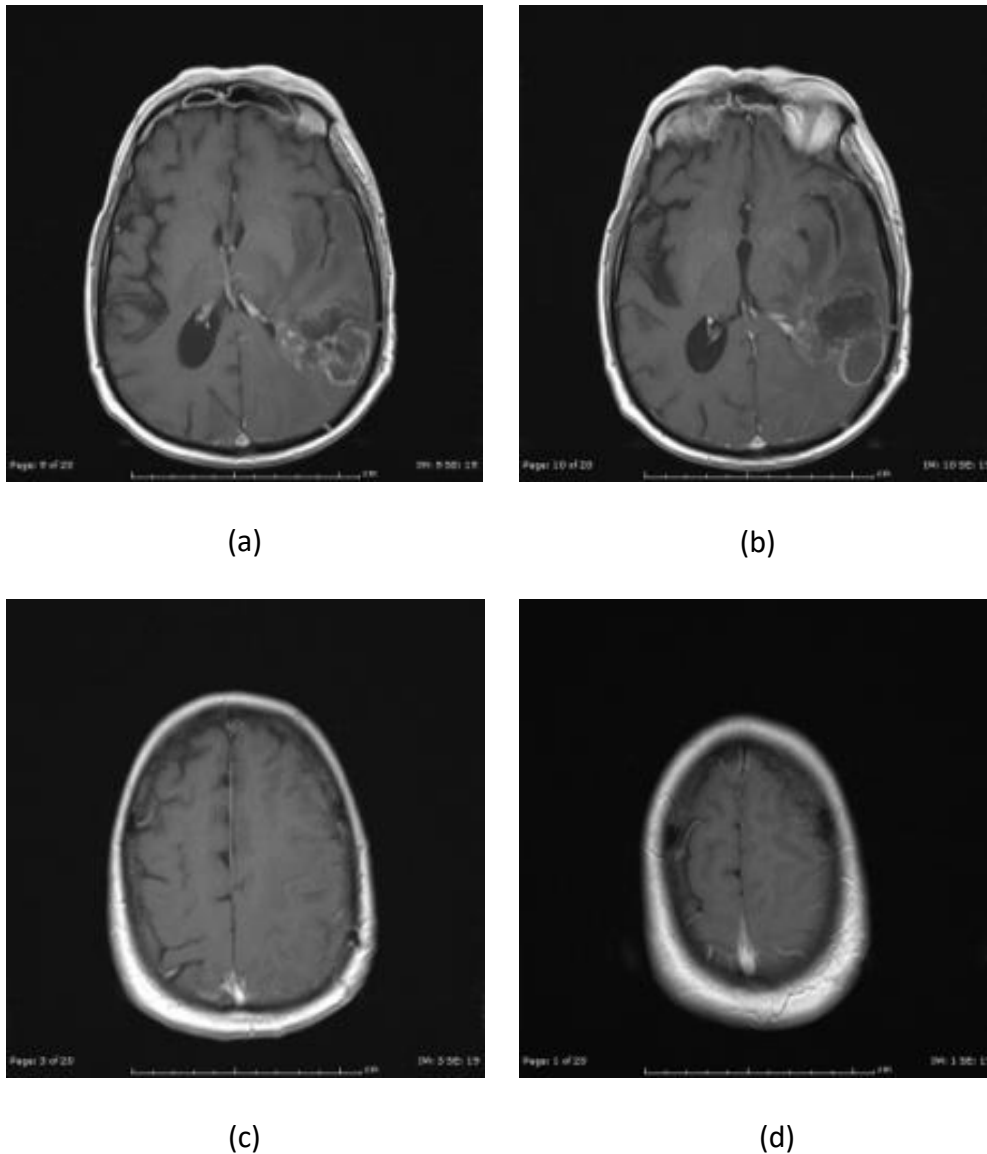
Figure 3.10: Sample of brain MRI Images from RGCI&RC: (a-b) abnormal brain;

(c-d) normal brain (RGCI&RC).

The features from the images are extracted using LBP as explained in section 3.2 and are given as input to the classification algorithms.
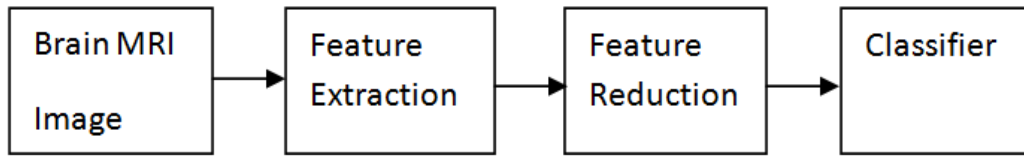
Figure 3.11 Methodology of Implemented Algorithm

The accuracy of the system's performance is assessed since it evaluates the system's overall performance. It is computed by identifying the properly categorised instances from all of the samples, as shown in equation 3.16,

$$Accuracy = \frac{TP + TN}{TP + FP + TN + FN}$$

3.16

where TP, FP, TN, and FN represent the number of true positive, false positive, true negative, and false negative cases, respectively.

The accuracy of the proposed algorithm(LBP+MCM) is compared with the KNN and SVM algorithms using LBP features. We found that LBP features give 90% accuracy when used with KNN, 95% accuracy with SVM(linear), 96.25% with SVM(polynomial & radial basis function). Also, the comparison is done with other brain image classification algorithms existing in the literature as shown in Table 3.1. The results in Table 3.1 shows that our method outperforms other classification methods in the literature with an accuracy of 98.75%. We can also see the comparative analysis of MRI brain image segmentation techniques in Figure 3.12.

Table 3.1: Classification Accuracy comparison for the same MRI dataset

Year	Author	Technique	Accuracy
2006	Chaplot *et al*.	DWT+SOM	86.25%
2006	Chaplot *et al*.	DWT+SVM(linear)	95.00%
2006	Chaplot *et al*.	DWT+SVM (polynomial)	96.25%
2006	Chaplot *et al*.	DWT+SVM (radial basis function)	96.25%
2010	Dahshan *et al*.	DWT+PCA+KNN	93.75%
2010	Dahshan *et al*.	DWT+PCA+ANN	91.25%
2011	Zhang *et al*.	DWT+PCA+BPNN	92.50%
2013	Sridhar *et al*.	DCT+PNN	88.75%
2015	Veeramuthu *et al*.	DWT+GLCM+PNN-RBF	90.00%
2015	Yazdani *et al*.	EM+GLCM+SVM	91.25%
2015	Machhale *et al*.	SVM+KNN	88.75%
2017	Gupta *et al*.	EIFE+PCA+SVM	93.75%
2017	Proposed	ULBP+MCM	98.75%

3.5 Summary

In this chapter, we have implemented a feature extraction and classification algorithm for MRI brain images. We suggest using LBP as a feature to distinguish tumorous and non-tumorous MRI brain images. The LBP calculates the connection between the 3x3 window's centre pixel and its neighbours and provides a label to each window. The histogram of these labels is then sent into the classification step as a feature vector. The MCM method is used to classify the brain images for the first time and proved to efficient. The suggested approaches'

performance is evaluated based on estimated accuracy, and it is found that the classification rate is greater than other current algorithms. The method obtained 98.75% classification accuracy on test images of the selected datasets.
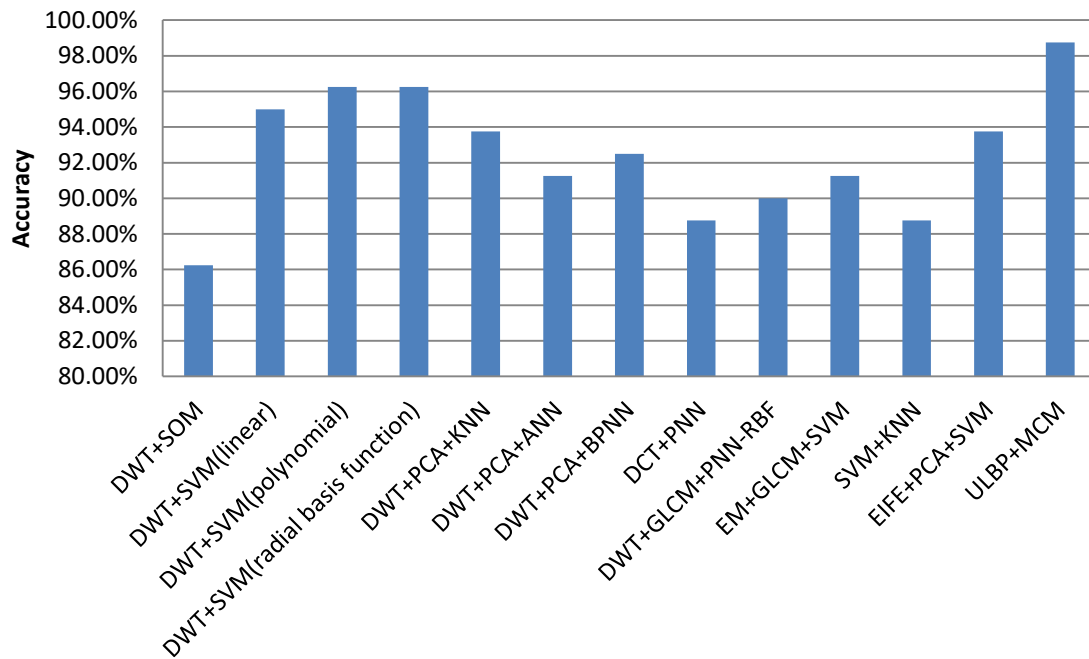
Figure 3.12: Comparative Analysis of MRI Brain Image segmentation Techniques

Chapter 4

Intuitionistic Fuzzy Co-Clustering Algorithm for Brain images

4.1 Introduction

Early detection and accurate treatment based on truthful diagnosis are the major concern to cure brain tumor. The important task in the diagnosis of brain tumor is to determine the exact location, orientation and area of the abnormal tissues. Detection of anatomical brain structure plays a major role in the planning of treatment. The automated segmentation method is composed of two phases: tumor detection and mapping.

There are two major challenges in segmentation of a brain image. First is to handle the uncertainty that arises on boundary between different tissues. Our approach addresses the issue of uncertainty with the help of intuitionistic algorithm. Second is to obtain distinct or non-overlapping clusters which is achieved with the help of co-clustering. We are able to overcome both the challenges with the help of proposed algorithm. In this chapter we have proposed a novel Intuitionistic Fuzzy Co-Clustering (IFCC) algorithm for brain tumor detection. The Co-clustering approach offers the advantage of assigning membership functions for both object as well as features. The intuitionistic fuzzy set theory is incorporated as it is more suitable for handling uncertainty as compared to fuzzy sets theory.

4.2 Background

4.2.1 Fuzzy Sets

Let there be data set $A = \{a_1, a_2, ..., a_I\}$ where I is the number of elements. Then Zadeh[101] defined a Fuzzy set(FS) B for the set A as in equation 4.1:

$$B = \{\langle a, \mu_B(a) \rangle : \forall a \in A\}$$ 4.1

where $\mu_B(a)$ denotes the membership of element $a \in A$ and lies between[0,1]. Also, the non-membership degree is defined as $\nu_B = 1 - \mu_B$. The following properties holds true for two FS B and C[102] are given as:

$$B \subseteq C \text{ iff } \forall a \in A, \ \mu_B(a) \leq \mu_C(a)$$ 4.2

$$B = C \text{ iff } \forall a \in A, \ \mu_B(a) = \mu_C(a)$$ 4.3

$$\overline{B} = \{\langle a, 1 - \mu_B(a) \rangle : \forall a \in A\}$$ 4.4

$$B \cup C = \{\langle a, \max(\mu_B(a), \mu_C(a)) \rangle : \forall a \in A\}$$ 4.5

$$B \cap C = \{\langle a, \min(\mu_B(a), \mu_C(a)) \rangle : \forall a \in A\}$$ 4.6

4.2.2 Intuitionistic Fuzzy Sets:

In real world when someone needs to take a decision, uncertainty is introduced due to hesitation in expressing their opinion. Intuitionistic Fuzzy sets(IFS) takes into account the degree of hesitation in addition to the membership and non-membership degree as in the FS. The IFS is defined by Atnassov[103] and is given as:

$$I = \{\langle a, \mu_I(a), \nu_I(a) \rangle : \forall a \in A\}$$ 4.7

with constraint

$$0 \le \mu_I(a) + v_I(a) \le 1 \qquad\qquad\qquad 4.8$$

where $\mu_I(a)$ and $v_I(a)$ denotes the membership and non-membership degree of element $a \in A$

and lies between[0,1].

The hesitation degree of the element $a \in A$ is given by equation 4.9.

$$\pi_I(a) = 1 - \mu_I(a) - v_I(a) \qquad\qquad\qquad 4.9$$

where $\pi_I(a)$ is hesitation degree, $\mu_I(a)$ and $v_I(a)$ denotes the membership and non-membership degree of element $a \in A$ and lies between[0,1].

If the value of $\pi_I(a) = 0$ in equation 4.9, then the IFS is reduced to FS.

The properties[104] that holds true for two IFS H and I are given as:

$$I \subseteq H \;\; iff \;\; \forall a \in A, \;\; \mu_I(a) \le \mu_H(a) and v_I(a) \ge v_H(a) \qquad 4.10$$

$$I = H \;\; iff \;\; \forall a \in A, \;\; \mu_I(a) = \mu_H(a) and v_I(a) = v_H(a) \qquad 4.11$$

$$\bar{I} = \left\{ \langle a, v_I(a), \mu_I(a) \rangle : \forall a \in A \right\} \qquad\qquad 4.12$$

$$I \cup H = \left\{ \langle a, \max(\mu_I(a), \mu_H(a)), \min(v_I(a), v_H(a)) \rangle : \forall a \in A \right\} \qquad 4.13$$

$$I \cap H = \left\{ \langle a, \min(\mu_I(a), \mu_H(a)), \max(v_I(a), v_H(a)) \rangle : \forall a \in A \right\} \qquad 4.14$$

For the construction of IFS, the negation function is given by Sugeno[105] as:

$$\theta_\lambda(a) = \frac{1-a}{1+\lambda a} \qquad\qquad \lambda > 0 \qquad\qquad\qquad 4.15$$

The IFS I is defined using the Sugeno's negation function as in equation 4.16.

$$I = \left\{ \left\langle a, \mu_I(a), v_I(a) = \frac{1-\mu_I(a)}{1+\lambda(\mu_I(a))} \right\rangle : \forall a \in A \right\} \qquad 4.16$$

4.2.3 Intuitionistic Fuzzification of images:

The intuitionistic fuzzification of images gives the appropriate membership and non-membership functions to describe the properties of the image in terms of IFS. A digital image I in the form of IFS can be represented as

$$I = \left\{ \left\langle a_j, \mu_I(a_j), v_I(a_j) \right\rangle : j = 1, 2, ..., N \right\} \qquad 4.17$$

where N is the total number of pixels of the image (N=N1*N2 is the size of the image), with L number of gray levels varying from 0 to L-1, the membership degree of pixels a_j is indicated by $\mu_I(a_j)$ and non-membership degree of pixels a_j is indicated by $v_I(a_j)$ .After normalizing the intensity level we obtain the membership degree of every pixel a_j of the image as given in equation 4.18.

$$\mu_I(a_j) = \frac{a_j - (a_j)_{\min}}{(a_j)_{\max} - (a_j)_{\min}}, \quad j = 1, 2, ..., N, \ x_j \in \{0, ..., L-1\} \qquad 4.18$$

where $(a_j)_{\min}$ and $(a_j)_{\max}$ are the minimum and maximum values of the gray levels of the image respectively.

4.2.4 Fuzzy Co-clustering for Images Algorithm

The aim of Co-clustering is to group both objects and features concurrently. We have used FCCI algorithm[105] instead of FCM in our work as it offers several advantages over the later. Fist advantage is that it performs well in high dimensions and also it gives us better clusters as compared to FCM clustering.

The objective function of the FCCI algorithm is given in equation 4.19. We can observe that there are three terms in the equation, the first term is $\sum\limits_{i=1}^{C} \sum\limits_{j=1}^{N} \sum\limits_{k=1}^{R} u_{ij} f_{ik} D_{ijk}$ which accounts for dissimilarity between the data point and cluster centre of the feature matrix by incorporating the distance function. In the next two terms regularization of objective function is done using

entropies. The entropy of objects is taken as $\sum\limits_{i=1}^{C}\sum\limits_{j=1}^{N}u_{ij}logu_{ij}$ and entropy of features is taken as

$\sum\limits_{i=1}^{C}\sum\limits_{k=1}^{R}f_{ik}logf_{ik}$. The images captured for applying the FCCI algorithm are first converted from

RGB to CIELAB color space and two features A and B of the CIELAB color space are then

further used to perform the clustering. The luminance vector obtained after transformation is

not taken into consideration in the clustering process as it is only used to determine the darkness

or fairness of the image segments and does not have any effect on the segmentation process.

The objective function J given in equation 4.19 is minimized in the FCCI algorithm[113]:

$$J = \sum_{i=1}^{C}\sum_{j=1}^{N}\sum_{k=1}^{R}u_{ij}f_{ik}D_{ijk} + T_U\sum_{i=1}^{C}\sum_{j=1}^{N}u_{ij}logu_{ij} + T_V\sum_{i=1}^{C}\sum_{k=1}^{R}f_{ik}logf_{ik} \qquad 4.19$$

The total membership of all attributes in a cluster must sum to 1, hence equation 4.19 is

subjected to the constraints in equations 4.20 and 4.21:

$$\sum_{i=1}^{C}u_{ij} = 1, \qquad u_{ij} \in [0,1], \quad \forall j = 1,...,N \qquad 4.20$$

$$\sum_{k=1}^{R}f_{ik} = 1, \qquad f_{ik} \in [0,1], \quad \forall i = 1,...,C \qquad 4.21$$

where, C is the number of clusters, N is the number of data points i.e., $N = N1 \times N2$ (N1*N2

is the dimension of the input image), R is the number of color features, u_{ij} is membership

function of data point j to cluster i given in equation 4.22, f_{ik} is membership function of

feature k to cluster i given in equation 4.23, T_U and T_V are the weighting parameters that

determine the degree of fuzziness and D_{ijk} is the Euclidean distance between data point x_{jk}

and cluster centroid p_{ik} given in equation 4.24.

$$u_{ij} = \frac{e^{\left(-\sum_{k=1}^{R}\frac{f_{ik}D_{ijk}}{T_U}\right)}}{\sum_{i=1}^{C} e^{\left(-\sum_{k=1}^{R}\frac{f_{ik}D_{ijk}}{T_U}\right)}}$$

<div align="right">4.22</div>

$$f_{ik} = \frac{e^{\left(-\sum_{j=1}^{N}\frac{u_{ij}D_{ijk}}{T_V}\right)}}{\sum_{k=1}^{R} e^{\left(-\sum_{j=1}^{N}\frac{u_{ij}D_{ijk}}{T_V}\right)}}$$

<div align="right">4.23</div>

$$D_{ijk} = d^2(x_{jk}, p_{ik}) = (x_{jk} - p_{ik})^2$$

<div align="right">4.24</div>

where,

$$p_{ik} = \frac{\sum_{j=1}^{N} u_{ij} x_{jk}}{\sum_{j=1}^{N} u_{ij}}$$

<div align="right">4.25</div>

4.2.5 Intuitionistic Fuzzification of images for Co-Clustering:

The membership, non-membership and hesitation degree of every pixel x_{jk} of the matrix for k

features in terms of normalize intensity level are illustrated in equations 4.26 to 4.28

$$\mu_I(x_{jk}) = \frac{x_{jk} - (x_{jk})_{min}}{(x_{jk})_{max} - (x_{jk})_{min}}, \quad j = 1, 2, ..., N, k = 1, 2 \ \ x_j \in \{0, ..., L-1\}$$

<div align="right">4.26</div>

$$\nu_I(x_{jk}) = \frac{1 - \mu_I(x_{jk})}{1 + \lambda(\mu_I(x_{jk}))}$$

<div align="right">4.27</div>

$$\pi_I(x_{jk}) = 1 - \mu_I(x_{jk}) - \nu_I(x_{jk})$$

<div align="right">4.28</div>

where $(x_{jk})_{min}$ and $(x_{jk})_{max}$ are the minimum and maximum values of the gray levels of the

image respectively.

4.3 Proposed Work

4.3.1 Intuitionistic Fuzzy Co-Clustering Algorithm

Let $X^{IFS} = \{x_1^{IFS}, x_2^{IFS}, ..., x_N^{IFS}\}$ be the set of N data points of the image I(total number of pixels

N=N1*N2, where N1 and N2 are rows and columns of the image respectively) and R be the

number of features linked with each data point. Then, to denote each data point for a particular

feature we can write k^{th} feature of the jth data point as, x_{jk}.

Let $(P^{IFS})^{(b)} = ((p_{1k})^{(b)}, (p_{2k})^{(b)}, ..., (p_{ik})^{(b)})$ be the set of feature centroid for each feature k of

cluster i and $D_{ijk}^{IFS} = Dist(x_{jk}^{IFS}, p_{ik}^{IFS})$ be the square of the Euclidean distance between feature

data point x_{jk} and feature cluster centroid p_{ik}.

The distance is given by the equation 4.29:

$$D_{ijk}^{IFS} = d^2(x_{jk}^{IFS}, p_{ik}^{IFS}) = (x_{jk}^{IFS} - p_{ik}^{IFS})^2 \qquad\qquad 4.29$$

Let object membership function matrix is $U = \{u_{ij}\}$ where u_{ij} is the object membership of the

data point j to cluster i and the feature membership matrix is $F = \{f_{ik}\}$ where f_{ik} is the feature

membership of the feature k to the cluster i.

The minimization optimization problem of the IFCC algorithm is defined as:

$$J_{IFCC}(U, F, P^{IFS} : X^{IFS}) = \sum_{i=1}^{C}\sum_{j=1}^{N}\sum_{k=1}^{R} u_{ij} f_{ik} D(x_{jk}^{IFS}, p_{ik}^{IFS}) + T_U \sum_{i=1}^{C}\sum_{j=1}^{N} u_{ij} \log u_{ij} + T_f \sum_{i=1}^{C}\sum_{k=1}^{R} f_{ik} \log f_{ik} \qquad 4.30$$

subject to the constraints:

$$\sum_{i=1}^{C} u_{ij} = 1. \qquad\qquad u_{ij} \in [0,1], \forall j = 1, ..., N \qquad\qquad 4.31$$

$$\sum_{k=1}^{R} f_{ik} = 1. \qquad f_{ik} \in [0,1], \forall i = 1,...,C \tag{4.32}$$

Now, we use Lagrangian multiplier method to solve the optimization problem and constrained optimization problem can now be formed as:

$$J^*_{IFCC}(U,F,P^{IFS}:X^{IFS}) = \sum_{i=1}^{C}\sum_{j=1}^{N}\sum_{k=1}^{R} u_{ij}f_{ik}D(x_{jk}^{IFS},p_{ik}^{IFS}) + T_U\sum_{i=1}^{C}\sum_{j=1}^{N} u_{ij}\log u_{ij} + T_f\sum_{i=1}^{C}\sum_{k=1}^{R} f_{ik}\log f_{ik} + \tag{4.33}$$

$$\sum_{j=1}^{N}\lambda_j(\sum_{i=1}^{C} u_{ij} - 1) + \sum_{i=1}^{C}\gamma_i(\sum_{k=1}^{R} f_{ik} - 1)$$

where λ_j and γ_i are multiplier constants.

Now, we calculate the partial derivatives of $J^*_{IFCC}(U,F,P^{IFS}:X^{IFS})$ with respect to U and setting the gradient to zero we get

$$u_{ij} = \frac{e^{\left(-\sum_{k=1}^{R}\frac{f_{ik}D(x_{jk}^{IFS},p_{ik}^{IFS})}{T_U}\right)}}{\sum_{i=1}^{C} e^{\left(-\sum_{k=1}^{R}\frac{f_{ik}D(x_{jk}^{IFS},p_{ik}^{IFS})}{T_U}\right)}} \tag{4.34}$$

Similarly, we calculate the partial derivatives of $J^*_{IFCC}(U,F,P^{IFS}:X^{IFS})$ with respect to F and setting the gradient to zero we get

$$f_{ik} = \frac{e^{\left(-\sum_{j=1}^{N}\frac{u_{ij}D(x_{jk}^{IFS},p_{ik}^{IFS})}{T_V}\right)}}{\sum_{k=1}^{R} e^{\left(-\sum_{j=1}^{N}\frac{u_{ij}D(x_{jk}^{IFS},p_{ik}^{IFS})}{T_V}\right)}} \tag{4.35}$$

Now, taking the partial derivatives of $J^*_{IFCC}(U,F,P^{IFS}:X^{IFS})$ with respect to $\mu(p_{ik})$, $v(p_{ik})$ and $\pi(p_{ik})$ and setting the gradient to zero we get

$$\mu(p_{ik}) = \frac{\sum\limits_{j=1}^{N} u_{ij}\mu(x_{jk})}{\sum\limits_{j=1}^{N} u_{ij}}$$

4.36

$$\nu(p_{ik}) = \frac{\sum\limits_{j=1}^{N} u_{ij}\nu(x_{jk})}{\sum\limits_{j=1}^{N} u_{ij}}$$

4.37

$$\pi(p_{ik}) = \frac{\sum\limits_{j=1}^{N} u_{ij}\pi(x_{jk})}{\sum\limits_{j=1}^{N} u_{ij}}$$

4.38

The centroids P^{IFS} of the IFCC algorithm are given as:

$$p_{ik}^{IFS} = (\mu(p_{ik}), \nu(p_{ik}), \pi(p_{ik}))$$

4.39

The IFCC algorithm is summarized as:

Step 1. Fix the number of cluster $C=2$, number of features $k=2$, fuzzifier constant $m=1$ and termination criterion $\varepsilon = 10^{-2}$.

Step 2. Calculate $x_{jk}^{IFS} = (\mu(x_{jk}), \nu(x_{jk}), \pi(x_{jk}))$, for $j=1,2,...,N$ and $k=1,2$ using equations 4.26 to 4.28

Step 3. Initialize the membership matrix $U^{(o)}$ with setting the loop counter $b=0$.

Step 4. Update the centroids, where $(P^{IFS})^{(b)} = ((p_{1k})^{(b)}, (p_{2k})^{(b)}, ..., (p_{ik})^{(b)})$, where $(p_{ik}^{IFS})^{(b)} = ((\mu(p_{ik}))^{(b)}, (\nu(p_{ik}))^{(b)}, (\pi(p_{ik}))^{(b)})$ using equations 4.36 to 4.38.

Step 5. Calculate D_{ijk} and f_{ik} using equations 4.29 and 4.35.

Step 6. Update the membership matrix $U^{(b)} = ((u_{ij})_{C \times N})^{b}$ using equation 4.34

Step 7. If $\max \left\| U^{(b+1)} - U^{(b)} \right\| < \varepsilon$ then stop, otherwise set counter b=b+1 and go to step 4.

4.3.2 Tumor Detection Using IFCC

The proposed tumor detection system consists of three modules namely pre-processing, building the intracranial mask and tumor extraction. In the first module we process the brain images before giving them as input to the system. Then, the intracranial mask is build so as to remove undesirable part from MRI images in the next module. And finally the proposed algorithm is applied to extract the tumor using the intracranial mask.

4.3.2.1 Preprocessing

In the first step the MRI scan images are fed to the median filter to remove the effect of various types of noises such as irregularities. The main objective of performing this pre-processing step is to guarantee the determination of the tumor accurately.

4.3.2.2 Building the intracranial mask

The intent of this step in the proposed system is to derive out the intra-cranial mask from the entire image. The extra-cranial region comprises of bones which do not contain tumor and hence its inclusion in the brain image is insignificant in segmentation of tumor. After studying and analyzing the images we see that there is remarkable difference in the intensity of intra-cranial and extra-cranial region. This difference is taken as a measure to derive the intracranial mask and remove the extra cranial mask from the MRI images. A threshold value is used to isolate the intra-cranial and extra-cranial masks. The threshold value at which the intra-cranial and extra-cranial regions are separated is 0.5. The extra-cranial mask obtained is subtracted from the original image to obtain the desired intra-cranial mask as shown in Figure1. If *G(a,b)* be the original MRI image and *E(a,b)* is the extracranial mask obtained after thresholding then, intracranial mask *F(a,b)* is determined using equation 4.40:

$$G(a,b) = F(a,b) - E(a,b) \qquad\qquad 4.40$$

where, a is the number of rows and b is the number of columns in the image.

<div align="center">

(a)   (b)   (c)   (d)   (e)

</div>
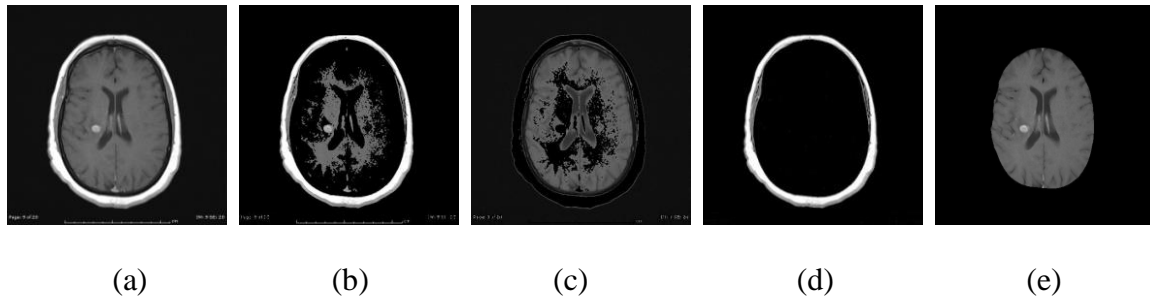
Figure 4.1: (a) Original MRI image, (b-c) Images after thresholding, (d) Extracranial mask, (e) Intracranial Mask

The algorithm for obtaining the desired intracranial mask is described below:

Step 1.   Read the input MRI image as shown in Figure 4.1(a).

Step 2.   Apply thresholding on the input image with threshold value t=0.5. As a result, we get two images as shown in Figure 4.1(b) and (c).

Step 3.   From the images obtained in step 2 choose the image with higher intensity values. Hence, we choose Figure 4.1(b)

Step 4.   From the chosen image, i.e., Figure 5.1(b) take only the connected component region i.e., the extracranial mask as shown in Figure 4.1(d).

Step 5.   The extracranial mask obtained in Figure 4.1(d) is subtracted from the original image to obtain the desired intracranial mask as shown in Figure 4.1(e).

4.3.2.3 Initialization of IFCC Using Particle swarm optimization

Kennedy and Eberhart [107] developed PSO, a population-based stochastic optimization method inspired by bird flocking and fish schooling, for the first time. The problem is approached by studying a population of particles, each of which represents a potential solution. The particle's initial locations and velocities are picked at random. Each particle's location is changed at each iteration step in the widely used standard PSO, based on its own personal best

position and the swarm's best solution. The swarm's evolution is regulated by the following equations:

$$VEL(iter+1) = w.VEL(iter) + c1.rand1.(pbest(iter) - POS(iter)) + c2.rand2.(gbest(iter) - POS(iter))\quad 4.41$$

$$POS(iter+1) = POS(iter) + VEL(iter+1) \qquad\qquad 4.42$$

where, POS is the particle's location, VEL is its velocity, w is its inertia weight, pbest is the particle's personal best position, and gbest is the swarm's global best position Iter is the number of iterations, while rand1, rand2 are random numbers between 0 and 1, c1, c2 are positive constants that define the impact of the personal best solution and the global best solution on the search process, respectively.

The PSO algorithm [107] is used to optimise the parameters and in the IFCC method for each picture. The parameters are set to the numbers 10 and 107, which were determined empirically. These starting values are determined by a series of hit-or-miss random trials. Because all of our tests converge within 100 iterations, the number of particles is set to 10 and the maximum number of iterations is set to 100.

4.3.2.4 Detection of Brain Tumor

Given an intracranial mask, our sole aim is now to detect the tumor. IFCC algorithm is applied for the clustering of the given MRI images. Using the image obtained after applying the clustering technique and the intra-cranial mask the tumor can be detected.

The algorithm of the proposed approach is described in the steps below:

    Step 1.   Read the input color MRI scan image.

    Step 2.   Convert the input color image into grayscale image.

    Step 3.   Apply median filter to remove noise.

    Step 4.   The desired intracranial mask is obtained.

Step 5.   Apply IFCC algorithm explained in section 4.3.2.1 with values of *C=2* to the intracranial mask.

Step 6.   Select the clustered image which has a greater number of pixels with values close to 1 as that cluster will contain tumor.

Step 7.   Apply morphological operation close to remove unwanted part and to get the exact shape of the tumor.

Step 8.   Calculate the area of tumor by calculating the number of white pixels in the tumorous image.

4.4 Experimental Results & Discussion

The algorithm is implemented on personal computer (2.0 GHz CPU, 2GB RAM) using MATLAB 7.9.0 (2009b). The tumorous images have been provided from a database of T1 weighted brain MRI images of 20 patients by the radiologist of Rajiv Gandhi Cancer Institute & Research Centre(RGCI&RC), Delhi, India. Each patient dataset had 20 MRI images in form of horizontal slices of brain resulting in a total of 400 images. The proposed scheme is applied on 50 tumorous MRI images obtained from real time database of RGCI&RC. After mapping the tumor on the original MRI image using the proposed tumor detection system, the calculated tumor area is compared with the ground truth tumor manually mapped by the radiologist. The radiologist analyzed the outputs based on four terminologies; ground truth, true positive, false positive and false negative as shown in Figure 4.2.

The area accurately measured is termed as *True Positive* and the errors encountered are termed as *False Positive* and *False Negative*. False positive counts the total number of pixels that our system classifies but is not present in ground truth and True negative counts the total number

55

of pixels that our system doesn't classifies but is present in the ground truth as belonging to particular cluster.
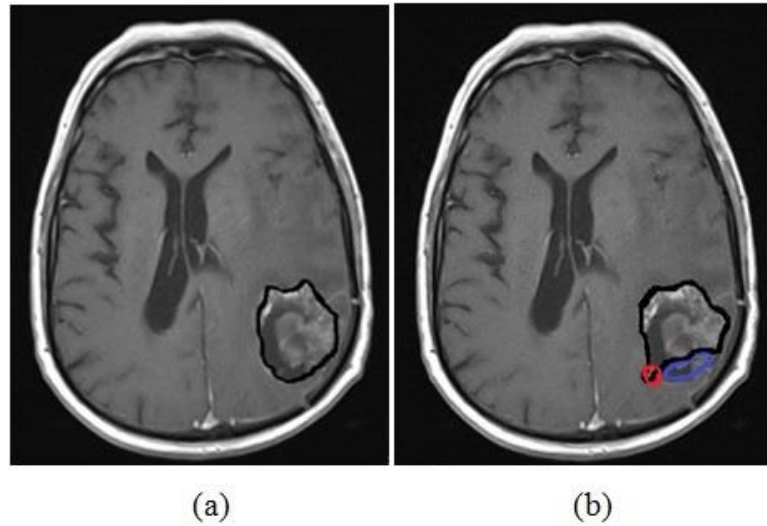
Figure 4.2. (a) Ground truth tumor (b) True positive, false positive and false

negative markings

To evaluate how well the system performs in segmenting the tumor, we use four quantitative measures namely, Match Score, Accuracy Score, Dice Coefficient(DC) and Jaccard's similarity(JS) score which are formulated from the parameters given by the radiologist and can be seen in equations 4.43 to 4.46. The number of True Positive pixels divided by the number of ground truth pixels results in *Match Score* which indicates the performance of proposed algorithm in comparison with the ground truth given by the radiologist. *Accuracy Score* is calculated to account for the presence of error in segmenting tumor and therefore the formula incorporates both false positive and false negative.

Match Score = No. of True positive pixels / No. of Ground truth pixels   4.43

$$\text{Accuracy Score} = \frac{\text{No. of True positive pixels} - 0.5(\text{No. of False positive pixels} + \text{No. of False negative pixels})}{\text{No. of Ground truth pixels}}$$

4.44

The Dice Coefficient[108] is defined as

$$DC(S,W) = 2(|S \cap W|)/(|S| + |W|)$$

4.45

where S and W are two sets.

In case of MRI brain image Dice Coefficient is calculated as:

$$DC = 2 * \frac{MIN(GT,TP)}{GT + TP}$$

4.46

Where, DC is Dice Coefficient, GT is number of ground truth pixels and TP is number of true positive pixels.

The value of Dice Coefficient lies between 0 and 1. 0 signifies no match/overlap and 1 signifies complete match/overlap. In terms of segmentation, *'S'* represents the segmented image containing tumor and '*W*' represents the ground truth given by the radiologist. The JS, also termed as Jaccard index the coefficient was originally given by Paul Jaccard[108], is a statistic used for comparing the similarity and diversity of sample sets. The JS measures similarity between finite sample sets, and is defined as the size of the intersection divided by the size of the union of the sample sets as given in equation 4.46:

$$JS = (|S \cap W|)/(|S \cup W|)$$

4.46

The value of JS also lies within 0 and 1. 0 signifies no match/overlap and 1 signifies complete match/overlap. The coefficient values of 1 are desired for dice score as well as JS. Relationship between DC and JS is as follows:

$$DC = 2 * JS / (1 + JS)$$
<div align="right">4.47</div>

The match score, accuracy score, Dice Coefficient and Jaccard Similarity have been calculated for 50 images using IFCC algorithm and shown in Table 4.1. The more the value of DC is close to 1, the better is the segmentation accuracy. It is studied that dice coefficient's value >0.7 implies good segmentation. Similar to DC is the JS measure. Both these parameters are not sensitive to volume overestimations and underestimations. However, DC is more famous than JS as it may sometimes result in a mismatch when there is a strong volumetric overlap. We have presented the estimated results using JS as well to have a better outlook of classification system. As we can see from the Table that the proposed system has an average match score of 0.92 which indicates high degree of similarity between the ground truth and the brain tumor segmented using the proposed algorithm. The average accuracy score is 0.87, as it also incorporates the errors that occurred in extracting tumor. The average Dice Coefficient and Jaccard Similarity have been reported 0.96 and 0.93 respectively.

Table 4.1. Quantitative results of tumor detection using IFCC algorithm

S.No	Patient No.	Ground Truth	True Positive	False Negative	False Positive	Match Score	Accuracy Score	Dice Coefficient	Jaccard Score
1	1	1928	1800	128	0	0.93	0.90	0.97	0.93
2	1	4360	4194	166	0	0.96	0.94	0.98	0.96
3	1	4916	4867	49	0	0.99	0.99	0.99	0.99
4	1	2056	2056	0	0	1.00	1.00	1.00	1.00
5	1	1150	1150	0	0	1.00	1.00	1.00	1.00
6	2	1651	1420	231	48	0.86	0.78	0.92	0.86
7	2	1884	1866	18	0	0.99	0.99	1.00	0.99
8	2	2324	2312	12	157	0.99	0.95	1.00	0.99

9	2	514	514	0	0	1.00	1.00	1.00	1.00
10	3	8265	5951	2314	102	0.72	0.57	0.84	0.72
11	3	10102	7880	2222	481	0.78	0.65	0.88	0.78
12	4	744	707	37	0	0.95	0.93	0.97	0.95
13	4	1498	1498	0	0	1.00	1.00	1.00	1.00
14	5	5212	4706	506	521	0.90	0.80	0.95	0.90
15	5	5680	5413	267	0	0.95	0.93	0.98	0.95
16	5	4794	4794	0	0	1.00	1.00	1.00	1.00
17	6	13422	13422	0	0	1.00	1.00	1.00	1.00
18	6	11022	10912	110	3306	0.99	0.84	0.99	0.99
19	6	9164	9073	91	2749	0.99	0.84	1.00	0.99
20	7	1983	1884	99	0	0.95	0.93	0.97	0.95
21	7	1802	1442	360	0	0.80	0.70	0.89	0.80
22	7	1686	1686	0	33	1.00	0.99	1.00	1.00
23	7	2704	2569	135	0	0.95	0.93	0.97	0.95
24	7	3845	3845	0	0	1.00	1.00	1.00	1.00
25	7	2705	2705	0	1082	1.00	0.80	1.00	1.00
26	8	5500	4510	990	0	0.82	0.73	0.90	0.82
27	8	6705	5834	871	335	0.87	0.78	0.93	0.87
28	8	6171	4937	1234	0	0.80	0.70	0.89	0.80
29	8	7412	5930	1482	1482	0.80	0.60	0.89	0.80
30	9	1315	1302	13	0	0.99	0.99	1.00	0.99
31	9	1968	1575	393	0	0.80	0.70	0.89	0.80
32	10	6748	6681	67	0	0.99	0.99	1.00	0.99

33	10	5758	5471	287	0	0.95	0.93	0.97	0.95
34	10	3495	3461	34	0	0.99	0.99	1.00	0.99
35	11	4295	4081	214	0	0.95	0.93	0.97	0.95
36	11	4434	4434	0	0	1.00	1.00	1.00	1.00
37	11	4360	4360	0	0	1.00	1.00	1.00	1.00
38	11	2903	2323	580	0	0.80	0.70	0.89	0.80
39	12	2362	2339	23	0	0.99	0.99	1.00	0.99
40	13	1889	1871	18	0	0.99	0.99	1.00	0.99
41	13	2891	2313	578	0	0.80	0.70	0.89	0.80
42	14	6288	5031	1257	0	0.80	0.70	0.89	0.80
43	15	5028	4719	309	26	0.93	0.90	0.97	0.94
44	15	4824	4342	482	0	0.90	0.85	0.95	0.90
45	15	2918	2918	0	0	1.00	1.00	1.00	1.00
46	16	1496	1378	118	0	0.92	0.88	0.96	0.92
47	16	4913	4581	332	0	0.93	0.89	0.97	0.93
48	16	5295	5295	0	52	1.00	0.99	1.00	1.00
49	16	4106	3833	273	0	0.93	0.90	0.97	0.93
50	16	1754	1611	143	38	0.92	0.87	0.96	0.92

Table 4.2. DC values of proposed technique and other segmentation algorithms

		FCM		IFCM		IIFCM		IFCC	
S. No.	Ground Truth	True Positive	Dice Score	True Positive	Dice Score	True Positive	Dice Score	True Positive	Dice Score
1	1928	2376	0.90	1786	0.96	1600	0.91	1800	0.97

2	4360	4867	0.95	5990	0.84	4142	0.97	4194	0.98
3	4916	4765	0.98	4812	0.99	4802	0.99	4867	0.99
4	2056	2018	0.99	2035	0.99	2043	1.00	2056	1.00
5	1150	1098	0.98	1109	0.98	1128	0.99	1150	1.00
6	1651	1324	0.89	1387	0.91	1404	0.92	1420	0.86
7	1884	1765	0.97	1812	0.98	1840	0.99	1866	0.99
8	2324	1866	0.89	1765	0.86	2301	1.00	2312	1.00
9	514	683	0.86	528	0.99	514	1.00	514	1.00
10	8265	5466	0.80	5699	0.82	5800	0.82	5951	0.84
11	10102	7435	0.85	7567	0.86	7785	0.87	7880	0.88
12	744	602	0.89	654	0.94	689	0.96	707	0.97
13	1498	1347	0.95	1438	0.98	1450	0.98	1498	1.00
14	5212	4170	0.89	4023	0.87	4278	0.90	4706	0.95
15	5680	5031	0.94	3805	0.80	5112	0.95	5413	0.98
16	4794	4983	0.98	4126	0.93	4794	1.00	4794	1.00
17	13422	12002	0.94	12123	0.95	12567	0.97	13422	1.00
18	11022	10099	0.96	10265	0.96	10542	0.98	10912	0.99
19	9164	8645	0.97	8865	0.98	8907	0.99	9073	1.00
20	1983	1789	0.95	1800	0.95	1832	0.96	1884	0.97
21	1802	1278	0.83	1206	0.80	1289	0.83	1442	0.89
22	1686	1345	0.89	1456	0.93	1598	0.97	1686	1.00
23	2704	2176	0.89	2245	0.91	2386	0.94	2569	0.97
24	3845	3476	0.95	3578	0.96	3657	0.97	3845	1.00
25	2705	2576	0.98	2634	0.99	2689	1.00	2705	1.00

26	5500	4087	0.85	4082	0.85	4280	0.88	4510	0.90
27	6705	5469	0.90	5573	0.91	5788	0.93	5834	0.93
28	6171	4021	0.79	4327	0.82	4756	0.87	4937	0.89
29	7412	4862	0.79	4987	0.80	5488	0.85	5930	0.89
30	1315	1180	0.95	1256	0.98	1287	0.99	1302	1.00
31	1968	1368	0.82	1421	0.84	1539	0.88	1575	0.89
32	6748	5978	0.94	6098	0.95	6234	0.96	6681	1.00
33	5758	4876	0.92	4921	0.92	5298	0.96	5471	0.97
34	3495	3103	0.94	3196	0.96	3400	0.99	3461	1.00
35	4295	3876	0.95	3543	0.90	4024	0.97	4081	0.97
36	4434	4086	0.96	4127	0.96	4312	0.99	4434	1.00
37	4360	3972	0.95	4096	0.97	4256	0.99	4360	1.00
38	2903	1943	0.80	2012	0.82	2256	0.87	2323	0.89
39	2362	1976	0.91	2109	0.94	2312	0.99	2339	1.00
40	1889	1743	0.96	1798	0.98	1843	0.99	1871	1.00
41	2891	2091	0.84	2167	0.86	2213	0.87	2313	0.89
42	6288	4031	0.78	4569	0.84	4988	0.88	5031	0.89
43	5028	4676	0.96	4342	0.93	4526	0.95	4719	0.94
44	4824	3876	0.89	3898	0.89	4257	0.94	4342	0.95
45	2918	2457	0.91	2543	0.93	2864	0.99	2918	1.00
46	1496	1186	0.88	1294	0.93	1343	0.95	1378	0.96
47	4913	5231	0.97	4451	0.95	4451	0.95	4581	0.93
48	5295	3833	0.84	5371	0.99	5182	0.99	5295	0.92
49	4106	3124	0.86	3426	0.91	3623	0.94	3833	0.93

| 50 | 1754 | 1496 | 0.92 | 1456 | 0.91 | 1602 | 0.95 | 1611 | 0.92 |

It can be observed from Table 4.2 that the values of Dice Score are highest for the proposed algorithm, hence IFCC outperforms other segmentation algorithms for detection of brain tumor from MRI images. On observing all the cases we can see that the proposed algorithm is most efficient in segmenting the tumor from the MRI. Tumor mapping, indicated by black outline, done on all the segmented images can be seen in Figure 4.3.

Table 4.3. Comparative analysis of MRI image segmentation algorithms

Segmentation Technique	Dice Score	Jaccard's Score	Error Percentage(%)
PIGFCM[12]	0.91	0.85	8.1
LIPC[13]	0.83	0.75	16.4
GWS[14]	0.80	0.74	17
KIFCM[15]	0.88	0.82	9.2
GLCM-CA[16]	0.92	0.86	7.4
TLBO[17]	0.91	0.89	6.0
AFBPNN[18]	0.92	0.86	8.0
GRBF[19]	0.93	0.88	7.5
IIFCM[76]	0.94	0.91	5.3
RLS[36]	0.91	0.89	7.8
CNN[77]	0.93	0.90	6.2
IFCM[68]	0.91	0.89	5.9
IFCC[81]	0.94	0.91	5.3
Proposed Algorithm: IFCC	0.96	0.93	3.7

To evaluate the effectiveness of IFCC algorithm we compare our results with other tumor detection algorithms from the literature. The proposed algorithm is compared with the state-of-the-art methods including both automatic and semi-automatic segmentation methods as shown in Table 4.3. The comparison is done with prior information guided FCM(PIGFCM). LIPC based method, GWS, KIFCM, GLCM-CA, TLBO, AFBPNN, IIFCM, RLS, CNN, IFCM, IFCC and GRBF based segmentation. The results shows that the proposed IFCC algorithm performs better than other segmentation techniques and has lowest error percentage and highest DS and JS values.
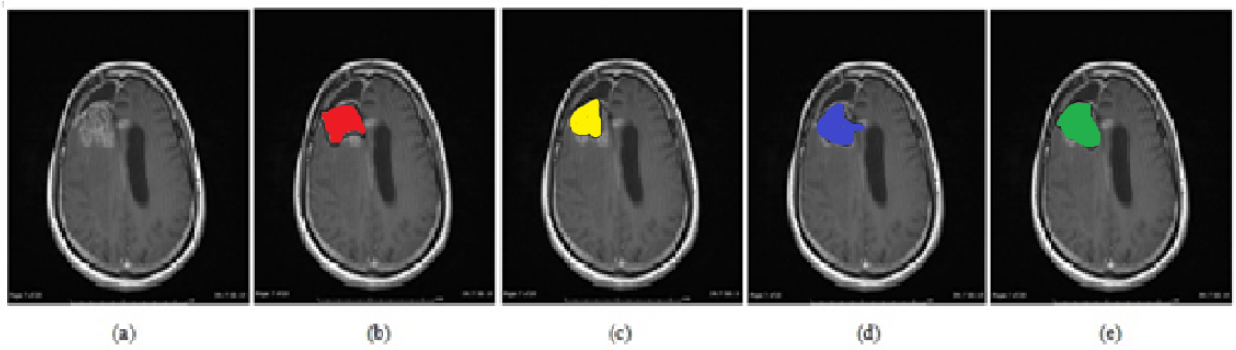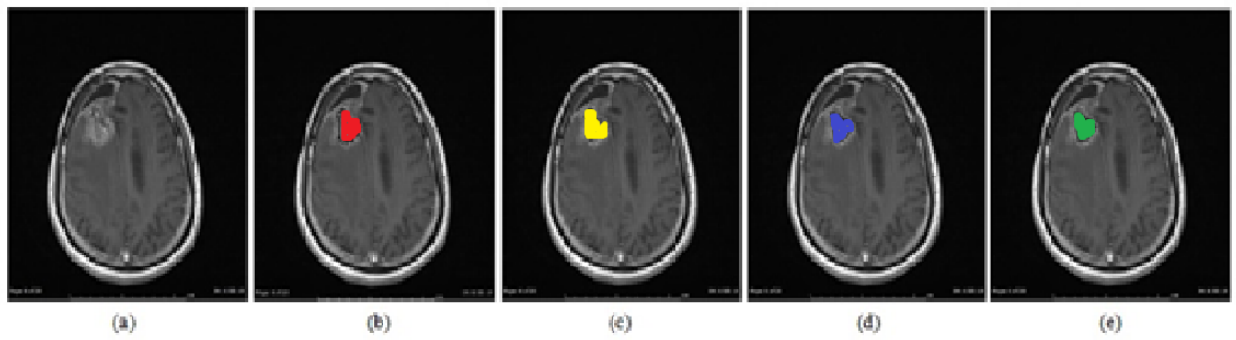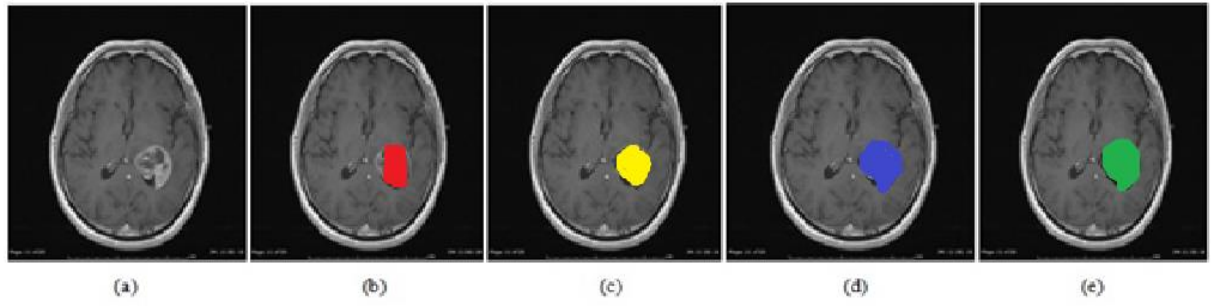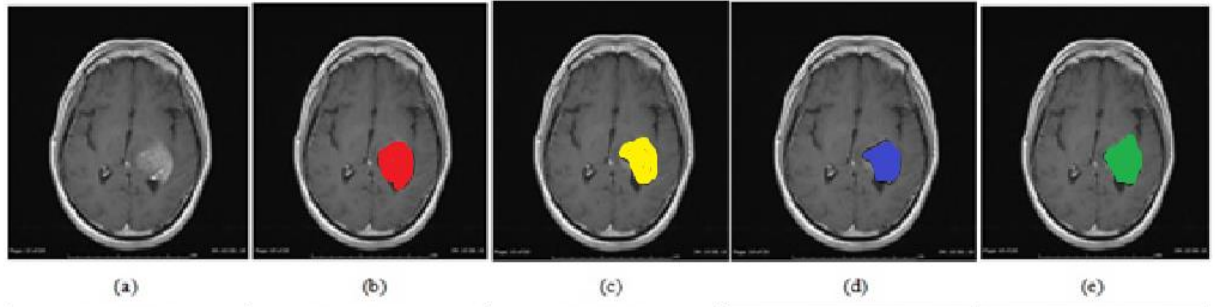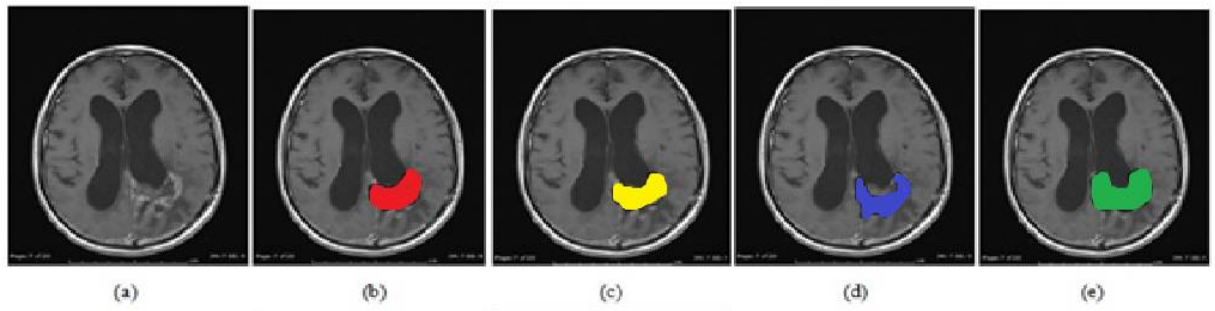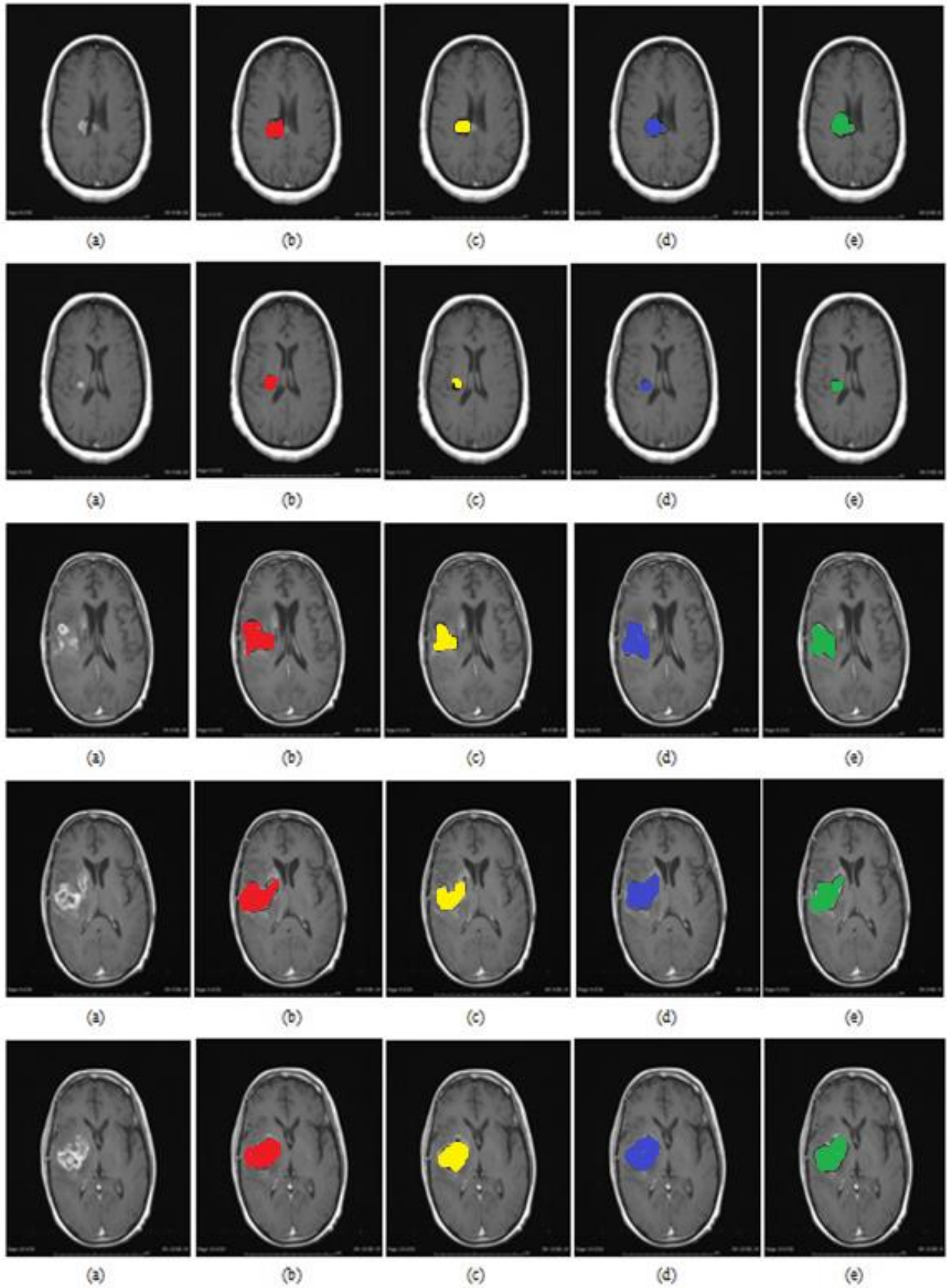
Figure 4.3: (a) Input MRI image, Tumor mapping with (b) FCM (c) IFCM (d) IIFCM (e) IFCC

66
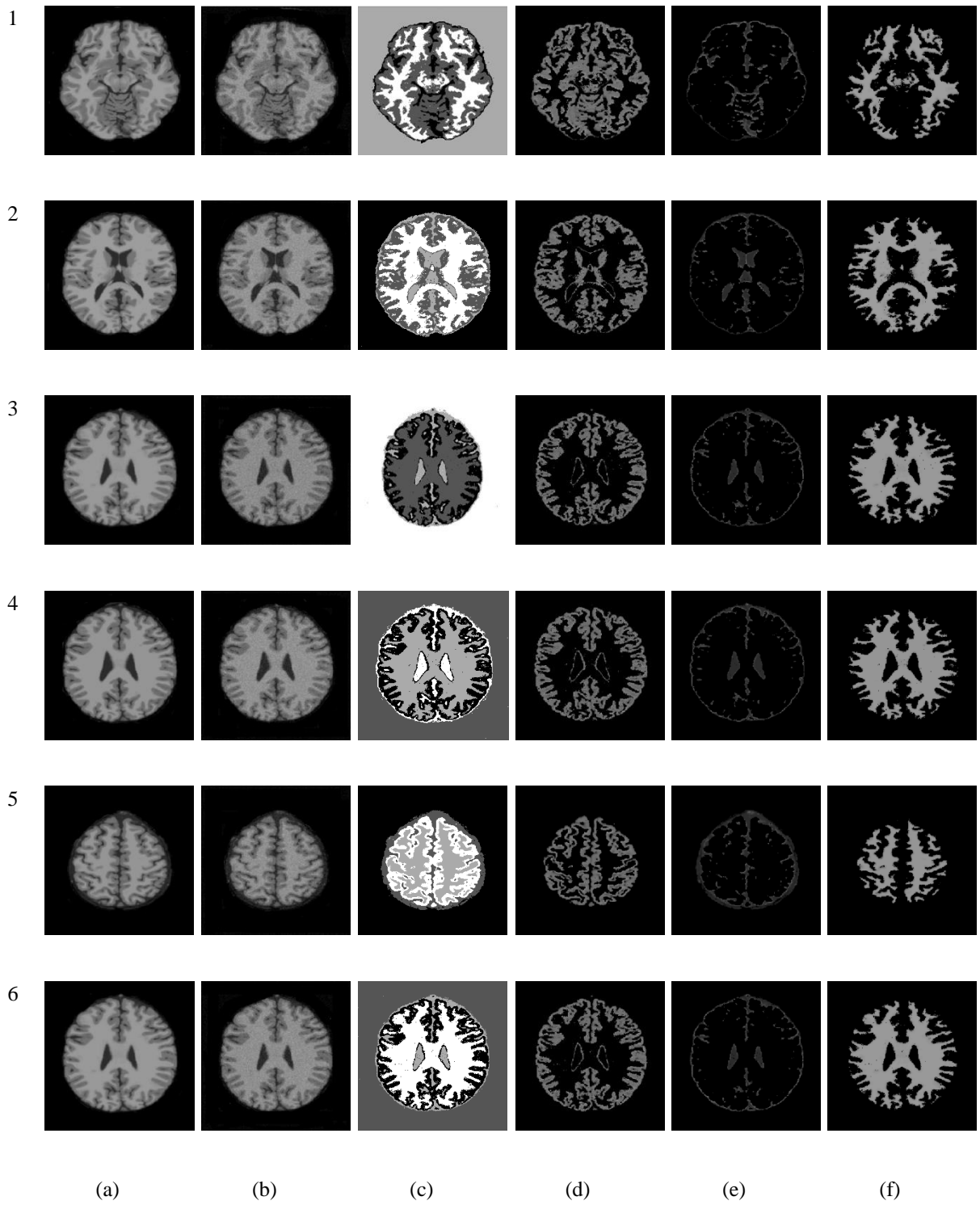
Figure 4.4: (a) Normal Brain, (b) Normal brain (noise 3%), (c) Segmented result, (d) Gray matter, (e) CSF, (f) White matter

4.5 Summary

An automatic brain tumor detection technique from real time MRI images has been presented in the thesis. A novel intutionistic and co-clustering based IFCC algorithm has been proposed. The Co-clustering approach offers the advantage of assigning membership functions for both object as well as features. The intuitionistic fuzzy set theory is found to be apt for handling uncertainty as compared to fuzzy sets theory. The proposed system is highly automatic as it produces tumor segmentation results in limited time and without any user intervention. The tumor detection result obtained by the proposed framework have been evaluated by experienced radiologist at Rajiv Gandhi Cancer Institute and Research Centre.

Chapter 5

Optimal Fuzzy C-Means Algorithm for Brain Image Segmentation

5.1 Introduction

This chapter presents an automated system for segmentation of brain tissues from brain Magnetic Resonance Imaging (MRI) images. Segmentation of three main brain tissues is carried out namely white matter, gray matter and cerebrospinal fluid. In this work, we performed the initialization step for fuzzy C-means (FCM) clustering algorithm using Ant Colony Optimization (ACO). Clustering results are often dependent upon the initial solution. The clustering process is further followed by inclusion of spatial information in segmenting brain tissues. Grouping of pixels into different clusters is influenced by its local neighborhood as neighboring pixels have higher probability of belonging to same class. Also, Mahalanobis distance metric is used instead of Euclidean distance metric in clustering process to avoid any relative dependency upon the geometrical shapes of different clustering classes. The results of the system are evaluated and validated against the ground truth images for both real and simulated brain image database.

5.2 Ant Colony Optimization

Ant Colony Optimization (ACO) technique is influenced by the behavior of ants in real life scenario. It is basically used in cases when the problem statement belongs to NP-hard class. [110] ACO is the probabilistic approach which focuses on providing solution to discrete optimization based difficult problems.[111]

In real world, ant locomote from one place to another in search of food. These ants are almost blind. They are generally influenced by the movement of other ants and try to find the shortest route to destination. The shortest path is ascertained by the pheromone trail deposited on that path by any of the ant. The more is the pheromone deposition on the path, the more is the chance/probability of that path being chosen. ACO tries to find out the optimal or close to optimal solution. Its solution might take time to converge but convergence is guaranteed.

ACO was firstly used for solving travelling salesman problem (TSP). To solve a new problem by using ACO, we try to find out whether that problem can be thought of or mapped in travelling salesman problem or not.

5.2.1 Overview of ACO Implementation:

Step 1.   Parameter setting: Initialize pheromone matrix and other required data.

Step 2.   DO While some defined stopping criteria is not met (Outer/cycle loop)

Step 3.   Do Until every ant completes a move/tour (Inner/tour loop)

- Update the pheromone/trail locally

Step 4.   End Do (Inner)

- Analyze the solution and trail

- Update the pheromone globally

- Get the best solution

Step 5.   End Do (Outer)

Movement of ants from one node to another is dependent upon the probability of choosing that path. The higher the probability, the more likely is the path to be selected. The movement of an ant from node i to node j is judged by the following probabilistic equation:

$$p_{i,j} = (\tau_{i,j}{}^{\alpha})(\eta_{i,j}{}^{\beta}) / \left(\sum_{\Omega \in allowed} (\tau_{i,j})(\eta_{i,j}) \right) \qquad 5.1$$

where,

$\tau_{i,j}$ denotes the amount of pheromone/trail laid by an ant on edge (i,j)

$\eta_{i,j}$ denotes the amount of heuristic matrix whose value is typically $1/d(i,j)$

α regulates the impact of $\tau_{i,j}$

β regulates the impact of $\eta_{i,j}$

Pheromone Update

Updation in pheromone is done according to the equation:

$$\tau_{i,j} = (1 - \rho) * \tau_{i,j} + \Delta \tau_{i,j} \qquad 5.2$$

Where,

ρ is the rate of evaporation of pheromone

$$\Delta \tau_{i,j}{}^{k} = \begin{cases} 1/L_k, & \text{if } k^{th} \text{ ant travels/covers edge (i,j)} \\ 0, & \text{otherwise} \end{cases}$$

Where L_k denotes the length of the kth ant travel/tour

5.3 Proposed Work

In this chapter, an automatic framework for segmentation of brain tissue classes namely, white matter, gray matter and cerebrospinal fluid has been proposed. The brain MRI images are used for the purpose of segmenting these tissues. The results of segmentation are often dependent upon the initialization step. MRI images are often subjected to some random noise. Segmentation algorithm such as FCM is very sensitive to noise. To avoid any stuck in local optimal results, Ant Colony Optimization technique is used. ACO is used to determine the value of initial cluster centres. The centres thus obtained are fed into the system to perform segmentation. Modified Fuzzy C-means clustering approach is used to segment an image into WM, GM and CSF. In modified FCM, Mahalanobis distance is used instead of Euclidean distance as Euclidean distance takes into account only the super spherical shapes about the centre of mass for clustering the data points. Whereas, data points belonging to same cluster may not be located in that area only. Also the local neighbourhood information is also considered as neighbouring pixels are more likely to belong to same cluster.

5.3.1 Initialization Step Using Ant Colony Optimization

ACO is the probabilistic based optimization technique inspired by the behaviour of ants in this real world. Various optimization problems can be reduced to finding the shortest path from source/nest to destination/food source depending upon the pheromone concentration on that path. In case of noisy problems,[71] Fuzzy c-means clustering algorithm can easily get stuck into local optimal solution as FCM is very sensitive to noise. One can run the algorithm many a times with different initial values each time to get the best solution by comparing the results each time with the best solution.[75] But this process is very cumbersome. Therefore, meta-heuristic approach can be used to solve this problem [110]. Meta-heuristic optimization techniques can be used to solve the problems when the available data is incomplete, noisy or

uncertain. Main purpose of using ACO technique is to get the global optimal solutions without getting trapped in local optimal results.

In the proposed approach, ACO technique is mapped to our problem of segmentation of brain tissues. Basically, ACO is used to obtain the initial values of clusters required for segmenting the brain MRI images.

Table 5.1 Parameters values used in ACO initialization

Parameters	Values
$\alpha = \beta$	1.5
total_NumberOfAnts	10
Max_iteration	150
Rho (ρ)	0.1

Algorithm for Initialization using ACO (ACO-FCM)

Requirements: Fix the number of clusters; initialize all the parameters mentioned in Table 5.1

Step 1.   Input data matrix/image say $X = \{x_1, x_2 \ldots x_n\}$ where n is the total number of pixels in an image.

Step 2.   Calculate another matrix X' of same dimension as X, such that value of each pixel in X' is the mean value of 4*4 neighbourhood of corresponding pixel in X.

Step 3.   for iter =1 to max_iteration do

Step 4.   for ants=1 to total_NumberOfAnts do

Step 5.   Randomly initialize cluster centre values for all clusters 'c'

73

Step 6. Calculate the heuristic matrix η, where $\eta = 1/D$ (D is the distance of pixels from all cluster centres)

Step 7. Find the probability of belongingness of each pixel to a particular cluster using the equation 6.1

Step 8. Based on the indexing of each pixel into different clusters calculated using above probability, cluster centres are then updated using the formula:

$$v_j = (\sum_{i \subseteq S}(u_{i,j})^m x_i + \alpha * x_i^{'})/(\sum_{i \subseteq S}(1+\alpha)*(u_{i,j})^m), \forall j = 1,2...nc \qquad 5.3$$

where, S is the set of pixels having similar index i.e. cluster numbers

Step 9. Calculate the Euclidean distance using the updated cluster centres.

Step 10. Calculate the objective function using the above calculated distance:

$$J = \sum_{i=1}^{n}\sum_{j=1}^{c}(u_{i,j})^m d^2(x_i,c_j) + \alpha \sum_{i=1}^{n}\sum_{j=1}^{c}(u_{i,j})^m d^2(x_i^{'},c_j) \qquad 5.4$$

Step 11. Compare the value of objective function with the best fitness. Our goal is to minimize the fitness function. Update best fitness, best centres and corresponding index for each pixel of an image.

Step 12. END for (Loop at Step4)

Step 13. Calculate the distance using the best centres after each iteration

Step 14. Update the membership matrix using the updated distance as

$$u_{i,j} = (d^2(x_i,c_j) + \alpha d^2(x_i^{'},c_j))^{(1/m-1)} / \sum_{k=1}^{nc}(d^2(x_i,c_k) + \alpha d^2(x_i^{'},c_k))^{(1/m-1)} \qquad 5.5$$

Step 15. Calculate the best index of each pixel using the best solution obtained after each iteration

Step 16.   Update the pheromone matrix using the best indexes obtained in previous step:

$$\tau_{i,j} \;=\; (1-\rho) * \tau_{i,j} \;+\; \Delta\tau_{i,j}$$ 5.6

$\Delta\tau_{i,j}$ equals to 1/distance corresponding to same location where updation of pheromone is being done.

Step 17.   END for (Loop for max_iteration Step3)

Step 18.   Return the best centres obtained and membership matrix corresponding to those best centres.

Simply running FCM for a noisy image doesn't make much difference in segmentation result. Resultant image does not show any reduction in noise thus quality of segmentation is degraded. Using ACO based initialization rather than random initialization, significant improvement can be noticed in segmented image. Reduction in noise and better segmentation quality can be observed.

5.4 Clustering Algorithm

5.4.1 Mahalanobis Distance

Unlike Euclidean distance, Mahalanobis distance takes into consideration the co-relation among data points or data sets. P.C. Mahalanobis introduced this distance in 1936. [112] It gives the measurement of distance of a data point say M and a distribution say D. It is also defined as the distance of the test point p from the centre of mass q divided by the width of ellipsoid measured in the direction of test point.

$$D(p,q) = \sqrt{(p-q)^T C^{-1} (p-q)}$$ 5.7

Where, C is the covariance matrix of vector P

When the data points are distributed or spread in a non-spherical manner, then the possibility of data point belonging to a particular cluster or set is not only dependent upon the distance of data point from the center of mass or we can say the average of sample points but it is also dependent upon the direction of the data point in consideration. Data point must be closer in shorter axis of ellipse and farther in longer/major axis of ellipse. This state can be formulated by defining the covariance matrix of the sample data points.

Firstly we try to frame out the covariance matrix of sample points belonging to each class. Then distance of given test point is calculated from all N classes. The test point is classified to a particular cluster for which the distance is minimal. The mahalanobis distance involving fuzzy logic is described by G & K [70] and is given as:

$$d^2(x_j, c_i) = (x_j - c_i)^T C_i (x_j - c_i) \qquad 5.8$$

$$C_i = | \sum_i |^{1/p} \sum_i \qquad 5.9$$

$$\sum_i = \sum_{j=1}^{N} \sum_{i=1}^{nc} u_{i,j}{}^m (x_j - c_i)(x_j - c_i)^T / \sum_{j=1}^{N} \sum_{i=1}^{nc} u_{i,j}{}^m \qquad 5.10$$

5.4.2 Spatial Information for Clustering

As we know that MRI images are subjected to random noise during its acquisition. It sometimes becomes difficult to view its anatomy or analyze the brain main tissues in the presence of noise in an image. FCM converges to local solution in case of noise. So, performing clustering of data points using FCM will not be effective. As FCM does not takes into account the spatial information of the data points to be clustered. The pixels surrounding the particular pixel are more likely to be segmented into same class. Therefore, we include the information of

4*4 neighbouring pixels surrounding the pixel being examined for clustering. This spatial information is the average of the neighbouring pixels in the defined window and is included in the process of clustering or assigning labels to pixels [67].

Clustering Algorithm

Requirements: Cluster centres and membership matrix returned by algorithm, total number of iterations (max_iter=100), error (10^{-6})

Step 1. for ij=1:max_iter

Step 2. Calculate the mahalanobis distance using the equation

Step 3. Update the membership degree/matrix using the equation given below:

$$u_{i,j} = (d^2(x_i, c_j) + \alpha d^2(x_i', c_j))^{(1/m-1)} / \sum_{k=1}^{nc} (d^2(x_i, c_k) + \alpha d^2(x_i', c_k))^{(1/m-1)} \qquad 5.11$$

Step 4. Update the cluster centres as:

$$v_j = (\sum_{i=1}^{N} (u_{i,j})^m x_i + \alpha * x_i') / (\sum_{i=1}^{N} (1+\alpha) * (u_{i,j})^m), \forall j = 1, 2...nc \qquad 5.12$$

Step 5. If ||U(ij+1) - U(ij)|| < error, then go to Step8.

Step 6. END If

Step 7. END for (loop for maximum iteration)

Step 8. Return U, perform clustering using degree of belongingness of each pixel in clusters.

5.5 Experimental Results and Discussion

The real time database of Brain MRI images has been taken from Insight Journal. One of the Insight Journals is MIDAS. Midas community include National Alliance for medical

image computing (NAMIC) which presents the data for two autistic and two normal children (male and female).[113] Three type of MRI scanning is presented i.e. T1 weighted, T2 weighted, PD weighted images. Coronal slices are obtained with slice thickness of 1.5mms. The quantitative analysis of MRI brain images shown in Figure 5.1 is done in comparison with the ground truth images and is presented in Table 5.1.

Dice Coefficient[108] is the volume overlap metric that evaluates the segmentation results quantitatively given the segmentation volumes pairs. The value of dice coefficient lies between 0 and 1. 0 signifies no match/overlap and 1 signifies complete match/overlap. It is observed from Table 1 that the significant improvement can be seen in the result obtained from our approach (ACO-FCM) as compared to standard FCM. The classification of brain tissues is more promising in case of ACO-FCM as there are a greater number of correctly classified pixels. Our approach uses spatial information which helps in better classification of such tissues. Similar to Dice Coefficient is the Jaccard's similarity measure. Both these parameters are not sensitive to volume overestimations and underestimations. However, Dice Coefficient is more famous than Jaccard's ratio [109] as it may sometimes result in a mismatch when there is a strong volumetric overlap. In Table 5.1, patient numbers refer to the slices of dataset. It can be noticed that classification/segmentation accuracy is highly dependent upon the classification of cerebrospinal fluid. The accuracy of both gray matter and white matter tissues is also improved but significant change can be seen in case of segmentation of CSF tissue. CSF is a very complex tissue and it is sometimes difficult to segment such a flowing matter from brain MRI. Therefore, there is a requirement to get better classification of data points belonging to CSF class. This improvement can be seen in our approach as compared to standard FCM. The ACO-FCM approach for segmenting brain MRI images is also applied and validated for simulated 3D brain MRI images with varying level of noise from brain web database. The simulated dataset from brain web is provided by McGill University and can be obtained with different file extensions.

[114] It contains normal anatomical brain structures with size of each image is 181*217. The results are tested and validated for T1-weighted images with 3%, 5% noise levels and slice thickness of 1mm as shown in Figure 5.2 and Figure 5.3. It can be noticed from Table 5.2 and Table 5.3 that ACO-FCM performs better for both levels of noise as compared to standard FCM. The efficiency of FCM is reduced with higher level of noise. This can be seen from the slice 100 corrupted with both 3% and 5% noise. Accuracy of FCM reduces significantly whereas ACO-FCM performs efficiently in higher level of noise as well.

Table 5.2: This Table presents the value of Dice Coefficient for three brain tissues namely, Gray matter, White matter, CSF using our approach (ACO-FCM) and standard FCM

	Dice Coefficient							
	ACO-FCM				FCM			
Patient	GM	WM	CSF	Avg.	GM	WM	CSF	Avg.
P11	0.928	0.889	0.755	0.857	0.917	0.848	0.57	0.778
P12	0.86	0.927	0.785	0.857	0.838	0.848	0.68	0.788
P21	0.902	0.933	0.878	0.904	0.849	0.83	0.784	0.821
P22	0.899	0.806	0.759	0.821	0.872	0.751	0.617	0.746
P31	0.887	0.802	0.796	0.828	0.841	0.793	0.652	0.762
P32	0.903	0.888	0.798	0.863	0.852	0.817	0.716	0.795
P41	0.924	0.94	0.859	0.907	0.887	0.846	0.838	0.857
P42	0.954	0.814	0.853	0.873	0.918	0.744	0.697	0.786
Average	**0.907**	**0.874**	**0.81**	**0.863**	**0.871**	**0.809**	**0.694**	**0.791**

Table 5.3: This Table presents the value of Jaccard's overlap ratio for three brain tissues namely, Gray matter, White matter, CSF using our approach (ACO-FCM) and standard FCM

	Jaccard's overlap ratio							
	ACO-FCM				FCM			
Patient	GM	WM	CSF	Avg.	GM	WM	CSF	Avg.
P11	0.865	0.8	0.606	0.757	0.846	0.736	0.398	0.66
P12	0.754	0.863	0.646	0.754	0.721	0.736	0.515	0.657
P21	0.821	0.874	0.782	0.825	0.737	0.709	0.644	0.696
P22	0.816	0.675	0.611	0.7	0.773	0.601	0.446	0.606
P31	0.796	0.669	0.611	0.692	0.725	0.657	0.483	0.621
P32	0.823	0.798	0.663	0.761	0.742	0.69	0.557	0.663
P41	0.858	0.886	0.752	0.832	0.796	0.733	0.721	0.75
P42	0.912	0.686	0.743	0.78	0.848	0.592	0.534	0.658
Average	**0.83**	**0.781**	**0.676**	**0.762**	**0.773**	**0.681**	**0.537**	**0.663**

	(a)		(b)

	(c)		(d)
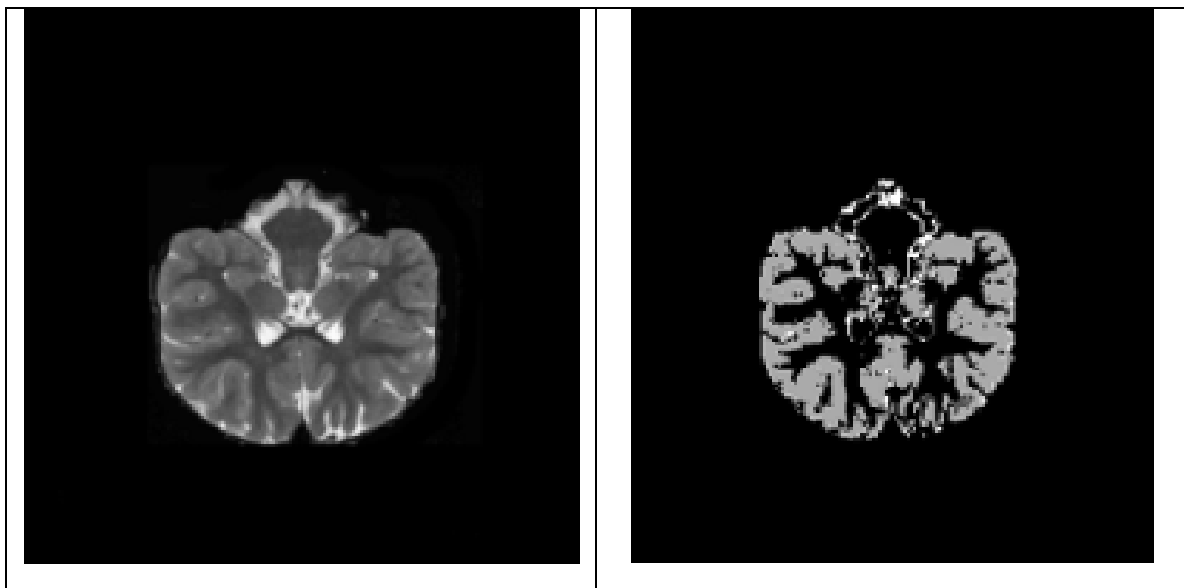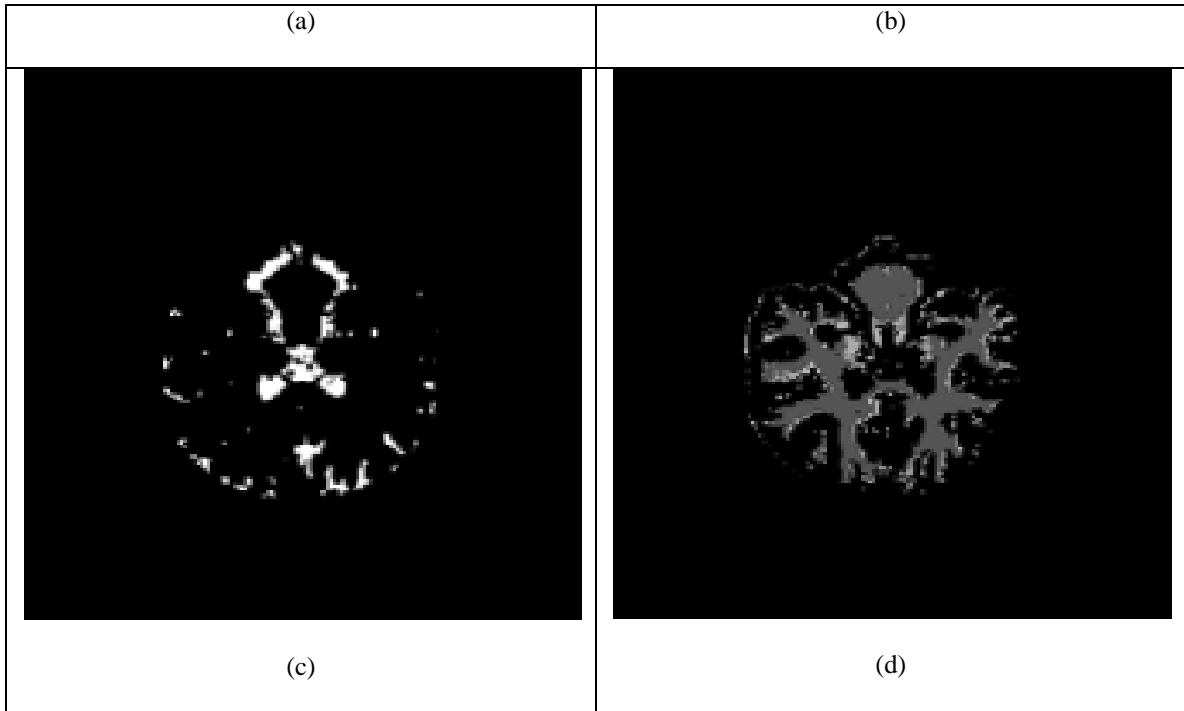
Figure 5.1. (a)Autistic Female T2-weighted MRI(slice 140), (b) Gray matter, (c) CSF, (d) White matter.

Table 5.4: This Table presents the value of Dice Coefficient for three brain tissues namely, Gray matter, White matter, CSF using our approach (ACO-FCM) and standard FCM for Brain Web database.

Slice#	Noise	GM	WM	CSF	Avg.	Slice#	Noise	GM	WM	CSF	Avg.
60	3%	0.962	0.911	0.812	0.895	60	3%	0.947	0.845	0.675	0.822
88	3%	0.929	0.963	0.89	0.927	88	3%	0.879	0.933	0.822	0.878
100	3%	0.9	0.97	0.837	0.902	100	3%	0.88	0.948	0.793	0.873
Average		**0.93**	**0.948**	**0.846**	**0.908**	**Average**		**0.902**	**0.908**	**0.763**	**0.857**
99	5%	0.915	0.967	0.841	0.907	99	5%	0.9	0.955	0.818	0.891

81

126	5%	0.934	0.902	0.874	0.903	126	5%		0.896	0.841	0.849	0.862
100	5%	0.902	0.962	0.835	0.899	100	5%		0.876	0.948	0.764	0.862
Average		**0.917**	**0.943**	**0.85**	**0.903**	**Average**			**0.89**	**0.914**	**0.81**	**0.871**
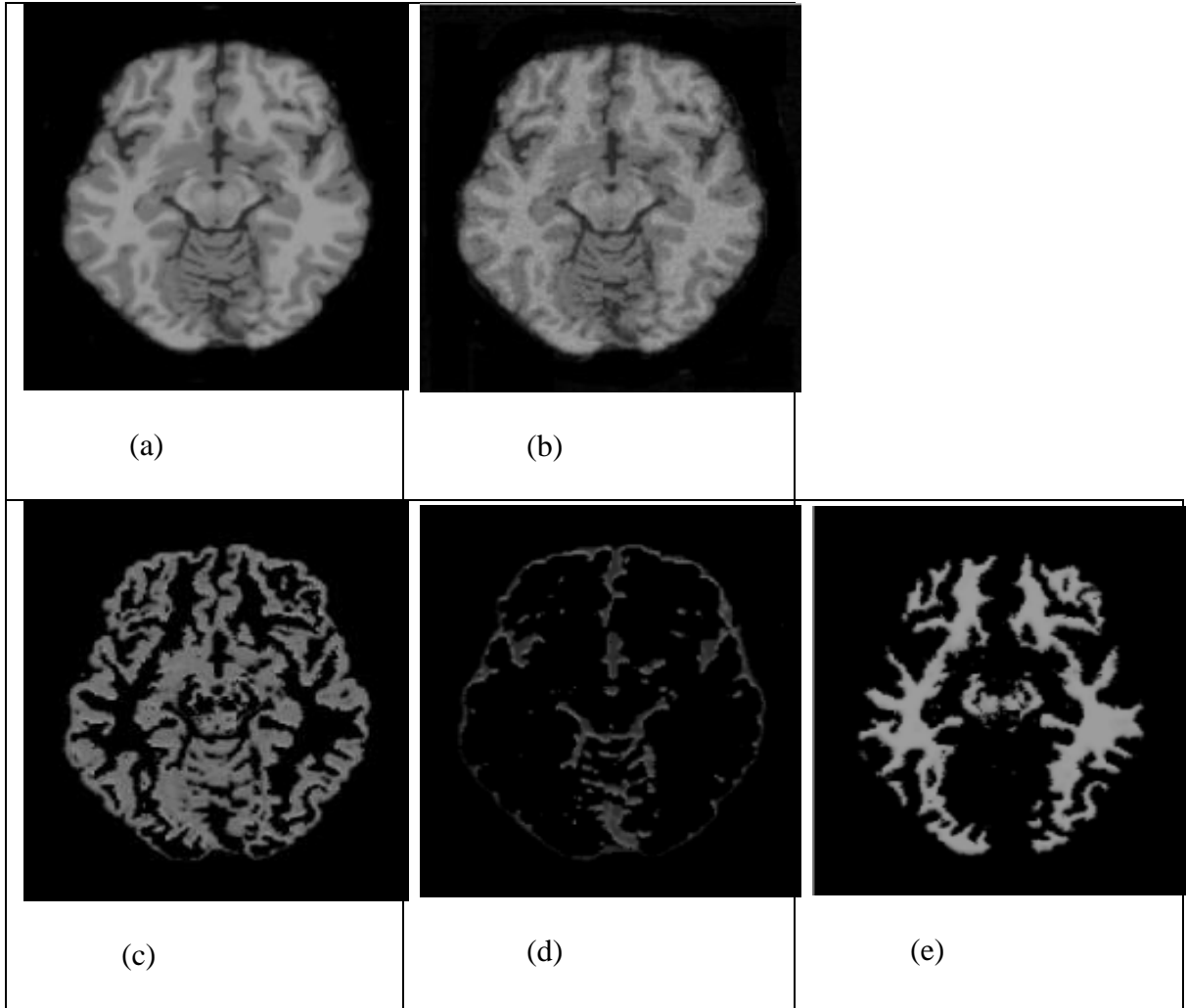
Figure 5.2: (a) Normal Brain(T1-weighted slice 60), (b) Normal brain (noise 3%), (c) Gray matter, (d) CSF, (e) White matter
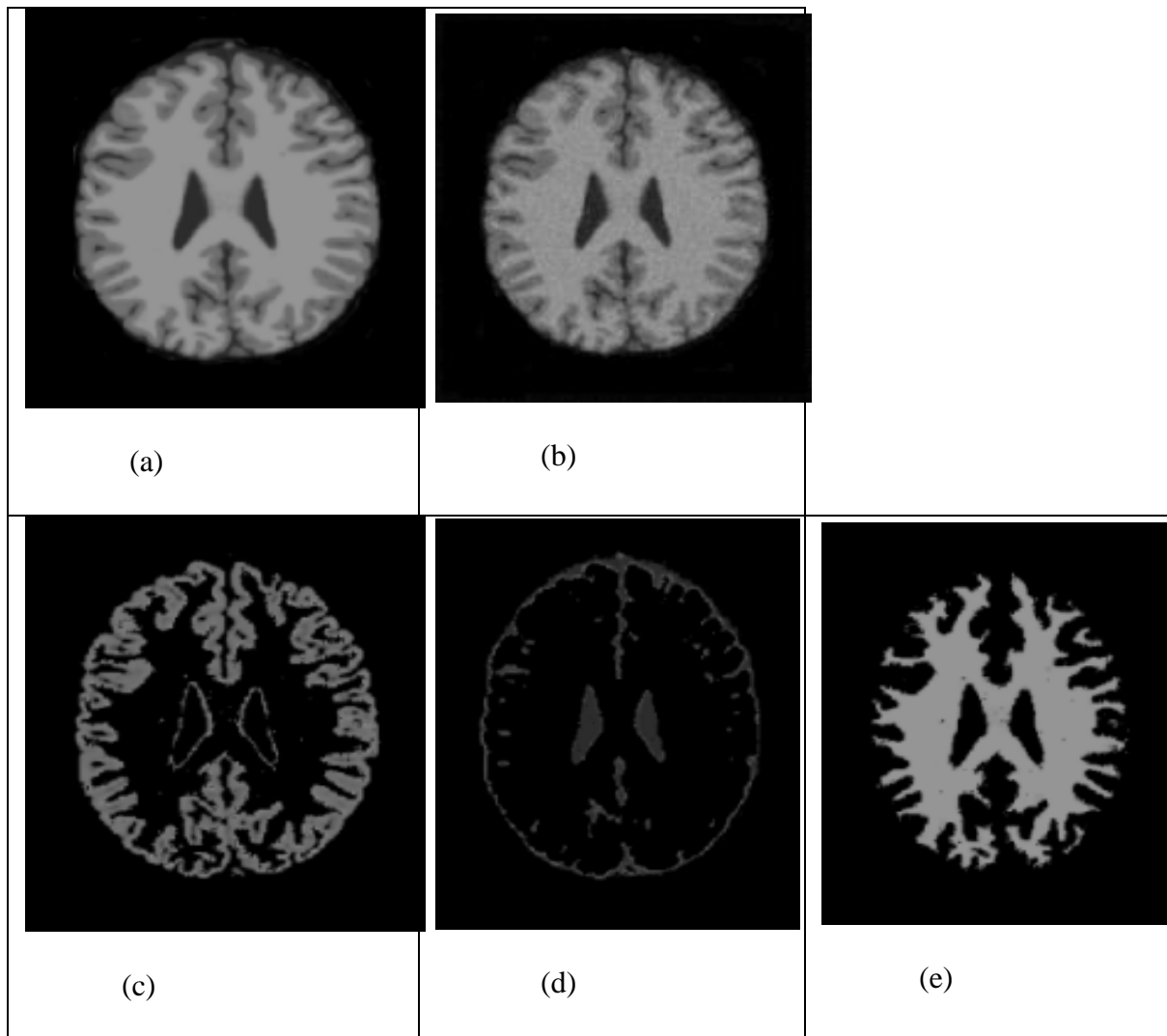
Figure 5.3: (a) Normal Brain(T1-weighted slice 99), (b) Normal brain (noise 5%), (c) Gray matter, (d) CSF, (e) White matter

5.6 Summary

In the chapter, image segmentation is done using 'Fuzzy Logic' technique. Step by step methodology for automated brain MRI image segmentation is presented. Classification of three main tissues of brain is performed. These tissues include- gray matter, white matter and cerebrospinal fluid. The Ant Colony Optimization technique is used to obtain the results of segmentation as ACO is a meta-heuristic approach that tends to give close to optimal solution. Also, inclusion of spatial information of pixels ensures better clustering as neighbouring pixels are more likely to belong to the same class/cluster. Consideration of geometrical shape of

clustering classes is also taken into account. Therefore, Mahalanobis distance is included to solve the purpose. Brain MRI acquisition are also subjected to random noise. Our work ensures better classification in presence of such noise as well. The results of our work have been evaluated and validated against ground truth. Both real time database and simulated database with varying level of noise is used to test the accuracy. Significant improvement in correct classification of brain tissues can be seen as compared to standard FCM.

Chapter 6

Fuzzy Clustering Using Gravitational Search Algorithm for Brain Images

6.1 Introduction

Clustering is a key activity in numerous data mining applications such as information retrieval, text mining, image segmentation. Clustering also plays a major role in medical image processing. Manual image segmentation is very tedious and time consuming. Also results of manual segmentation are subjected to errors due to huge and varying data. Therefore, automated segmentation systems are gaining enormous importance nowadays. This study presents an automated system for segmentation of brain tissues from brain MRI images. Segmentation of three main brain tissues is carried out namely white matter, gray matter and cerebrospinal fluid. In this work, we propose a clustering approach, Fuzzy-Gravitational Search Algorithm(GSA) and its application to MRI brain image segmentation. The proposed approach is based on GSA, and uses fuzzy inference rules for controlling the parameter α as search progresses. The results of the system are compared with GSA and recent work on brain image segmentation algorithms for both real and simulated database on the basis of Dice Coefficient values and is found to outperform.

6.2 Gravitational Search Algorithm

GSA is an optimization algorithm proposed by Rashedi[115] in 2009. It is based on the Newton's laws of gravity and motion. The law of gravity states that "Every particle in the universe attracts every other particle with a force that is directly proportional to the product of

85

the masses of the particles and inversely proportional to the square of the distance between them". By this definition, the gravitational force is determined using the following equation [115]:

$$F = G \frac{M_1 M_2}{R^2}$$

6.1

where, F is the gravitational force acting between two masses M_1 and M_2, G is the gravitational constant with a value of 6.67259×10^{-11} N m2/kg2, and R is the distance between the two masses.

Newton's second law of motion states that when a force acts on a mass, acceleration is produced. The magnitude of acceleration produced is obtained using the equation below [115]:

$$a = \frac{F}{M}$$

6.2

where, F and M denote the net force acting on a given particle and its mass, respectively.

The GSA employs this physical phenomenon for solving optimization problems. Consider a system with N masses or agents. The position of ith mass is defined as:

$$X_i = (x_i^1, \ldots, x_i^d, \ldots, x_i^n), \text{ for } i = 1, 2, \ldots, N,$$

6.3

where, x_i^d is the position of ith agent in d^{th} dimension and n is the total number of dimensions in the search space. The positions of agents correspond to the solutions of the problem. The mass of each agent is computed, after evaluating the present population's fitness, using the following equations:

$$m_i(t) = \frac{fit_i(t) - worst(t)}{best(t) - worst(t)}$$

6.4

$$M_i(t) = \frac{m_i(t)}{\sum_{j=1}^{N} m_j(t)}$$

6.5

where, $fit_i(t)$, denotes the fitness value of ith agent at time t, and best(t) and worst(t) are computed as follows(for minimization problems):

$$best(t) = \min fit_j(t) \, , \quad j = 1, 2, \ldots, N \tag{6.6}$$

$$worst(t) = \max fit_j(t) \, , \quad j = 1, 2, \ldots, N \tag{6.7}$$

Similarly, for maximization problems best(t) and worst(t) are computed by taking the maximum and minimum fitness values respectively.

The acceleration of an agent is computed next, by considering the total forces from a set of heavier masses using the laws of gravity and motion using Equations 6.8 and 6.9. The new velocity of an agent is computed next by adding a fraction of its current velocity to its acceleration (Equation 6.10), followed by the calculation of its new position (Equation 6.11).

$$F_i^d(t) = \sum_{j \in kbest, j \neq i} rand_j \, G(t) \frac{M_j(t)M_i(t)}{R_{ij}(t) + \varepsilon} \left(x_j^d(t) - x_i^d(t)\right) \tag{6.8}$$

$$a_i^d(t) = \frac{F_i^d(t)}{M_i(t)} = \sum_{j \in kbest, j \neq i} rand_j \, G(t) \frac{M_j(t)}{R_{ij}(t) + \varepsilon} \left(x_j^d(t) - x_i^d(t)\right) \tag{6.9}$$

$$v_i^d(t + 1) = rand_i \times v_i^d(t) + a_i^d(t) \tag{6.10}$$

$$x_i^d(t + 1) = x_i^d(t) + v_i^d(t + 1) \tag{6.11}$$

where, $rand_i$ and $rand_j$ are two random numbers uniformly distributed in the range of [0, 1], ε is a small value to prevent division by zero, $R_{ij}(t)$ is the Euclidean distance between agent i and agent j. kbest is the set of first K agents with best fitness values and thus, largest mass. kbest is dependent on time, initialized to Ko at the start and decreases as time progresses. The gravitational constant, $G(t)$, decreases with time to control the search accuracy. The value of $G(t)$ is calculated using the following equation:

$$G(t) = G_o e^{\frac{-\alpha t}{T}} \tag{6.12}$$

where, Go is the initial value of gravitational constant, α is a parameter which governs the degree of exploration versus exploitation of the search and T is the maximum number of iterations.

6.3 Proposed Work

In this chapter, an automatic framework for segmentation of brain tissue classes namely, white matter, gray matter and cerebrospinal fluid has been proposed. The brain MRI images are used for the purpose of segmenting these tissues. We describe the proposed method, called Fuzzy-GSA, for segmentation of brain images. The proposed approach is based on GSA, described in section 6.2 and uses fuzzy inference rules for controlling the parameter α as search progresses. This section is divided into two subsections. Section 6.3.1 describes the Fuzzy Inference System(FIS) developed, and the section 6.3.2 presents the proposed Fuzzy-GSA algorithm for clustering.

6.3.1 The Developed Fuzzy Inference System

The FIS is developed with two input variables and one output variable. The input variables are as follows:

IT: The current iteration number.

Fbest: The best value of fitness achieved till the current iteration.

IT enables us to consider how far we have reached in the search process. During the initial iterations, i.e. when *IT* is low, a lower value of α is desired since lower the value of α, higher the value of gravitational constant, *G(t)*, will be (Equation 6.12) and thus, higher the force, *F*, (Equation 6.8) resulting in a higher acceleration, *a*, (Equation 6.9) and velocity, *v(t)* (Equation 6.10). This allows for higher exploration at the beginning of search. Similarly, towards the final few iterations, i.e. when *IT* is high, a higher value of α is desired to promote higher exploitation. Figure 6.1 depicts the membership function for *IT*. The iterations are represented as a fraction of the maximum number of iterations allowed, such that 0.5 means half of the total iterations and 1 represents the maximum iterations.
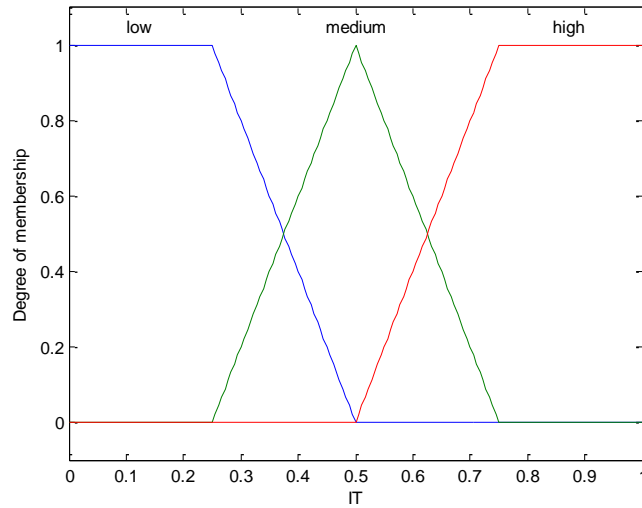
Figure 6.1: Membership Function for *IT*
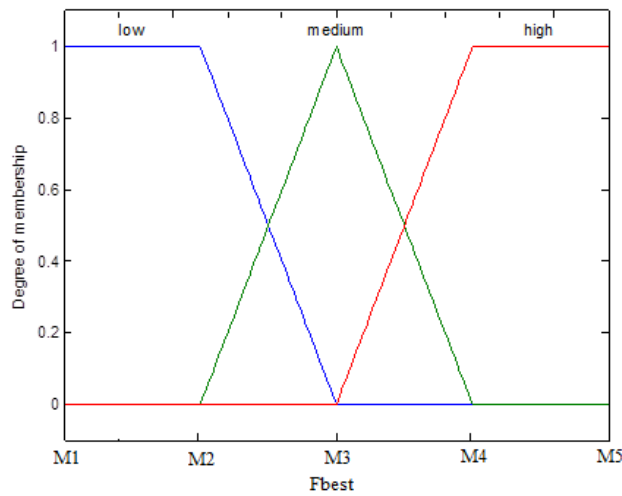
Figure 6.2: Membership Function for *Fbest*

Fbest represents the lowest value of fitness, since clustering is a minimization problem with the fitness function as mean square error, achieved till the current iteration. If the value of *Fbest* is high, then we need to reduce α to promote a greater exploration, since higher values for *Fbest* mean we are still far from the solution. However, if *Fbest* is low, we should increase α to allow

for a higher exploitation as we are near the solution. Figure 2 shows the membership function for *Fbest*. Note that the membership function for *Fbest* needs to be tuned as per the input dataset being considered, since the accepTable values of fitness function will vary for different datasets.

To obtain the marked value M5 in Figure 3, we executed five independent runs of GSA for a single iteration and equated M5 to the maximum value of *Fbest* obtained, after adding hundred and then rounding it off to the nearest hundred. For the value of M3, we considered the integer part of the best fitness value obtained using GSA, taken from [116], for that dataset. M4 was computed by adding one to the value of M3, and M2 was calculated by rounding off M3 to the nearest ten smaller than M3. Finally, M1 was obtained by subtracting ten from M2.

Note that the fitness function, representing the total mean square error or the sum of intra-cluster distances, is computed using the following equation [116]:

$$f(O, C) = \sum_{l=1}^{k} \sum_{O_i \in C_l} D(O_i, CC_l)^2$$

6.13

where, CC_l represents the centroids of the cluster C_l , $D(O_i, CC_l)$ denotes the distance or dissimilarity between object O_i and cluster centroid CC_l. The most popular and widely used distance metric is the Euclidean distance, which we have used in this work. Euclidean distance between two objects X_i and X_j with d dimensions is calculated as:

$$D(X_i, X_j) = \sqrt{\sum_{p=1}^{d} (x_i^p - x_j^p)^2}$$

6.14

where, x_i^p denotes the value of pth dimension for the object X_i and x_j^p denotes the value of pth dimension for the object X_j.

The developed FIS consists of one output variable, i.e. *alpha(t)*, which denotes the value of parameter α in Equation 6.12. Figure 6.3 shows the membership function for *alpha(t)*. The range of parameter α is taken as [0, 50] to provide a wide range of search on the value of *alpha(t)*.
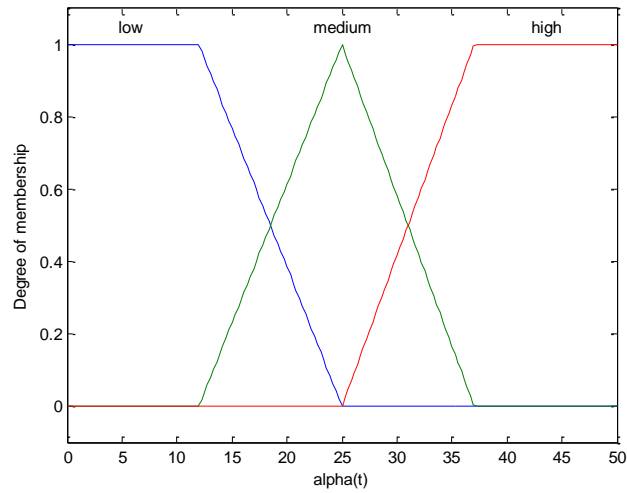
Figure 6.3: Membership Function for *alpha(t)*

The following eight fuzzy rules were formulated to control the parameter α in the calculation of the gravitational constant (Equation 6.12):

RULE 1: If (*IT* is low) and (*Fbest* is low) then (*alpha(t)* is high)

RULE 2: If (*IT* is low) and (*Fbest* is medium) then (*alpha(t)* is medium)

RULE 3: If (*IT* is low) and (*Fbest* is high) then (*alpha(t)* is low)

RULE 4: If (*IT* is medium) and (*Fbest* is high) then (*alpha(t)* is low)

RULE 5: If (*IT* is medium) and (*Fbest* is medium) then (*alpha(t)* is medium)

RULE 6: If (*IT* is high) and (*Fbest* is high) then (*alpha(t)* is medium)

RULE 7: If (*IT* is high) and (*Fbest* is medium) then (*alpha(t)* is medium)

RULE 8: If (*IT* is high) and (*Fbest* is low) then (*alpha(t)* is high)

The method used in the developed fuzzy inference system for "And" is min and for "Or" is max. The implication method is min, aggregation method is max and defuzzification method is centroid.

6.3.2 Fuzzy Gravitational Search Algorithm

The proposed algorithm, Fuzzy-GSA, comprises of two main steps. The first step is to generate an initial population for GSA. We have generated the initial population by considering three agents (or candidate solutions) corresponding to the maximum, minimum and median values for all features in a given dataset, respectively. This provides a better initial population which would allow for a higher exploration since a wide range of values, including maximum, minimum and median, are present while searching the solution space. The rest of the agents are generated randomly by considering the range of features in the given dataset.

The second step involves application of GSA, described in section 6.2, to the given dataset and using the fuzzy inference system developed to control the parameter α while searching for the solution. The flow diagram for the proposed Fuzzy-GSA algorithm is depicted by Figure 6.4. The step by step algorithm for the proposed approach is stated next. Let N denote the population size, Ci be the ith candidate solution or agent, k be the number of clusters, d be the number of features in a given dataset.

Step 1: Generate initial population, *P = {C1, C2, . . . , CN}*.

- Generate *C1* consisting of maximum values of all the features.

- Generate *C2* consisting of minimum values of all the features.

- Generate *C3* consisting of median values of all the features.

- Generate the remaining N-3 candidates randomly within the range of minimum to maximum values for all features.

Step 2: Apply GSA and use the developed FIS, described in Section 6.3.1, for parameter adaptation.

- Calculate the fitness function, as per Equation 13, for all the candidate solutions.

- Feed the values of *IT*, current iteration number, and *Fbest*, best fitness achieved, as inputs to the developed FIS, and obtain the value of parameter α.

- Calculate *G, F, M* and *a* for all the candidate solutions using Equations 5, 8, 9 and 12 as described in the Gravitational Search Algorithm (GSA).

- Update the velocity and position of each candidate solution as per Equation 10 and 11 respectively.

- Check if termination criteria, i.e. maximum number of iterations allowed is reached or fitness function is not exhibiting a minimum improvement, are met. If yes, then return the best value of fitness function achieved as the final solution, else reiterate through step 2.

The final solution consists of the best value of fitness function, i.e. the minimum mean square error, achieved by running the proposed Fuzzy-GSA algorithm.

6.4 Experimental Results & Discussions

The algorithm is implemented on personal computer (2.40 GHz CPU, 4GB RAM) using MATLAB R2010a. We have considered the population size to be 50, i.e. $N = 50$, and the maximum number of iterations to be 300. G_o in Equation 6.12 is taken as 100. The minimum acceptable improvement in the fitness values between two successive iterations is set as 1×10^{-6}. Each candidate solution, in the population, consists of cluster centers for each of the k clusters, and each cluster center comprises of values for each feature in a dataset. Figure 6.5 illustrates the representation of the ith candidate solution C_i. CC_{ij} denotes the jth cluster center of the ith

candidate solution and F_{ij} represents the value of jth feature for i^{th} cluster center. Therefore, each candidate solution consists of $(d \times k)$ values. Here, the value of $k=3$.
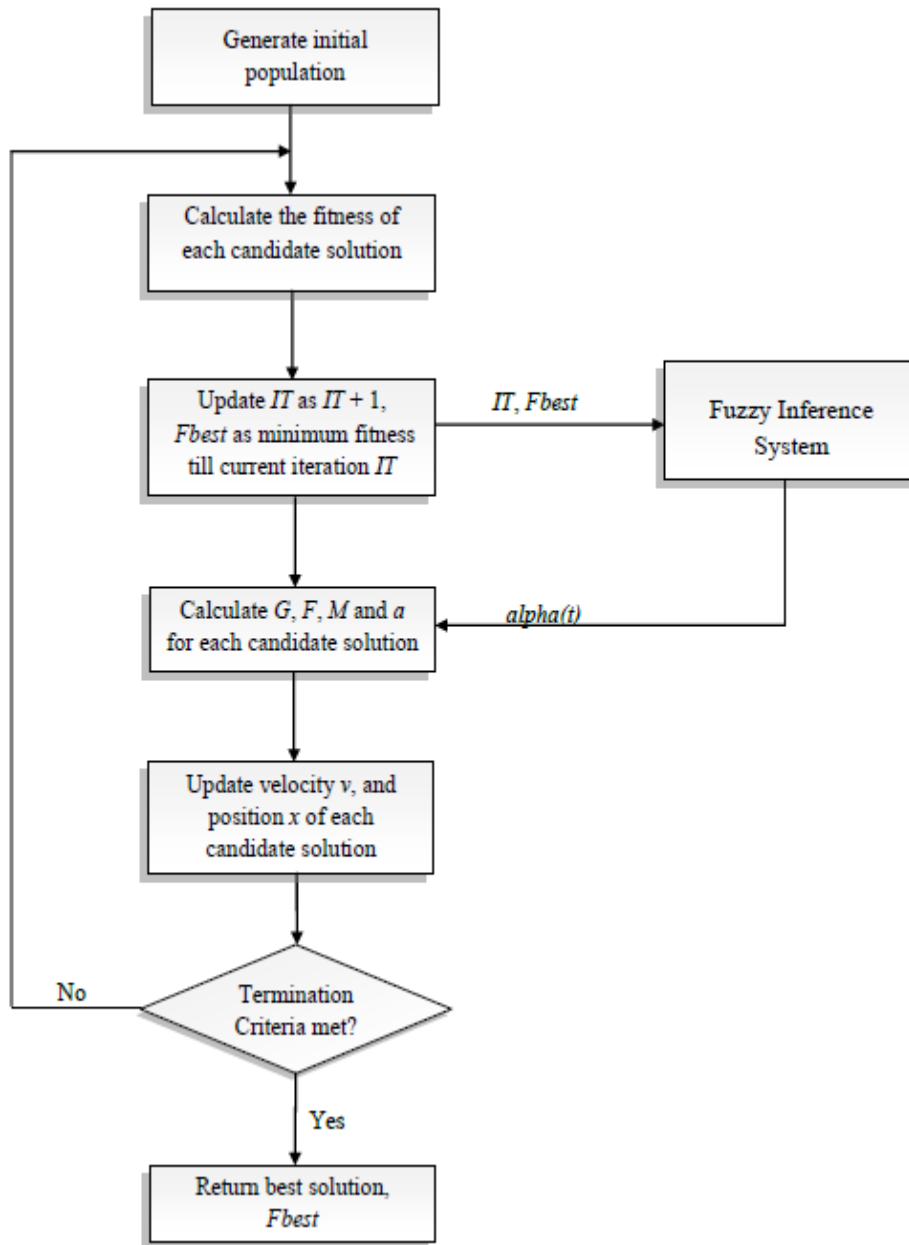

Figure 6.4: Flowchart for Fuzzy GSA algorithm

$$\begin{array}{|c|c|c|c|} \hline F_{11} & F_{12} & \ldots & F_{1d} \\ \hline \end{array}$$

$$\begin{array}{|c|c|c|c|} \hline CC_{i1} & CC_{i2} & \ldots & CC_{ik} \\ \hline \end{array}$$
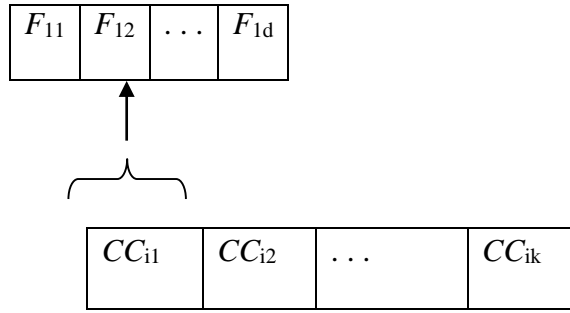
Figure 6.5: Representation of ith Candidate Solution, C_i

The real time database of Brain MRI images has been taken from Insight Journal. Insight Journal is an Open Access on-line publication that covers domain of medical image processing and visualization. One of its journals is MIDAS. Midas community include National Alliance for medical image computing (NAMIC) which presents the data for two autistic and two normal children (male and female).[113] Three type of MRI scanning is presented i.e. T1 weighted, T2 weighted, PD weighted images. Coronal slices are obtained with slice thickness of 1.5mms. Also the tissue segmentation label map is presented with the database. This tissue label is atlas based segmentation by making use of expectation-maximization scheme. The quantitative analysis of MRI brain images is done in comparison with the ground truth images for the sample image shown in Figure 6.6 and is presented in Table 6.1. True positive gives the measure of the correctly classified pixels. Whereas False positive counts the total number of pixels that our system classifies but is not present in ground truth and True negative counts the total number of pixels that our system doesn't classifies but is present in the ground truth as belonging to particular cluster. In the Table sensitivity is also calculated to measure the performance of the proposed approach. Here, we can see that average sensitivity is 0.926. Sensitivity in general can be calculated as

Sensitivity=TP/(TP+FN)

Where, TP is True Positive and FN is False Negative

95

Table 6.1 Classification of pixels for FUZZY GSA for real time MRI database

[37] Patient #	Ground Truth	True positive	False negative	False Positive	Sensitivity
Autistic Female slice100	34482	30110	4372	2012	0.873
Autistic Female slice140	33936	31569	2367	3982	0.930
Control Female slice80	33056	31247	1809	3250	0.945
Control Female slice114	28503	25727	2776	4981	0.903
Control Male slice110	33528	29653	3875	4905	0.884
Control Male slice67	39125	36728	2397	4286	0.939
Autistic Male slice70	30248	30118	130	2872	0.996
Autistic Male slice160	10960	10342	618	653	0.944

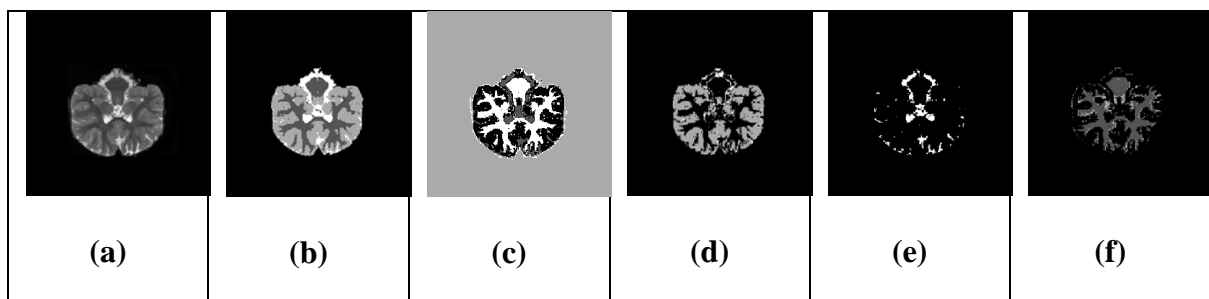| **(a)** | **(b)** | **(c)** | **(d)** | **(e)** | **(f)** |

Figure 6.6: (a)Autistic Female T2-weighted MRI(slice 140), (b)Ground truth, (c)

Segmentation result, (d) Gray matter, (e) CSF, (f) White matter

The Dice Coefficient(DC)[108] is defined as

$$DC(Y,Z) = 2(|Y \cap Z|)/(|Y| + |Z|)$$ 6.15

where Y and Z are two sets. The value of DC lies between 0 and 1. 0 signifies no match/overlap and 1 signifies complete match/overlap. In terms of segmentation, 'Y' represents the segmented image containing tumor and 'Z' represents the ground truth given by the radiologist.

Table 6.2 This Table presents the value of DC for three brain tissues namely, Gray matter, White matter, CSF using our approach(FUZZY GSA) and GSA

	FUZZY GSA				GSA		
	DC				DC		
Patient #	GM	WM	CSF	Patient #	GM	WM	CSF
P11	0.992	0.967	0.86	P11	0.932	0.871	0.631
P12	0.994	0.991	0.886	P21	0.873	0.862	0.699
P21	0.989	0.996	0.972	P21	0.862	0.846	0.815
P22	0.995	0.972	0.839	P22	0.9	0.782	0.688
P31	0.982	0.976	0.891	P31	0.869	0.799	0.681
P32	0.987	0.952	0.891	P32	0.872	0.843	0.739
P41	0.99	0.994	0.962	P41	0.899	0.876	0.867
P42	0.996	0.929	0.959	P42	0.924	0.782	0.714
Average	**0.991**	**0.972**	**0.908**	**Average**	**0.891**	**0.833**	**0.729**

The algorithm is run over several slices of both normal and autistic male and female dataset provided by NIMAC. The average of several runs was calculated using DC and is tabulated in Table 6.2. It is observed that the significant improvement can be seen in the result obtained from

our approach (FUZZY-GSA) as compared to GSA .The classification of brain tissues is more promising in case of FUZZY GSA as there are more number of correctly classified pixels.

The more the value of DC is close to 1, the better is the segmentation accuracy. It is studied that DC's value >0.7 implies good segmentation. Similar to DC is the JS measure. Both these parameters are not sensitive to volume overestimations and underestimations. However, DC is more famous than JS as it may sometimes result in a mismatch when there is a strong volumetric overlap. We have presented the estimated results in Table 6.3 using JS as well to have a better outlook of classification system.

In above Table patient numbers refers to following slices of dataset:

P11-5074-004-02_10_t2_fit.nnrd (slice 100)   P12- 5074-004-02_10_t2_fit.nnrd (slice 140)

P21-5128-004-01_10_T2_fit.nrrd (slice 80)   P22-5128-004-01_10_T2_fit.nrrd (slice 114)

P31-5150-004-02_10_T2_fit.nrrd (slice 110)   P32-5150-004-02_10_T2_fit.nrrd (slice 67)

P41-5157-004-02_10_T2_fit.nrrd (slice 70)   P42-5157-004-02_10_T2_fit.nrrd (slice 160)
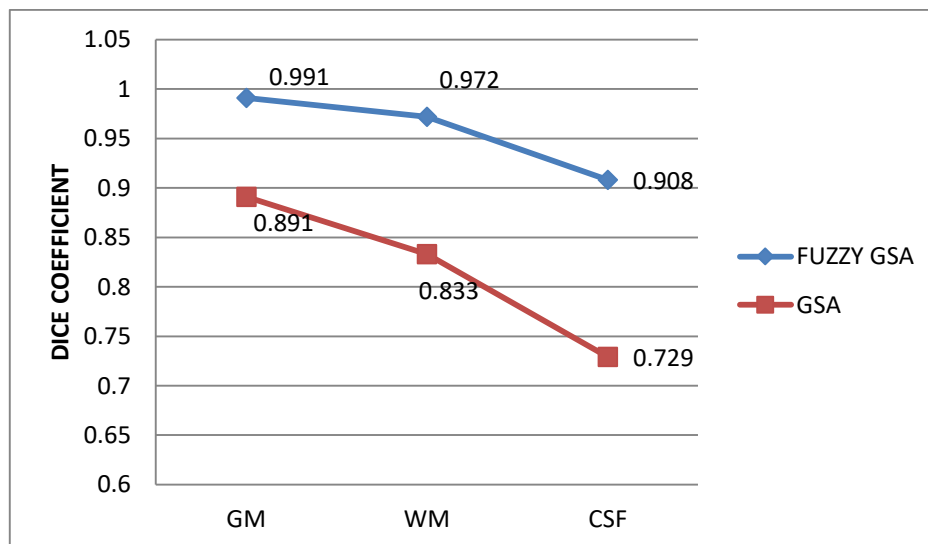

Figure 6.7: Comparison of DC values for GSA and Fuzzy GSA

It can be noticed that classification/segmentation accuracy is highly dependent upon the classification of cerebrospinal fluid. The accuracy of both gray matter and white matter tissues is also improved but significant change can be seen in case of segmentation of CSF tissue. CSF is a very complex tissue (fluid flowing in our brain). It is sometimes difficult to segment such a flowing matter from brain MRI. Therefore there is a requirement to get better classification of data points belonging to CSF class. This improvement can be seen in our approach as compared to standard FCM.

The FUZZY GSA approach for segmenting brain MRI images is also applied and validated for simulated 3D brain MRI images with varying level of noise from brain web database. The simulated dataset from brain web is provided by McGill University and can be obtained with different file extensions. [114] It contains normal anatomical brain structures with size of each image is 181*217. The results are tested and validated for T1-weighted images with 3%, 5% noise levels and slice thickness of 1mm in Table 6.3.

Table 6.3 This Table presents the value of DC for three brain tissues namely, Gray matter, White matter, CSF using our approach(FUZZY GSA) and GSA for Brain Web database

Slice#	Noise	GM	WM	CSF	Avg.	Slice#	Noise	GM	WM	CSF	Avg.
60	3%	0.981	0.938	0.827	0.912	60	3%	0.956	0.868	0.844	0.889
88	3%	0.985	0.973	0.914	0.941	88	3%	0.892	0.955	0.857	0.901
100	3%	0.968	0.985	0.846	0.924	100	3%	0.901	0.967	0.792	0.887
AVG.		**0.978**	**0.965**	**0.86**	0.926	**AVG.**		**0.916**	**0.93**	**0.831**	0.892

99	5%	0.973	0.981	0.866	0.923	99	5%	0.918	0.967	0.687	0.857
126	5%	0.962	0.927	0.883	0.918	126	5%	0.924	0.862	0.846	0.877
100	5%	0.945	0.973	0.847	0.911	100	5%	0.895	0.968	0.829	0.897
AVG.		**0.960**	**0.960**	**0.865**	0.918	**AVG.**		**0.912**	**0.932**	**0.787**	0.877
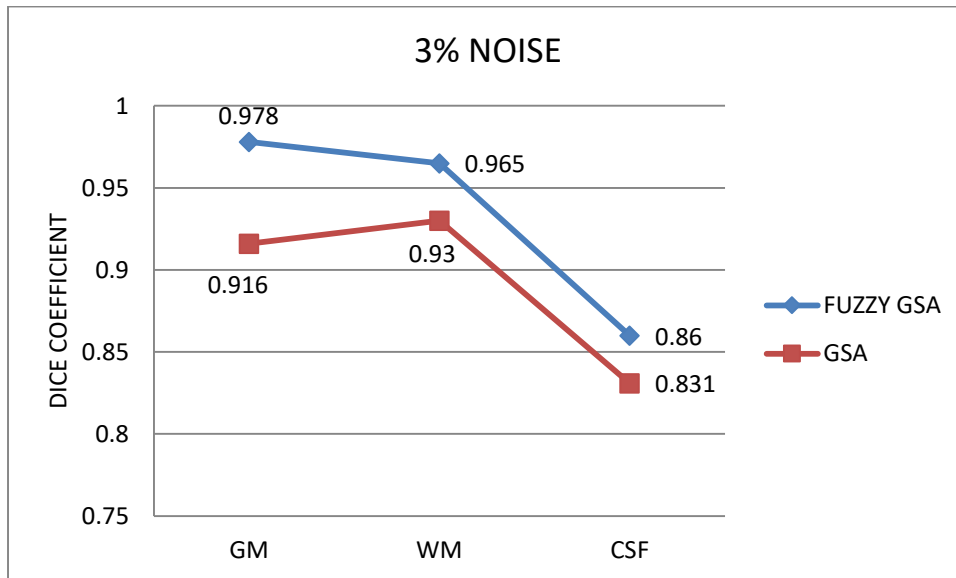
Figure 6.8: Comparison of DC values for GSA and Fuzzy GSA with noise level 3%

It can be noticed from Table 6.3 that FUZZY GSA performs better for both levels of noise as compared to GSA. The efficiency of GSA is reduced with higher level of noise as can be seen in Figure 6.7, Figure 6.8 and Figure 6.9. This can be seen from the slice 100 corrupted with both 3% and 5% noise. Accuracy of FCM reduces significantly whereas FUZZY GSA performs efficiently in higher level of noise as well.
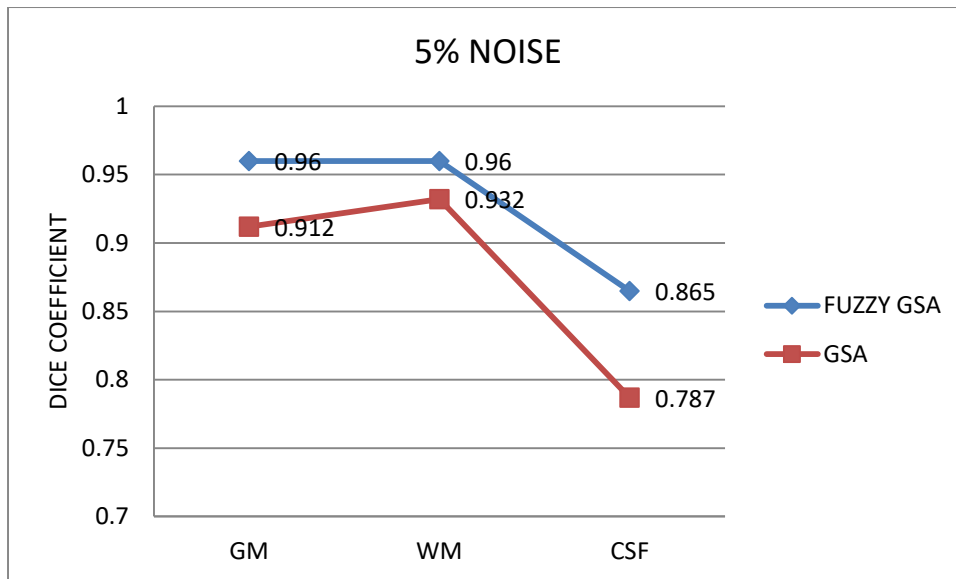
Figure 6.9: Comparison of DC values for GSA and Fuzzy GSA with noise level 5%
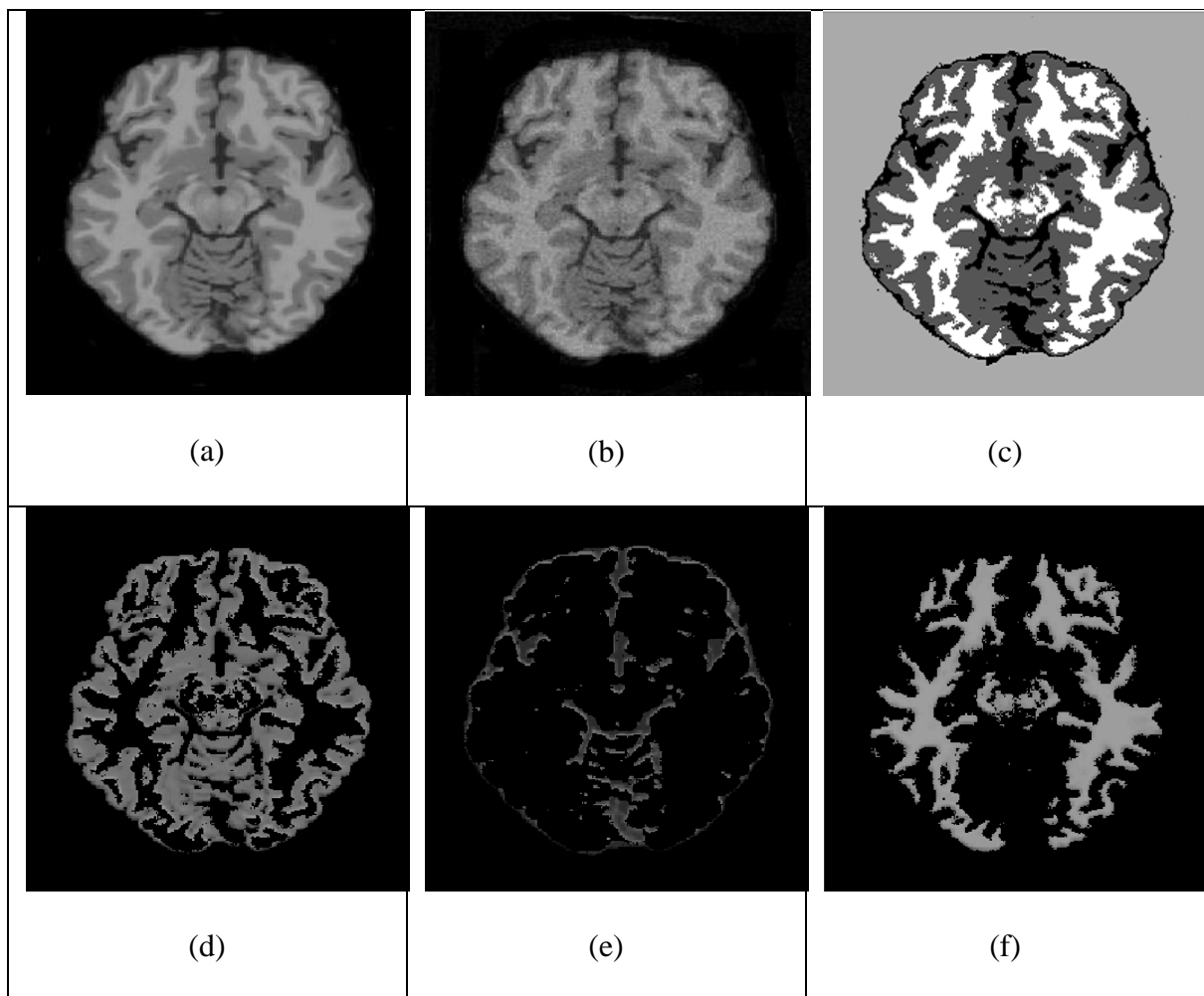
Figure 6.10. (a) Normal Brain(T1-weighted slice 60), (b) Normal brain (noise 3%), (c)

Segmented result using FUZZY GSA, (d) Gray matter, (e) CSF, (f) White matter

101
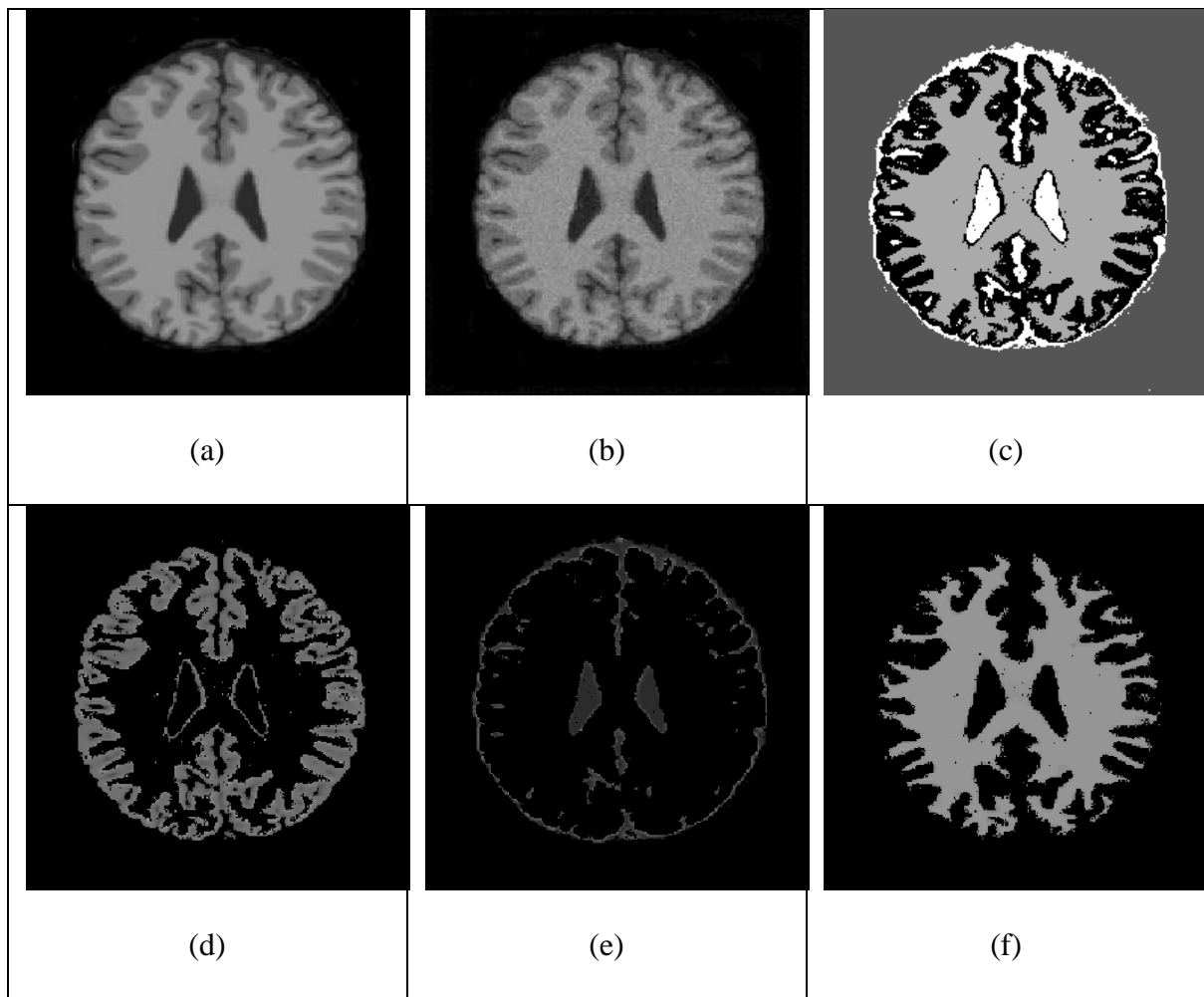
Figure 6.11. (a) Normal Brain(T1-weighted slice 99), (b) Normal brain (noise 5%), (c)

Segmented result using FUZZY GSA, (d) Gray matter, (e) CSF, (f) White matter

It can be noticed from Table 6.4 that FUZZY GSA performs better for both levels of noise as compared to GSA. The efficiency of GSA is reduced with higher level of noise as can be seen in Figure 6.7, Figure 6.8 and Figure 6.9. This can be seen from the slice 100 corrupted with both 3% and 5% noise. Accuracy of FCM reduces significantly whereas FUZZY GSA performs efficiently in higher level of noise as well.

The results of the proposed Fuzzy GSA algorithm are also compared with Growing Hierarchical Self Organising Map(GHSOM), Non-Local FCM(NLFCM), Improved Spatial FCM(IFCMS), combination of Mean Shift and FCM (MFCM), Local Information based Intutionistic

FCM(IIFCM), Repeated Level Set(RLS), Convolutional Neural Network(CNN), Non Local based Spatially Constrained Hierarchical FCM(NLSCHFCM), Improved FCM(IFCM), Generalised Rough Intuitionistic FCM(GRIFCM), Fuzzy Unsupervised Learning(FUSL) and Intutionistic Fuzzy Co-Clustering(IFCC) algorithm. Also, the comparison with the algorithms is done with varying levels of noise (3% and 5%). As, we can see from Table 6.4 that the proposed algorithm outperforms other segmentation algorithms and has the ability to accurately segment the brain images in the presence of noise as well.

Table 6.4: Comparative performance analysis of DC values for different segmentation algorithms on brain image with varying noise level.

| | | NOISE | | | | | | | | |
| | | 0% | | | 3% | | | 5% | | |
AUTHOR	ALGORITHMS	GM	WM	CSF	GM	WM	CSF	GM	WM	CSF
Ortiz's[73]	GHSOM	0.714	0.625	0.623	0.701	0.612	0.609	0.678	0.601	0.589
Chen 's[74]	NLFCM	0.785	0.773	0.630	0.747	0.685	0.621	0.724	0.687	0.617
Benaichouche's [75]	IFCMS	0.769	0.724	0.701	0.731	0.672	0.614	0.718	0.657	0.603
Mahmood's[66]	MFCM	0.795	0.705	0.676	0.768	0.693	0.662	0.748	0.710	0.649
Verma's[76]	IIFCM	0.881	0.842	0.846	0.854	0.792	0.724	0.832	0.757	0.711
Roy's[36]	RLS	0.891	0.864	0.850	0.834	0.803	0.794	0.812	0.773	0.729
Moeskops's [77]	CNN	0.923	0.891	0.882	0.919	0.871	0.811	0.894	0.800	0.782
Chen's[78]	NLSCHFCM	0.911	0.903	0.816	0.903	0.872	0.781	0.881	0.827	0.760
Kalaiselvi's[68]	IFCM	0.861	0.811	0.674	0.804	0.717	0.657	0.799	0.769	0.620
Namburu's[79]	GRIFCM	0.931	0.916	0.852	0.910	0.861	0.836	0.891	0.848	0.804
Keyvan's[80]	FUSL	0.938	0.922	0.851	0.919	0.892	0.838	0.899	0.857	0.824
Verma's[81]	IFCC	0.985	0.964	0.900	0.970	0.948	0.846	0.957	0.943	0.850
Proposed	FUZZY GSA	0.991	0.972	0.908	0.978	0.965	0.86	0.960	0.960	0.865

6.5 Summary

In this chapter we proposed an algorithm Fuzzy-GSA for MRI brain image segmentation which is based on the conventional GSA with a provision for adapting the value of parameter α used in the calculation of the gravitational constant. In the beginning, a smaller value of α is desired to achieve a higher exploration, whereas towards the end of search, a relatively higher value of α helps in achieving a higher exploitation. Step by step methodology for automated brain MRI image segmentation is presented. Classification of three main tissues of brain is performed. These tissues include- gray matter, white matter and cerebrospinal fluid. The performance of Fuzzy-GSA is evaluated in comparison with GSA by performing experiments on real time database and simulated database with varying level of noise. The proposed algorithm is also compared on the basis of DC values with various brain image segmentation algorithms and is seen to outperform even in the presence of noise.

Chapter 7

Hamming Distance based Local Binary Pattern for Biomedical Image Retrieval

7.1 Introduction

Patient diagnosis databases are available in a variety of formats, including computer tomography, magnetic resonance imaging, ultrasound, and X-ray. However, it is impossible to make use of this information unless it is arranged in a way that allows for easy access, search, and retrieval. Content-based biomedical image retrieval was created to solve this issue. The visual contents of a picture, such as colour, texture, form, faces, and spatial arrangement, are used to represent and index the image database in content-based image retrieval [82]. Automatic retrieval of images is of great importance in medical field as it helps in decision making for solving various problems. The feature extraction in content-based image retrieval is a crucial stage whose success is determined on the approach used to extract characteristics from pictures. There are two types of visual content descriptors: global and local. To describe an image, a global descriptor describes the visual features of the entire image, whereas a local descriptor represents the visual features of areas or objects. These are arranged as multi dimensional feature vectors and construct the feature database [117,118]. In this thesis, we have proposed a novel feature descriptor based on local binary pattern for retrieval of biomedical images. After obtaining the features the distance measure is used to retrieve the most similar images. The flowchart for image retrieval is depicted in Figure 7.1.
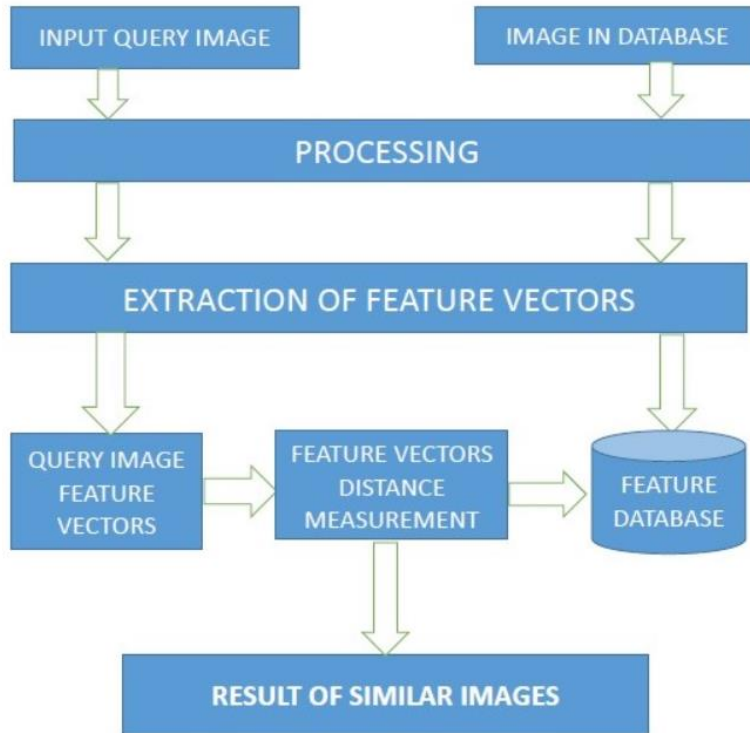
Figure 7.1: Flowchart for Image Retrieval

7.2. Review of Local Patterns

7.2.1 Local Binary Patterns(LBP)

Ojala *et al*. [84] initially introduced the LBP operator as a means for texture descriptor. In his basic LBP method, a binary code for each pixel of the image has been generated based on thresholding the 3 x 3 neighborhood of the pixel with the value of the center pixel and these binary values are concatenated in a clockwise direction starting from top-left neighbor (Figure 7.2 for illustration). The binary codes are converted into decimal number to label the pixel and termed as LBPs or LBP codes [84].

The local primitives like edges, spots, flat areas etc can be coded by the LBP method as shown in Figure 7.3.
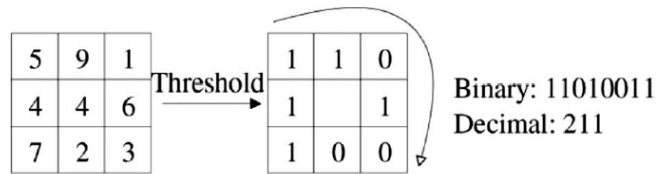
Figure 7.2 The basic LBP operator [85]
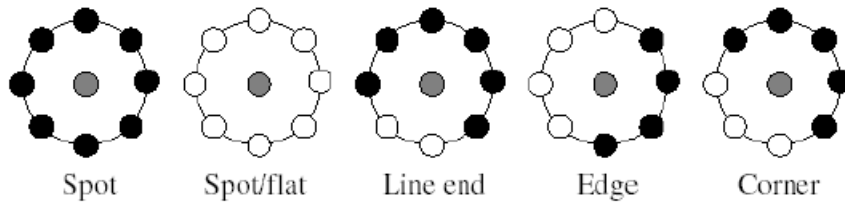
Figure 7.3 Texture primitives which can be detected by LBP [85]

The fixed 3 x 3 neighborhood may not capture the dominant features with large-scale structures. Hence to handle such texture, varying size neighborhood have been proposed by Ojala *et al.* [84]. The local neighborhood has been defined circularly in place of square and bilinear interpolation was employed to obtain value of sampling points not lying on a pixel. This generalization allowed flexibility in number of sampling points and radius of circle as shown in Figure 7.4 below. The *(P, R)* notation denotes *P* equally spaced sampling points lying over the circle of radius *R*.

Figure 7.4 Examples of Extended LBP operator : (8,1) , (16,2) and (24,3) circular

neighborhood

Writing in a more formal way, the ELBP code can be obtained in decimal number as follows[84]:

$$LBP_{P,R}(x,y) \ = \ \sum_{P=0}^{P-1} s(i_P - i_c)2^P \qquad 7.1$$

where(x,y) is the given central pixel with intensity i_c and i_P is the intensity of Pth neighboring pixel lying on the circle of radius R. The function $s(x)$ can be defines as:

$$s(x) \ = \ f(x) = \begin{cases} 1, & if \ x < 0 \\ 0, & if \ x \geq 0 \end{cases} \qquad 7.2$$

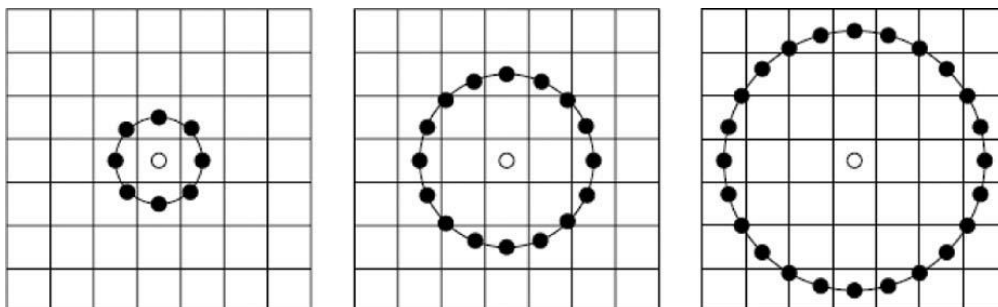The feature vector to describe the texture is the histogram of LBP labeled image. Ahonen *et al.* [92]reported that 90.6% of patterns in (8,1) neighborhood and 85.2% in (8,2) neighborhood are uniform while experimenting on FERET database. The concept of uniform patterns paved the way to a much reduced feature vector by accumulating the non-uniform patterns in a single bin while putting all the uniform patterns separately. Following this criterion, the histogram reduced to 59 bins in case of $LBP^{U2}_{(P,R)}$ against256 bins in standard LBP. The histogram of the LBP labeled image can be defined as[83].

$$H_i \ = \ \sum_{x,y} I(f(x,y) = i), \quad i = 0,1, \dots .. n - 1 \qquad 7.3$$

with n different labels produced by LBP operator and

$$I(A) = \begin{cases} 1, & A \ is \ true \\ 0, & A \ is \ false \end{cases} \qquad 7.4$$

This histogram forms the feature vector having local micro-pattern information like edges, spots and flat areas over the whole image [84]. Thus a statistical representation of the image is obtained, it can be visualized as a composition of micro-patterns and hence to describe them, the suitability of LBP is justified theoretically and later on experimentally by many studies[84, 85, 86].The micro-patterns encoded using LBP over the whole image does not contain their location and shape. So a block-based approach has been proposed in which the image is divided

into small regions $R0, R1, ... Rm$ and individual histogram were extracted from each region. The final, spatially enhanced, global feature vector is obtained by concatenating all the region specific histograms and is given as:

$$H_{i,j} = \sum_{x,y} I(f(x,y) = i) \; I((x,y) \in R_j) i = 0,1, ... n-1 \; and \; j = 0,1, ... m-1 \qquad 7.5$$

LBP methodology has been extensively researched and modified over different aspects. Some of the major modifications are carried out to increase the discriminative capacity and neighborhood selection to obtain better performance while not increasing much of the computational cost [86]. An Improved LBP ($ILBP$), which compares the neighboring pixels including the center pixel with the mean value of the window was proposed by Jin *et al*. [86]. But their method has increased the feature vector length by 511 ($2^9 - 1$, as all zeros and ones are the same).

7.2.2 Spatiotemporal LBP

Recently, dynamic feature extraction methods have been evolved over the years [87]. There are two spatiotemporal local pattern approaches: Volume Local Binary Pattern ($VLBP$) and LBP from Three Orthogonal Planes ($LBP - TOP$) by Zhao *et al*.[85]. They have reported that the LBP-TOP generates significantly less feature vectors as compared to VLBP with comparable accuracy of recognition. The dynamic texture (DT) analysis is performed over the sequence of image frames.

The basic LBP-TOP descriptor is further extended to block-level, but with a huge increase in the length of feature vector. Further, the concept of uniform pattern was also incorporated in LBP-TOP. Zhao *et al*. in[88] have reported an overall recognition rate of 96.26% using the LBP-TOP DT descriptors. [89].

Figure 7.5 shows the basic procedure of obtaining LBP-TOP feature vector.
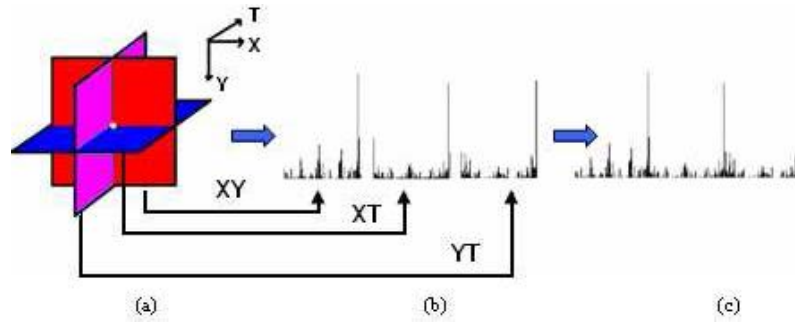
Figure 7.5 (a) Three DT planes (b) respective LBP histograms from three planes

(c) concatenated feature histogram[88]

7.2.3 Local Diagonal Extrema Patterns (LDEP)

Dubey *et al*. [89] proposed this new and efficient feature descriptor for CT image retrieval. They have considered only the diagonal and the center pixels in a $3 \, x \, 3$ neighborhood to obtain a binary representation of the center pixel. The method has reduced the feature vector dimensionality to 24 as against 59 in case of $LBP_{(P,R)}^{U2}$.

Since both the CT images are characterized primarily by their texture, hence the LDEP method proposed in [89] has been proven to be worthwhile.

First-order diagonal derivatives were used to obtain the values and indexes of local diagonal extremas. The discriminating ability of the feature vector is enhanced using the relationship of center pixel with local diagonal maxima and minima (extremas).

7.2.4 First-order Local Diagonal Derivatives

It has been reported by Gupta *et al*. [90] that most of the local information is contained in diagonal elements. This gives the justification behind use of diagonal elements only.

110

Formally, let $P_t^{i,j}$ be the tth diagonal neighbor of the pixel $P^{i,j}$ at a distance of R pixels, where $t \in [1,4]$ in a gray scale image M with m_1 rows and m_2 columns. Let $I_t^{i,j}$ and $I^{i,j}$ are the intensity values of $P_t^{i,j}$ and $P^{i,j}$ respectively as shown in Figure 6.5. $I_t^{i,j}$ is defined as

$$I_t^{i,j} = I^{i+\alpha, j+\beta} \tag{7.6}$$

where, α and β are constants defined as

$$\alpha, \beta = \begin{cases} -R, +R & t = 1 \\ -R, -R & t = 2 \\ +R, -R & t = 3 \\ +R, +R & t = 4 \end{cases} \tag{7.7}$$

where, $t \in [1,4]$ and $\gamma \in [0,2]$. Figure 7.6 illustrates an example image patch and the first-order derivatives of diagonal elements with three values of $\gamma = 0,1,2$.

7.2.5 Local Diagonal Extrema Pattern

The local diagonal extrema pattern for a pixel $P^{i,j}$ is a binary pattern denoted as $LDEP^{i,j}$ and is generated as

$$LDEP^{i,j} = (LDEP_1^{i,j}, LDEP_2^{i,j}, \dots \dots \dots \dots \dots, LDEP_{dim}^{i,j}) \tag{7.8}$$

where, dim is the length of the $LDEP$ pattern.

$LDEP_k^{i,j}$ is the kth element of the $LDEP^{i,j}$ pattern and is obtained using following equations:

$$LDEP_k^{i,j} = \begin{cases} 1, & if\ k = (\tau_{max} + 8\delta)\ or\ k = (\tau_{min} + 4 + 8\delta) \\ 0, & otherwise \end{cases} \tag{7.9}$$

where, δ is the factor representing the extrema-center relationship and is given as

$$\delta = \begin{cases} 0, & if\ (sign(\Delta_{max}^{i,j}) = 0\ and\ sign((\Delta_{min}^{i,j}) = 0) \\ 1, & if\ (sign(\Delta_{max}^{i,j}) = 1\ and\ sign((\Delta_{min}^{i,j}) = 1) \\ 2, & otherwise \end{cases} \tag{7.10}$$

and $\Delta_{max}^{i,j}$ and $\Delta_{min}^{i,j}$ are given as

$$\Delta_{min}^{i,j} = I_{\tau_{min}}^{i,j} - I^{i,j} \tag{7.11}$$

$$\Delta_{max}^{i,j} = I_{\tau_{max}}^{i,j} - I^{i,j} \tag{7.12}$$

111

First-order local diagonal derivative

$\gamma = 0$			$\gamma = 1$			$\gamma = 2$	
145	-41	85	104	41		24	
-60	-44	-104	-85	-145		60	

(a) — (b) — (c) — (d) — (e) — (f) — (g) — (h) — (i)

$I_2^{i,j}$		$I_1^{i,j}$
	$I^{i,j}$	
$I_3^{i,j}$		$I_4^{i,j}$

(a)

15		56
	50	
160		100

(b)

$I_{\tau_{max}}^{i,j} = 160$
$I_{\tau_{min}}^{i,j} = 15$
$I^{i,j} = 50$

(e)

$\tau_{max} = 3$
$\tau_{min} = 2$

(d)

$\Delta_{max}^{i,j} = 110$
$\Delta_{min}^{i,j} = -45$

(f)

$sign(\Delta_{max}^{i,j}) = 1$
$sign(\Delta_{min}^{i,j}) = 0$

(g)

$\delta = 2$

(h)

$(\tau_{max} + 8\delta) = 19$
$(\tau_{min} + 4 + 8\delta) = 22$

(i)

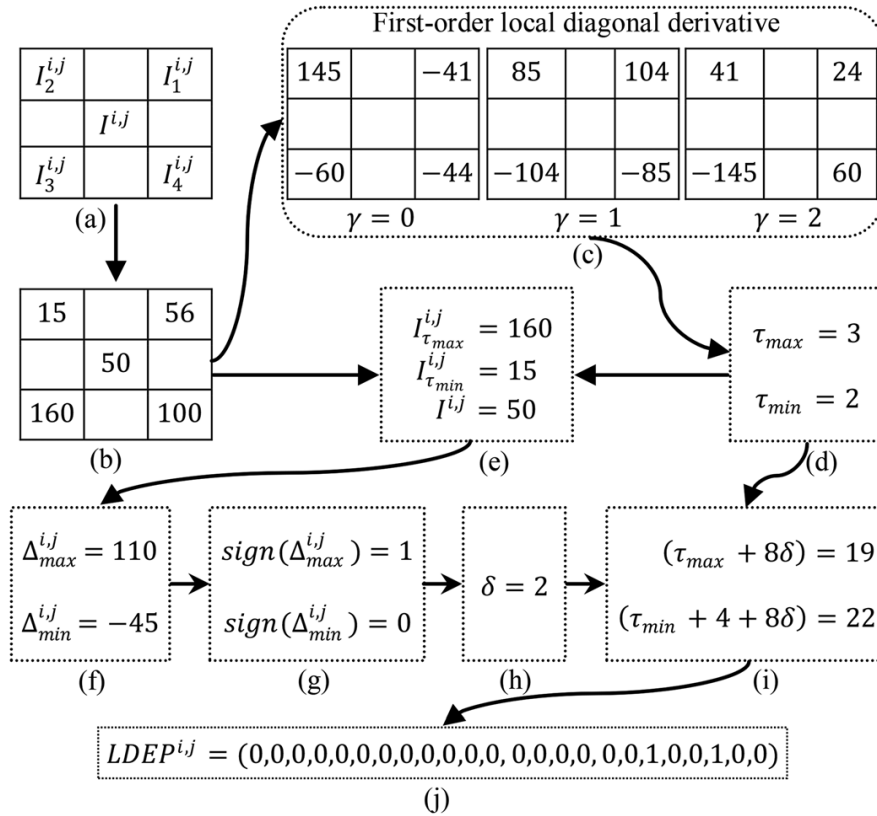$LDEP^{i,j} = (0,0,0,0,0,0,0,0,0,0,0,0,0,\ 0,0,0,0,\ 0,0,1,0,0,1,0,0)$

(j)

Figure 7.6. $LDEP^{i,j}$ computation process with an example image patch

It can be deduced from above formulas that the LDEP pattern is composed of all $0's$ and only two $1's$. This produces a unique discriminating pattern. The length dim of the LDEP depends upon the maximum value of k which is 24 obtained by putting $\tau_{min} = 4$ and $\delta = 2$. Thus the dimension of LDEP feature vector is 24.

7.3 Proposed System

Local binary pattern methodology has been extensively researched and modified over different aspects. Some of the major modifications are carried out to increase the discriminative capacity and neighborhood selection to obtain better performance while not increasing much of the computational cost. In this thesis we have modified the local binary pattern by calculating the transition between consecutive windows using hamming distance and then calculate the hamming code for building features. The feature set is used for retrieving images from the

database by evaluating the similarity between features using distance metric. The experiments are conducted on both real and simulated database and the proposed algorithm shows significant improvement over existing local binary pattern based image retrieval algorithms.

7.3.1 Feature Extraction

For extracting the features of the image for which we need to retrieve similar images we need to follow the following steps as given below and the sample image patch is shown in Figure 7.7:

Step 1: Load the input image.

Step 2: Compute the LBP for each 3X3 window in the entire image.

Step 3: Calculate the hamming distance between the two LBP codes.

Step 4: A 3 X 3 window of hamming distances by performing calculation in the eight neighborhood.

Step 5: Now compute LBP code using this hamming distance window.

Step 6: Following this pattern histogram is computed for 256 values.

Step 7: Form a feature vector by concatenating the histograms.

7.3.2 Similarity Measurement

Feature extraction yields the feature vector for query picture I, which is represented as $f_I = (f_{I_1}, f_{I_2}, \ldots, f_{I_{LG}})$.

Similarly, feature vectors $f_{DB_j} = (f_{DB_{j1}}, f_{DB_{j2}}, \ldots, f_{DB_{jLG}}); j = 1, 2, \ldots, |DB|$. are used to represent each image in the database. The aim is to find the n most similar photos to the query image. The distance between the query image and the images in the database |DB| is used to choose n top matched photos. We utilise the d1 similarity distance metric, which is calculated using Equation 7.13.

113

$$D(I_i, DB_{ji}) = \sum_{i=1}^{LG} \left| \frac{f_{DB_{ji}} - f_{I_i}}{1 + f_{DB_{ji}} + f_{I_i}} \right|$$

where $f_{DB_{ji}}$ is the ith characteristic of the jth picture in the database |DB|. The d1 similarity distance metric is used in this thesis to calculate the retrieval outcomes of the proposed technique and other current methods. The d1 distance metric has been utilised for picture retrieval in the literature [119-122].
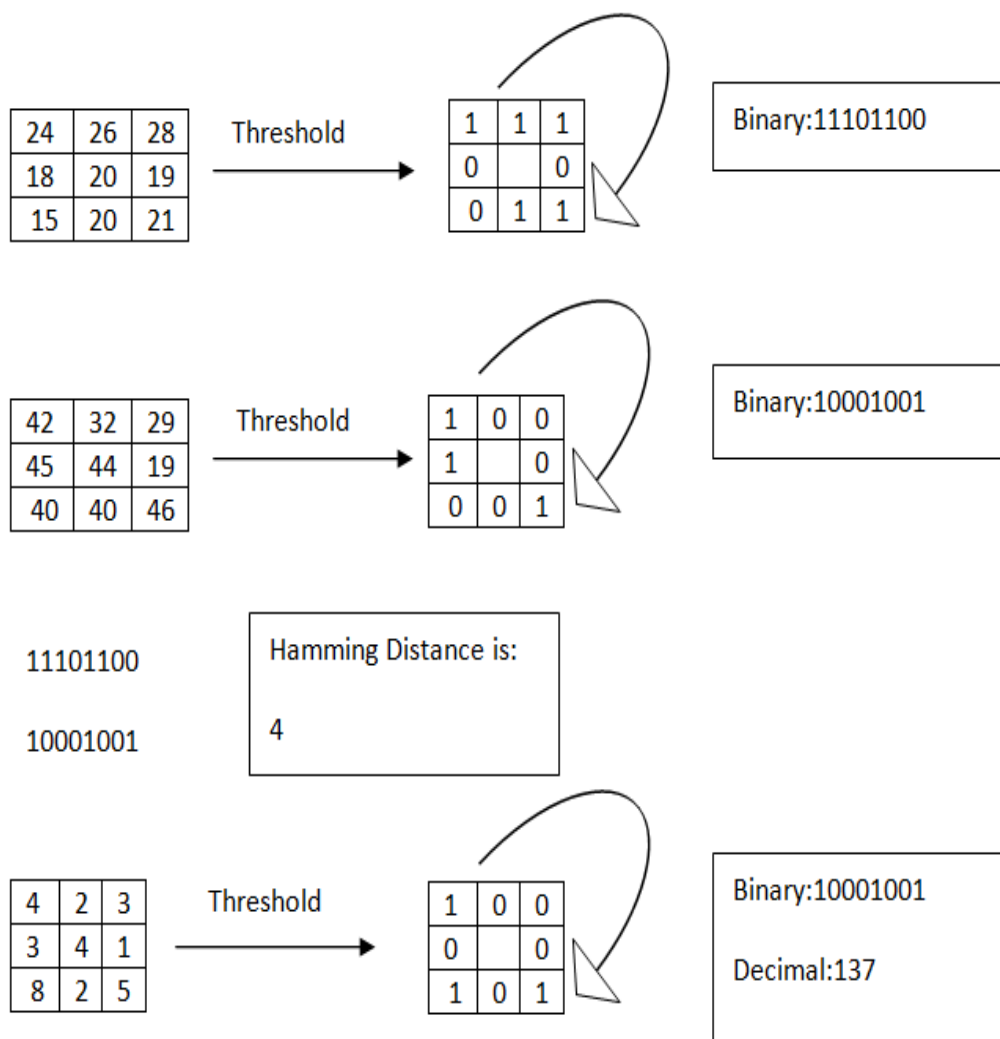

Figure 7.7: HDLBP computation process with an example image patch

7.3.3 Metrics for Evaluation

Precision is used to calculate the performance of the given method. It's a metric for precision, i.e. what proportion of data that's labelled positive is truly positive.

$$Precision = \frac{TP}{TP+FP} \qquad 7.14$$

Precision may be defined as the ratio of the total number of relevant pictures retrieved to the total number of images retrieved in the instance of image retrieval.

7.4. Experimental Results & Discussions

On a real-time Brain Image Database, the suggested technique is implemented. The real-time database comes from Delhi, India's Rajiv Gandhi Cancer Institute and Research Centre (RGCI&RC). The tumorous images have been provided from a database of T1 weighted brain MRI images of 20 patients by the radiologist of Rajiv Gandhi Cancer Institute & Research Centre(RGCI&RC), Delhi, India. Each patient dataset had 20 MRI images in form of horizontal slices of brain resulting in a total of 400 images.

As shown in Figure 7.8, (a) is the query image is supplied into the system as input, and top five comparable photos are retrieved from the database as shown in (b) to (e). Database stores all the images of the patients who have undergone treatment in the hospital. Retrieval of images similar to the new case can help in treatment planning of the patient.

The proposed algorithm is compared with other existing algorithms in the literature and is found to outperform as we can see from Table 7.1 and Figure 7.9.
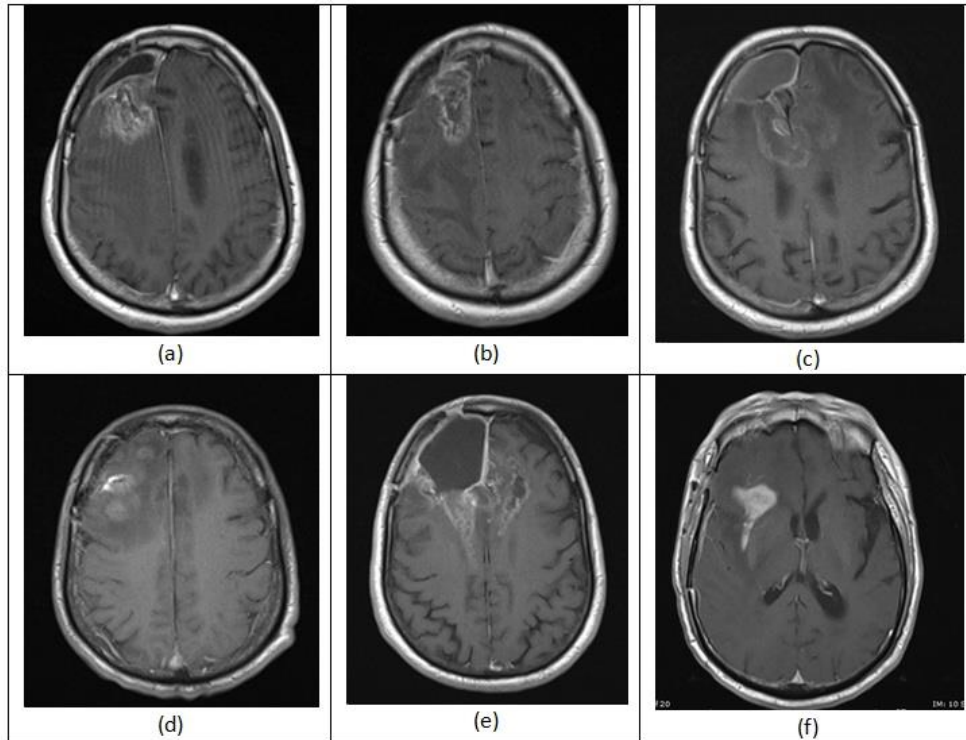
Figure 7.8: (a) Input Image (b-f)Top 5 Output Images Based on Similarity Measure
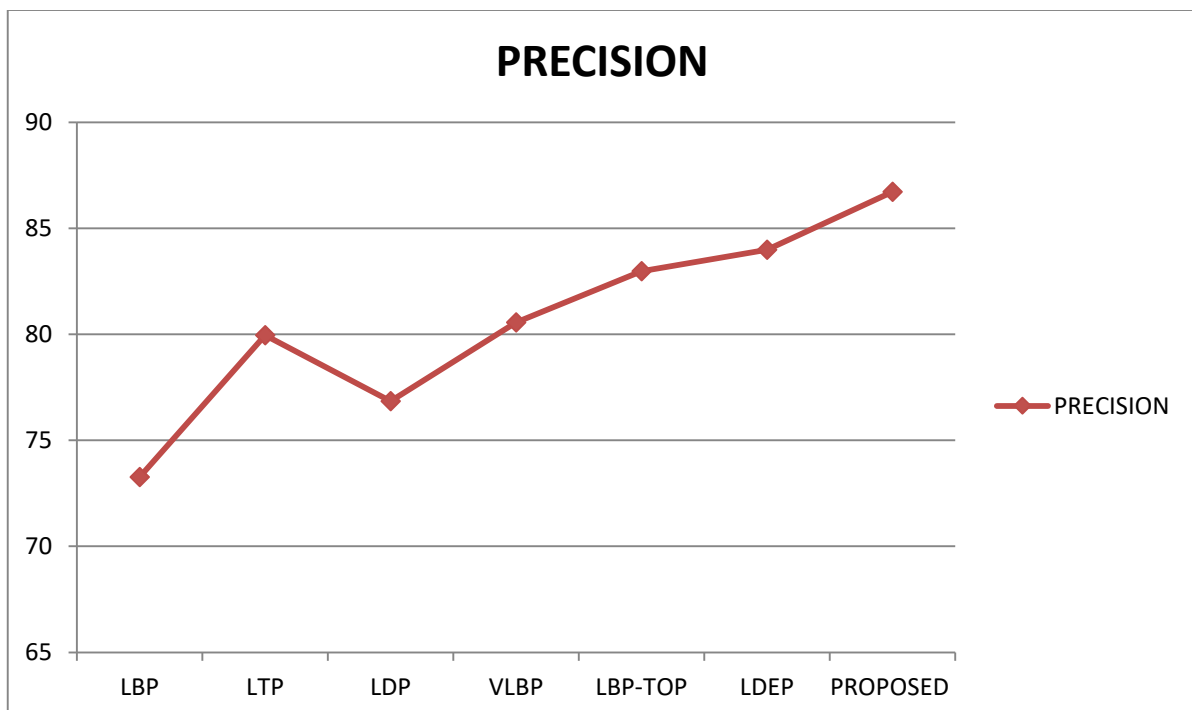

Figure 7.9: Comparative analysis of the proposed algorithm

Table 7.1: Comparative Analysis of the proposed algorithm

METHOD	PRECISION
LBP	73.26
LTP	79.96
LDP	76.84
VLBP	80.56
LBP-TOP	82.97
LDEP	83.98
PROPOSED	86.72

7.5 Summary

Image retrieval is a real world problem where we can extract images from the database on the basis of certain similarity. In this chapter, the local binary pattern was modified successfully by calculating the transition between consecutive windows using hamming distance and then calculate the hamming code for building features. The derived feature set proved to be very effective in the extraction of similar images from the database on the basis of distance similarity measure. The similar images thus extracted will further help the doctors and radiologists in treatment planning. The experiments were conducted on the real time database and the proposed algorithm outperforms other existing local binary pattern-based image retrieval algorithms.

Chapter 8

Conclusions and Future Work

Medical image processing is currently the foremost emerging and challenging area of research within the field of image processing. Processing and analysis of human brain images plays a major role in computer aided diagnosis and neuroscience research. It further helps in identification of several neurodegenerative and mental disorder diseases such as tumors, edema, Schizophrenia, Multiple Sclerosis, Alzheimer disease and Parkinson.

In order to beat the shortcomings of mapping the tumor manually, the researchers are keen to develop automatic tumor segmentation system. This thesis work tries to cater various aspects of MR brain image classification and segmentation. In order to classify the image into tumorous and non-tumorous. We have proposed to use binary patterns (LBP) as features. The images are classified using Minimal complexity machine (MCM) algorithm into tumorous and non-tumorous. The accuracy calculated is used to assess the performance of the proposed approaches.

K-Means Clustering, Fuzzy C-Means Clustering, and Region Growing are the picture segmentation algorithms used. The above stated picture segmentation approaches were compared, and it was discovered that utilising simply feature memberships might result in overlapping clusters, emphasising the requirement for both feature and object memberships. To

address this issue in the case of MR brain pictures, we present the Fuzzy Co-Clustering Algorithm for brain tumour identification. Co-clustering is combined with the Fuzzy method in this technique to produce unique clusters. These segmentation algorithms, on the other hand, are unable to deal with the ambiguity that emerges from tissue boundaries. To deal with this sort of uncertainty, intuitionistic fuzzy sets, an extension of fuzzy sets theory, is employed (IFS). In this thesis, we developed the Intuitionistic Fuzzy Co- Clustering Algorithm to deal with the ambiguity between various tissues.

Also, in computer-aided diagnosis and neuroscience research, segmenting a human brain picture from magnetic resonance imaging into three brain tissues: cerebrospinal fluid, grey matter, and white matter is an important component. Segmentation algorithms such as FCM is very sensitive to noise. To avoid any stuck in local optimal results, ACO technique is used. ACO is used to determine the value of initial cluster centers. The centers thus obtained are fed into the system to perform segmentation. In modified FCM, Mahalanobis distance is used instead of Euclidean distance as Euclidean distance takes into account only the super-spherical shapes about the center of mass for clustering the data points, whereas data points belonging to same cluster may not be located in that area only. These techniques are also compared with the state of art algorithms. Proposed algorithms excel in subjective as well as perceptible ways.

Image retrieval is a real world problem where we can extract images from the database on the basis of certain similarity. In this thesis, an image retrieval algorithm is also proposed. The local binary pattern was modified successfully by calculating the transition between consecutive windows using hamming distance and then calculate the hamming code for building features. The derived feature set proved to be very effective in the extraction of similar images from the database on the basis of distance similarity measure.

8.1 Contributions and Future Work

In this thesis existing methods for brain image classification, tumor detection, brain image segmentation and brain image retrieval are studied and their relative segmentation performance is compared on two publicly available real and simulated MRI brain data.

- The Local Binary Pattern based Minimal Complexity Machine algorithm is proposed in the thesis for brain image classification which can accurately help in identifying the brain image as tumorous or non-tumorous.

- The Intuitionistic Fuzzy Co-Clustering algorithm is proposed in the thesis for brain tumor detection that can help us to identify the tumor in the image and also maps it on the original image for further analysis by the radiologist on treatment planning.

- The optimal fuzzy c-means algorithm and Fuzzy Gravitational Search Algorithm are also proposed for segmentation of MR brain image into gray matter, white matter and cerebrospinal fluid which also caters to the problem of noise.

- A Hamming distance based Local Binary Pattern algorithm is also proposed for brain image retrieval where we can extract images from the database on the basis of certain similarity.

In future, the work of the thesis can be extended to further improve the accuracy and efficiency of the proposed algorithms. Also this work dealt with noise and partial volume effect, so it can be extended to work for images with intensity inhomegenity as well. In this thesis we have focused on only brain images, the work can be extended to lung images as well.

References

[1] K. M. Iftekharuddin, 'On techniques in fractal analysis and their applications in brain', Medical imaging systems: technology and applications, Analysis and Computational Methods, vol. 1, World Scientific Publications, ISBN 981-256-993-6, 2005.

[2] S. M. Bhandarkar, P. Nammalwar, 'Segmentation of Multispectral MR images Using a Hierarchical Self-Organizing Map', Proceedings of the 14th IEEE Symposium on Computer-Based medical system CBMS, Vol: 26, No: 27, pp: 294-299,2001.

[3] Yong Fan, Hengyi Rao, Joan Giannetta, Hallam Hurt, Jiongjiong Wang, Christos Davatzikos, and Dinggang Shen, 'Diagnosis of Brain Abnormality Using both Structural and Functional MR Images', In proceedings of the IEEE conference on Eng Med BioI Soc., 2006

[4] S. Bricq, C. Collet, J. P. Armspach:Unifying framework for multimodal brain MRI segmentation based on Hidden Markov Chains, Medical Image Analysis, pp. 639–652, 2008

[5] A.Mayer, H. Greenspan: An adaptive mean-shift framework for MRI brain segmentation, IEEE Transactions on Medical Imaging, Vol:28, No: 8, pp: 1238–1250, 2009.

[6] Benoit Caldairou, Nicolas Passat, Piotr A. Habas: A non-local fuzzy segmentation method: Application to Brain MRI, Biomedical Image Computing Group, Pattern Recognition 44 pp: 1916-1927, 2011.

[7] Zexuan Ji, Yong Xia: Fuzzy Local Gaussian Mixture Model for brain MR Image Segmentation, IEEE Transactions on Information Technology in Biomedicine, VOL.16 NO.3, May 2012

[8] Charles R. Noback, Norman L. Strominger, Robert J. Demarest and David A. Ruggiero: The Human Nervous System: Structure and Function, 6th ed., Humana Press, 2005.

[9] Wahba Marian: An Automated Modified Region Growing Technique for Prostate Segmentation in Trans-Rectal Ultrasound Images, Master's Thesis, Department of Electrical and Computer Engineering, University of Waterloo, Waterloo, Ontario, Canada, 2008.

[10] A.Nakib, H.Oulhadj, P.Siarry: A thresholding method based on two-dimensional fractional differentiation, Image Visual Computing, Vol: 27, pp: 1343–1357, 2009.

[11] Brown, M. and Semeka, R, 'MRI: Basic Principles and Applications. John Wiley and Sons, Inc., 3rd edition 2003.

[12] Charles R. Noback, Norman L. Strominger, Robert J. Demarest and David A. Ruggiero, The Human Nervous System: Structure and Function, 6th ed., Humana Press, 2005.

[13] Louis D.N., Ohgaki H., Wiestler O.D, Cavenee W.K. (Eds.), 'WHO Classification of Tumors of the Central Nervous System', International Agency for Research on Cancer (IARC), Lyon, France, 2007.

[14] Jan C. Buckner, 'Central Nervous System Tumors', Mayo Clinic Proceedings, Vol. 82, No. 10 , pp. 1271-1286, 2007.

[15] L. J. Erasmus, D. Hurter, M. Naude, H.G. Kritzinger and S Acho, 'A short overview of MRI artifacts', SA Journal of Radiology, Vol. 8 ,No. 2 , pp. 13-17, 2004.

[16] Schmidt M., Levner I., Greiner R., Murtha A. and Bistritz A., 'Segmenting Brain Tumors using Alignment-Based Feature', IEEE 4th International Conference on Machine Learning and Applications, ICMLA, pp. 215-220, Dec. 2005.

[17] N Abdullah, U.K. Ngah, S.A. Aziz, 'Image classification of brain MRI using support vector machine', IEEE International Conference on Imaging Systems and Techniques (IST), 17-18 May 2011, pp. 242-247

[18] S. Chaplot, L.M. Patnaik, N.R. Jagannathan, 'Classification of magnetic resonance brain images using wavelets as input to support vector machine and neural network', Biomedical Signal Processing and Control, Volume 1, Issue 1, January 2006, pp. 86–92.

[19] N. Nandha Gopal, Dr. M. Karnan, 'Diagnose Brain Tumor Through MRI Using Image Processing Clustering Algorithms Such As Fuzzy C Means Along With Intelligent Optimization Techniques', IEEE International Conference on Computational Intelligence and Computing Research (ICCIC), December 2010, pp. 1-4.

[20] El-Sayed A. El-Dahshan, Heba M. Mohsen, Kenneth Revett, Abdel-Badeeh M. Salem, 'Computer-aided diagnosis of human brain tumor through MRI: A survey and a new algorithm', Expert Systems with Applications, Volume 41, Issue 11, 1 September 2014, pp. 5526–5545.

122

[21] Yudong Zhang, Zhengchao Dong, Lenan Wua, Shuihua Wanga, 'A hybrid method for MRI brain image classification', Expert Systems with Applications, Elsevier, Volume 38, Issue 8, August 2011, pp. 10049–10053.

[22] El-Sayed Ahmed El-Dahshan, Tamer Hosny, Abdel-Badeeh M. Salem, 'Hybrid intelligent techniques for MRI brain images classification', Digital Signal Processing, Elsevier, Volume 20, Issue 2, March 2010, pp. 433–44.

[23] N.H. Rajini, R. Bhavani, 'Classification of MRI brain images using k-nearest neighbor and artificial neural network', IEEE International Conference on Recent Trends in Information Technology (ICRTIT), 3-5 June 2011, pp. 563-568,

[24] H.B. Nandpuru, S.S. Salankar, V.R. Bora, 'MRI brain cancer classification using Support Vector Machine', IEEE Students Conference on Electrical, Electronics and Computer Science (SCEECS), 1-2 March 2014, pp. 1-6.

[25] W.H. Ibrahim, A.A.A. Osman, Y.I. Mohamed, 'MRI brain image classification using neural networks', International Conference on Computing, Electrical and Electronics Engineering (ICCEEE), 26-28 Aug. 2013, pp. 253-258.

[26] D. Sridhar and I. Murali Krishna, "Brain Tumor Classification using Discrete Cosine Transform and Probabilistic Neural Network," *2013 International Conference on Signal Processing , Image Processing & Pattern Recognition*, Coimbatore, 2013, pp. 92-96.

[27] S. Yazdani, R. Yusof, M. Pashna and A. Karimian, "A hybrid method for brain MRI classification," *2015 10th Asian Control Conference (ASCC)*, Kota Kinabalu, 2015, pp. 1-5.

[28] K. Machhale, H. B. Nandpuru, V. Kapur and L. Kosta, "MRI brain cancer classification using hybrid classifier (SVM-KNN)," *2015 International Conference on Industrial Instrumentation and Control (ICIC)*, Pune, 2015, pp. 60-65.

[29] Tanvi Gupta, Tapan K. Gandhi, B.K. Panigrahi, "Multi-sequential MR brain image classification for tumor detection", Recent advancements in computer, communication and computational sciences, Journal of Intelligent & Fuzzy Systems, vol. 32, no. 5, pp. 3575-3583, 2017

[30] Tahia Tazin, Sraboni Sarker, Punit Gupta, Fozayel Ibn Ayaz, Sumaia Islam, Mohammad Monirujjaman Khan, Sami Bourouis, Sahar Ahmed Idris, Hammam Alshazly, "A Robust and Novel Approach for Brain

Tumor Classification Using Convolutional Neural Network", Computational Intelligence and Neuroscience, vol. 2021, Article ID 2392395, 11 pages, 2021.

[31] Vidhya s. Dessai, Megha P. Araker, Ram Mohana Reddy Guddeti, 'A Parallel Segmentation of Brain Tumor from Magnetic Resonance Images', IEEE Third International Conference on Computing Communication & Networking Technologies (ICCCNT), pp. 1-6, Jul. 2012.

[32] Kiran Thapaliya, Goo-Rak K won, 'Extraction of Brain Tumor Based on Morphological Operations', IEEE International Conference on Computing Technology and Information Management (ICCM), vol.1, pp. 515-520, Apr. 2012.

[33] Ishita Maiti, Dr. Monisha Chakraborty,'A new method for brain tumor segmentation based on watershed and edge detection algorithms in HSV colour model', IEEE National Conference on Computing and Communication Systems (NCCCS), pp.1-5, Nov. 2012.

[34] Dr. M. Karnan, T.Logheshwari,'Improved Implementation of Brain MRI image Segmentation using Ant Colony System', IEEE International Conference on Computational Intelligence and Computing Research (ICCIC), pp.1-4, Dec.2010.

[35] Dr. H. B. Kekre, Dr.Tanuja Sarode, Ms.Kavita Raut, 'Detection of tumor in MRI using Vector quantization Segmentation' IEEE International Journal of Engineering Science and Technology, Vol. 2(8), pp. 3753-3757, 2010.

[36] Sudipta Roy, Samir K. Bandyopadhyay,'Detection and Quantification of Brain Tumor from MRI of Brain and it's Symmetric Analysis', IEEE International Journal of Information and Communication Technology Research, vol. 2 No. 6, pp. 477-483, Jun. 2012.

[37] A. Rajendran and R.Dhanasekaran, 'A hybrid Method Based on Fuzzy Clustering and Active Contour Using GGVF for Brain Tumor Segmentation on MRI Images', European Journal of Scientific Research, Vol. 61, No. 2, 2011, pp. 305-313.

[38] M. Arfan Jaffar,Quratulain,and Tae Sun Choi, 'Tumor Detection From Enhanced Magnetic Resonance Imaging Using Fuzzy Curvelet', Microscopy Research and Technique, Wiley Online Library, Vol. 75, No. 6, April 2012, pp. 499- 504.

[39] R. B. Dubey, M. Hanmandlu, Shantaram Vasikarla,'Evaluation of Three Methods for MRI Brain Tumor Segmentation', IEEE Eighth International Conference on Information Technology, pp. 494-499, Apr.2012.

[40] Ming-Ni Wu, Chia-Chen Lin, Chin-Chen Chang, 'Brain Tumor Detection Using Color-Based K-Means Clustering Segmentation', IEEE Third International Conference on Intelligent Information Hiding and Multimedia Signal Processing(IIHMSP), vol.2, pp. 245-250, Nov.2007.

[41] N. Nandha Gopal, Dr. M. Karnan, 'Diagnose Brain Tumor Through MRI Using Image Processing Clustering Algorithms Such As Fuzzy C Means Along With Intelligent Optimization Techniques' IEEE International Conference on Computational Intelligence and Computing Research (ICCIC), pp. 1-4, Dec.2010.

[42] El-Melegy, Moumen T, Mokhtar, Hashim M., 'Tumor segmentation in brain MRI using a fuzzy approach with class center priors', EURASIP Journal on Image and Video Processing, 2014, 2014:21.

[43] M. Huang, W. Yang, Y. Wu, J. Jiang, W. Chen and Q. Feng, 'Brain Tumor Segmentation Based on Local Independent Projection-Based Classification', in IEEE Transactions on Biomedical Engineering, vol. 61, no. 10, pp. 2633-2645, Oct. 2014. doi: 10.1109/TBME.2014.2325410

[44] Nabizadeh N, Kubat M., 'Brain tumors detection and segmentation in MR images: Gabor wavelet vs. statistical features', Computers and Electrical Engineering, 2015. http://dx.doi.org/10.1016/j.compeleceng.2015.02.007

[45] Eman Abdel-Maksoud, Mohammed Elmogy, Rashid Al-Awadi, 'Brain tumor segmentation based on a hybrid clustering technique', Egyptian Informatics Journal, Volume 16, Issue 1, 2015, Pages 71-81, ISSN 1110-8665.

[46] C. Sompong, S. Wongthanavasu, 'An efficient brain tumor segmentation based on cellular automata and improved tumor-cut algorithm', Expert Systems With Applications, 2016. http://dx.doi.org/10.1016/j.eswa.2016.10.064

[47] V. Rajinikanth, Suresh Chandra Satapathy, Steven Lawrence Fernandes, S. Nachiappan, 'Entropy based segmentation of tumor from brain MR images – a study with teaching learning based optimization', Pattern Recognition Letters, Volume 94, 2017, Pages 87-95, ISSN 0167-8655, http://dx.doi.org/10.1016/j.patrec.2017.05.028.

[48] R. Deepa, A & R. Sam Emmanuel, An efficient detection of brain tumor using fused feature adaptive firefly backpropagation neural network. Multimedia Tools and Applications, 2018. 10.1007/s11042-018-6731-9.

[49] Amin, Javeria & Sharif, Muhammad & Raza, Mudassar & Yasmin, Mussarat, 'Detection of Brain Tumor based on Features Fusion and Machine Learning', Journal of Ambient Intelligence and Humanized Computing. 10.1007/s12652-018-1092-9, 2018.

[50] H. Hooda, O. P. Verma and T. Singhal, 'Brain tumor segmentation: A performance analysis using K-Means, Fuzzy C-Means and Region growing algorithm', IEEE International Conference on Advanced Communications, Control and Computing Technologies, Ramanathapuram, 2014, pp. 1621-1626.

[51] M. Prastawa, E Bullitt, S Ho, G Gerig, 'A brain tumor segmentation framework based on outlier detection', Medical Image Analysis, vol. 8, pp. 275-283, 2004.

[52] S.Xavierarockiaraj, K.Nithya, and R.Maruni Devi, 'Brain Tumor Detection Using Modified Histogram Thresholding-Quadrant Approach', Journal of Computer Applications (JCA), Vol. 5, No.1, 2012, pp. 21-25.

[53] Anam Mustaqeem, Ali Javed and Tehseen Fatima, 'An Efficient Brain Tumor Detection Algorithm Using Watershed and Thresholding Based Segmentation', International Journal of Image, Graphics and Signal Processing (IJIGSP), Vol. 4, No.10, 2012, pp. 34-39.

[54] Kadam D. B., Gade S. S., M. D. Uplaneand R. K. Prasad, 'Neural Network Based Brain Tumor Detection Using MR Images', International Journal of Computer Science and Communication (IJCSC), Vol. 2, No.2, July-Dec. 2011, pp. 325-331.

[55] Hassan Khotanlou, Olivier Colliot, Jamal Atif and Isabelle Bloch, '3D brain tumor segmentation in MRI using fuzzy classification, symmetry analysis and spatially constrained deformable models', Fuzzy Sets and Systems, Vol. 160, Issue 10, 2009, pp.1457–1473.

[56] Nandita Pradhan and A.K. Sinha, 'Fuzzy ANN Based Detection and Analysis of Pathological and Healthy Tissues in FLAIR Magnetic Resonance Images of Brain', international Journal of Information Technology and Knowledge Management, Vol. 4, No. 2, July-Dec. 2011, pp. 471-476.

[57] Noor Elaiza Abdul Khalid, Shafaf Ibrahim and Mazani Manaf, 'Brain Abnormalities Segmentation Performances Contrasting: Adaptive Network-Based Fuzzy Inference System (ANFIS) vs K-Nearest Neighbors (k-NN) vs Fuzzy c-Means (FCM)', 15th WSEAS International Conference on Computers, Corfu Island, Greece, July 2011, pp. 285-290.

[58] Salama, W.M., Shokry, A. A novel framework for brain tumor detection based on convolutional variational generative models. Multimed Tools Appl 81, 16441–16454 2022. https://doi.org/10.1007/s11042-022-12362-9

[59] Clark, M.C., Hall, L.O., Goldgof, D.B., Velthuizen, R., Reed Murtagh, F., Silbiger, M.S., 'Automatic tumor segmentation using knowledge-based techniques', IEEE Transactions on Medical Imaging, vol. 17, pp. 187-201,1999.

[60] Prastawa, M., Bullitt, E., Ho, S., Gerig, G., 'A brain tumor segmentation framework based on outlier detection, Medical Image Analysis', vol. 8, pp. 275-283, 2004.

[61] A.R.Kavitha, Dr.C.Chellamuthu, Ms.Kavin Rupa, 'An Efficient Approach for Brain Tumour Detection Based on Modified Region Growing and Neural Network in MRI Images', IEEE International Conference on Computing, Electronics and Electrical Technologies [ICCEET], pp. 1087-1095, 2012.

[62] A. Nakib, H. Oulhadj, P. Siarry, 'A thresholding method based on two-dimensional fractional differentiation', Image Vis. Computing, Vol. 27, 2009, pp:1343–1357.

[63] J.C. Bezdek, 'Pattern Recognition with Fuzzy Objective Function Algorithms', Kluwer Academic Publishers, Norwell, MA, USA, 1981.

[64] D. Pham, 'Fuzzy clustering with spatial constraints', Proceedings of the InternationalConference on Image Processing, vol.2, NewYork, USA, 2002, pp.II-65–II-68.

[65] S.Chen, D.Zhang, 'Robust image segmentation using FCM with spatial constraints based on new kernel-induced distance measure',IEEE Trans.Syst.ManCybern. PartB, Cybern.34, 2004, pp:1907–1916.

[66] Q. Mahmood, A. Chodorowski, M. Persson, 'Automated MRI brain tissue segmentation based on mean shift and fuzzy c-means using a priori tissue probability maps', In IRBM, Volume 36, Issue 3, 2015, Pages 185-196, ISSN 1959-0318, https://doi.org /10.1016/ j.irbm.2015.01.007.

[67] M.Ahmed, S.Yamany, N.Mohamed, A.Farag, T.Moriarty, 'A modified fuzzy c-means algorithm for bias field estimation and segmentation of MRI data', IEEE Trans. Med. Imag. 21, 2002, pp: 193–199.

[68] T.Kalaiselvi, P.Nagaraja, V.Ganapathy Karthick, 'Improved Fuzzy C-Means for Brain Tissue Segmentation Using T1- Weighted MRI Head Scans', International Journal of Innovative Science, Engineering & Technology, Vol. 3 Issue 7, July 2016.

[69] R.Krishnapuram, J.Kim, 'A note on the Gustafson Kessel and adaptive fuzzy clustering algorithms', IEEE Trans. Fuzzy Syst. 7, 1999, pp:453–461.

[70] D.E.Gustafson, W.C.Kessel, 'Fuzzy clustering with a fuzzy covariance matrix', IEEE Conference on Decision and Control including the 17th Symposium on Adaptive Processes, vol.17, SanDiego, CA, USA, 1978, pp.761–766.

[71] Thomas A. Runkler, 'Ant Colony Optimization of Clustering Models', International Journal of Intelligent Systems, vol. 20, 1233–1251, 2005.

[72] Yucheng Kao, Kevin Chang, 'An ACO based clustering algorithm', ANTS 2006, LNCS 4150, pp. 340–347, 2006.

[73] A. Ortiz, J. M. Górriz, J. Ramírez and D. Salas-Gonzalez, "MR brain image segmentation by growing hierarchical SOM and probability clustering," in Electronics Letters, vol. 47, no. 10, pp. 585-586, May 12 2011. doi: 10.1049/el.2011.0322.

[74] Y. Chen, J. Zhang, S. Wang and Y. Zheng, "Brain magnetic resonance image segmentation based on an adapted non-local fuzzy c-means method," in IET Computer Vision, vol. 6, no. 6, pp. 610-625, November 2012.

[75] A.N. Benaichouche, H. Oulhadj, P. Siarry, Improved spatial fuzzy c-means clustering for image segmentation using PSO initialization, Mahalanobis distance and post-segmentation correction, In Digital Signal Processing, Volume 23, Issue 5, 2013, pp: 1390-1400, ISSN 1051-2004.

[76] Hanuman Verma, R.K. Agrawal, Aditi Sharan, An improved intuitionistic fuzzy c-means clustering algorithm incorporating local information for brain image segmentation, In Applied Soft Computing, Volume 46, 2016, Pages 543-557, ISSN 1568-4946.

[77] P. Moeskops, M. A. Viergever, A. M. Mendrik, L. S. de Vries, M. J. N. L. Benders and I. Išgum, "Automatic Segmentation of MR Brain Images With a Convolutional Neural Network," in IEEE Transactions on Medical Imaging, vol. 35, no. 5, pp. 1252-1261, May 2016

[78] Y. Chen, J. Li, H. Zhang, Y. Zheng, B. Jeon and Q. J. Wu, "Non-local-based spatially constrained hierarchical fuzzy C-means method for brain magnetic resonance imaging segmentation," in IET Image Processing, vol. 10, no. 11, pp. 865-876, 11 2016.

[79] Anupama Namburu, Srinivas Kumar Samayamantula, Srinivasa Reddy Edara, " Generalised rough intuitionistic fuzzy c-means for magnetic resonance brain image segmentation", IET Image Processing, Volume 11, Issue 9, p. 777 –785.

[80] Saneipour, Keyvan & Mohammadpoor, Mojtaba, Improvement of MRI Brain Image Segmentation Using Fuzzy Unsupervised Learning. Iranian Journal of Radiology. In Press. 10.5812/iranjradiol.69063, 2019.

[81] Om Prakash Verma and Heena Hooda, "A Novel Intuitionistic Fuzzy Co-Clustering Algorithm for Brain Images", Multimedia Tools and Applications, Volume 79, 31517–31540, 2020.

[82] Subrahmanyam Murala, Jonathan Wu QM, "Local mesh patterns versus local binary patterns: Biomedical image indexing and retrieval". IEEE Journal of Biomedical Health Informatics 2014.

[83] Geetha, A., Investigation and Survey of Content Based Image Retrieval for MRI Brain Images. International Journal of Health & Allied Sciences, 2016.

[84] T. Ojala, M. Pietikäinen, and D. Harwood, "A comparative study of texture measures with classification based on featured distributions," Pattern recognition, vol. 29, pp. 51-59, 1996.

[85] Hooda H., Verma O.P. (2019), "Classification of Magnetic Resonance Brain Images Using Local Binary Pattern as Input to Minimal Complexity Machine", In Computing, Communication and Signal Processing, Advances in Intelligent Systems and Computing, Springer, Singapore, International Conference on Computing, Communication and Signal Processing 2018, 26-27 Jan 2018, vol 810, pp. 883-893.

[86] H. Jin, Q. Liu, H. Lu, and X. Tong, "Face detection using improved LBP under bayesian framework," in Multi-Agent Security and Survivability, 2004 IEEE First Symposium on, 2004, pp. 306-309.

[87] J. N. Bassili, "Emotion recognition: the role of facial movement and the relative importance of upper and lower areas of the face," Journal of personality and social psychology, vol. 37, p. 2049, 1979.

[88] G. Zhao and M. Pietikäinen, "Boosted multi-resolution spatiotemporal descriptors for facial expression recognition," Pattern recognition letters, vol. 30, pp. 1117-1127, 2009.

[89] S. R. Dubey, S. K. Singh, and R. K. Singh, "Local Diagonal Extrema Pattern: A New and Efficient Feature Descriptor for CT Image Retrieval," Signal Processing Letters, IEEE, vol. 22, pp. 1215-1219, 2015.

[90] R. Gupta, H. Patil, and A. Mittal, "Robust order-based methods for feature description," in Computer Vision and Pattern Recognition (CVPR), 2010 IEEE Conference on, 2010, pp. 334-341.

[91] Zhou Guohua, Lu Bing, Hu Xuelong, Ni Tongguang, "Sparse Representation-Based Discriminative Metric Learning for Brain MRI Image Retrieval", Frontiers in Neuroscience, VOLUME 15, 2022. https://www.frontiersin.org/article/10.3389/fnins.2021.829040,

[92] T. Ahonen, A. Hadid, and M. Pietikäinen, "Face recognition with local binary patterns," in Computer vision-eccv 2004, ed: Springer, 2004, pp. 469-481.

[93] A. Hadid, M. Pietikainen, and T. Ahonen, "A discriminative feature space for detecting and recognizing faces," in Computer Vision and Pattern Recognition, pp. II-797-II-804 Vol. 2, 2004.

[94] T. Ojala, M. Pietikainen, and T. Maenpaa, "Multiresolution gray-scale and rotation invariant texture classification with local binary patterns," Pattern Analysis and Machine Intelligence, IEEE Transactions on, vol. 24, pp. 971-987, 2002.

[95] T. Ahonen, A. Hadid, and M. Pietikainen, "Face description with local binary patterns: Application to face recognition," Pattern Analysis and Machine Intelligence, IEEE Transactions on, vol. 28, pp. 2037-2041, 2006.

[96] C. Shan, S. Gong, and P. W. McOwan, "Facial expression recognition based on local binary patterns: A comprehensive study," Image and Vision Computing, vol. 27, pp. 803-816, 2009.

[97] Padraig Cunningham, Sarah Delany, 'k-Nearest neighbour classifiers', Mult Classif Syst., 2007

[98] V.N. Vapnik, Statistical Learning Theory, Wiley, New York, 1998.

[99] Jayadeva, 'Learning a hyperplane classifier by minimizing an exact bound on the VC dimension', Neurocomputing Volume 149, Part B, 3 February 2015, pp: 683–689.

[100] Harvard Medical School, Web: data available at http://www.med.harvard.edu/AANLIB/.

[101] L.A. Zadeh, Fuzzy sets, Inf. Control, Vol: 8 (3), 1965, pp: 338–353.

[102] L.K. Hyung, Y.S. Song, K.M. Lee, Similarity measure between fuzzy sets andbetween elements, Fuzzy Sets Syst., Vol: 62 (3), 1994, pp: 291–293.

[103] K.T. Atanassov, Intuitionistic fuzzy sets, Fuzzy Sets Syst., Vol: 20 (1), 1986, pp: 87–96.

[104] Z. Xu, Some similarity measures of intuitionistic fuzzy sets and their appli-cations to multiple attribute decision making, Fuzzy Optim. Decis. Mak., Vol: 6 (2), 2007, pp:109–121.

[105] M. Sugeno, Theory of Fuzzy Integrals and Its Applications, Ph.D. Dissertation, Tokyo Institute of Technology, 1974

[106] Madasu Hanmandlu, Om Prakash Verma, Seba Susan, V.K. Madasu, 'Color Segmentation by Fuzzy co-clustering color features', Neurocomputing, Volume 120, November 2013.

[107] J. Kennedy, R. C. Eberhart, 'Particle swarm optimization', Proceedings of IEEE International Conference on Neural Networks, 1995, pp: 1942-1948.

[108] L. R. Dice, 'Measures of the amount of ecologic association between species', Ecology 1945; Vol: 26 pp:297–302.

[109] P. Jaccard, 'The distribution of flora in the alpine zone', New Phytologist 1912; Vol: 11, pp:37–50.

[110] B. Biswal, P.K. Dash, S. Mishra, 'A hybrid ant colony optimization technique for power signal pattern classification', Expert Systems with Applications, Vol: 38, 2011, pp: 6368–6375.

[111] K. Selvanayaki, P. Kalugasalam, 'Brain tumor segmentation using algorithmic and non algorithmic approach' International Journal of research in Commerce, IT and Management, volume no. 2 (2012), issue no. 10 (October)

[112] P.C. Mahalanobis, 'On the generalized distances in statistics: Mahalanobis distance', Journal Soc. Bengal, Vol. XXVI, pp. 541-588, 1936.

[113] http://www.insight-journal.org/midas/community/

[114] http://www.bic.mni.mcgill.ca/brainweb

[115] E. Rashedi, H. Nezamabadi-pour, S. Saryazdi, "GSA: a gravitational search algorithm", Information Sciences, vol. 179, issue 13, pp. 2232–2248, 2009.

[116] A. Hatamlou, S. Abdullah, H. Nezamabadi-pour, "Application of gravitational search algorithm on data clustering", Rough Sets and Knowledge Technology, Springer, pp. 337–346, 2011.

[117] Subrahmanyam Murala, Q.M. Jonathan Wu."MRI and CT image indexing and retrieval using local mesh peak valley edge patterns", Signal Processing: Image Communication, 2014.

[118] C.H. Lin, R.T. Chen, Y.K.A. Chan, Smart content-based image retrieval system based on color and texture feature, ImageVis.Comput., Vol: 27, 2009, pp:658–665.

[119] Subrahmanyam Murala, R.P. Maheshwari, R.Bala subramanian, Local maximum edge binary patterns: a new descriptor for image retrieval and object tracking, Signal Process.92(2012)1467–1479.

[120] Subrahmanyam Murala, R.P. Maheshwari, R. Balasubramanian, Directional local extrema patterns: a new descriptor for content based image retrieval, Int. J.Multimed.Inf.Retr.1(3)(2012)191–203.

[121] Subrahmanyam Murala, R.P. Maheshwari, R.Balasubramanian, Directional binary wavelet patterns for biomedical image indexing and retrieval, J. Med. Syst., Vol 36(5), 2012, pp. 2865–2879.

[122] Subrahmanyam Murala, R.P. Maheshwari, R. Balasubramanian, Local tetra patterns: a new feature descriptor for content based image retrieval, IEEE Trans. Image Processing, Vol 21(5), pp. 2874–2886, 2012.